

ATTACHMENT 3 TO AEP:NRC:4054-06

WESTINGHOUSE WCAP-14118-NP

**“STRUCTURAL INTEGRITY EVALUATION OF REACTOR VESSEL UPPER HEAD
PENETRATIONS TO SUPPORT CONTINUED OPERATION: D. C. COOK UNITS 1 AND 2”
REVISION 7, DATED MAY 2004**

NON-PROPRIETARY

Westinghouse Non-Proprietary Class 3

**WCAP-14118-NP
Revision 7
(Supersedes WCAP-15753 Rev. 1)**

May 2004

Structural Integrity Evaluation of Reactor Vessel Upper Head Penetrations to Support Continued Operation: D. C. Cook Units 1 and 2




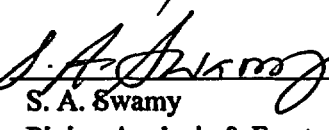
WCAP-14118-NP
Revision 7
(Supersedes WCAP-15753 Rev. 1)

Structural Integrity Evaluation of Reactor Vessel Upper Head Penetrations to Support Continued Operation: D. C. Cook Units 1 and 2

S. Jirawongkraisorn

May 2004

Verifier: 
C. K. Ng
Piping Analysis & Fracture Mechanics

Approved: 
S. A. Swamy
Piping Analysis & Fracture Mechanics

Westinghouse Electric Company LLC
P.O. Box 355
Pittsburgh, PA 15230-0355

© 2004 Westinghouse Electric Company LLC
All Rights Reserved

TABLE OF CONTENTS

| | |
|--|-----|
| List of Tables..... | v |
| List of Figures..... | vi |
| 1 Introduction | 1-1 |
| 2 History of Cracking in Head Penetrations | 2-1 |
| 3 Overall Technical Approach..... | 3-1 |
| 3.1 Penetration Stress Analysis | 3-1 |
| 3.2 Flaw Tolerance Approach | 3-1 |
| 4 Material Properties, Fabrication History and Crack Growth Prediction | 4-1 |
| 4.1 Materials and Fabrication | 4-1 |
| 4.2 Crack Growth Prediction | 4-1 |
| 5 Stress Analysis..... | 5-1 |
| 5.1 Objectives of the Analysis | 5-1 |
| 5.2 Model | 5-1 |
| 5.3 Stress Analysis Results – Outermost CRDM Penetration (50.5°) | 5-2 |
| 5.4 Stress Analysis Results – Intermediate CRDM Penetrations..... | 5-3 |
| 5.5 Stress Analysis Results – Center CRDM Penetration..... | 5-3 |
| 5.6 Stress Analysis Results – Head Vent | 5-3 |
| 6 Flaw Tolerance Charts..... | 6-1 |
| 6.1 Introduction..... | 6-1 |
| 6.2 Overall Approach | 6-1 |
| 6.3 Axial Flaw Propagation | 6-3 |
| 6.4 Circumferential Flaw Propagation | 6-4 |
| 6.5 Flaw Acceptance Criteria..... | 6-5 |
| 6.6 Example Calculations | 6-7 |
| 7 Summary..... | 7-1 |
| 7.1 Safety Assessment..... | 7-1 |
| 8 References | 8-1 |

TABLE OF CONTENTS (Cont.)

| | | |
|-------------------|---|------------|
| Appendix A | Allowable Areas of Lack of Fusion: Weld Fusion Zone..... | A-1 |
| Appendix B | D. C. Cook Units 1 & 2: CRDM Hoop Stress Vs Distance from Bottom of Weld Plots.B-1 | |

LIST OF TABLES

| | | |
|-----------|---|------|
| Table 1-1 | D. C. Cook Unit 1 Head Penetration Nozzles with the Intersection Angles Identified..... | 1-3 |
| Table 1-2 | D. C. Cook Unit 2 Head Penetration Nozzles with the Intersection Angles Identified..... | 1-4 |
| Table 2-1 | Operational Information and Inspection Results for Units Examined (Results through April 30, 2002) | 2-4 |
| Table 4-1 | D. C. Cook Unit 1 R/V Head Adapter Material Information | 4-7 |
| Table 4-2 | D. C. Cook Unit 2 R/V Head Adapter Material Information | 4-8 |
| Table 6-1 | Summary of R.V. Head Penetration Flaw Acceptance Criteria (Limits for Future Growth)..... | 6-10 |
| Table 6-2 | D. C. Cook Units 1 & 2 Penetration Geometries [11, 12] | 6-10 |
| Table B-1 | Hoop Stress Vs Distance from Bottom of Weld Data for the Center CRDM Penetration | B-2 |
| Table B-2 | Hoop Stress Vs Distance from Bottom of Weld Data for the 27.0 Degrees Row of Penetration, Uphill Side..... | B-3 |
| Table B-3 | Hoop Stress Vs Distance from Bottom of Weld Data for the 27.0 Degrees Row of Penetration, Downhill Side..... | B-4 |
| Table B-4 | Hoop Stress Vs Distance from Bottom of Weld Data for the 45.8 Degrees Row of Penetration, Uphill Side..... | B-5 |
| Table B-5 | Hoop Stress Vs Distance from Bottom of Weld Data for the 45.8 Degrees Row of Penetration, Downhill Side..... | B-6 |
| Table B-6 | Hoop Stress Vs Distance from Bottom of Weld Data for the 47.0 Degrees Row of Penetration, Uphill Side..... | B-7 |
| Table B-7 | Hoop Stress Vs Distance from Bottom of Weld Data for the 47.0 Degrees Row of Penetration, Downhill Side..... | B-8 |
| Table B-8 | Hoop Stress Vs Distance from Bottom of Weld Data for the 50.5 Degrees Row of Penetration, Uphill Side..... | B-9 |
| Table B-9 | Hoop Stress Vs Distance from Bottom of Weld Data for the 50.5 Degrees Row of Penetration, Downhill Side..... | B-10 |

LIST OF FIGURES

| | | |
|------------|---|------|
| Figure 1-1 | Reactor Vessel Control Rod Drive Mechanism (CRDM) Penetration..... | 1-5 |
| Figure 1-2 | Location of Head Penetrations for D. C. Cook Unit 1 [11C]..... | 1-6 |
| Figure 1-3 | Location of Head Penetrations for D. C. Cook Unit 2 [12C]..... | 1-7 |
| Figure 2-1 | EDF Plant R/V Closure Head CRDM Penetrations – Penetrations with Cracking | 2-5 |
| Figure 3-1 | Schematic of a Head Penetration Flaw Growth Chart for Part-Through Flaws | 3-3 |
| Figure 3-2 | Schematic of a Head Penetration Flaw Tolerance Chart for Through-Wall Flaws..... | 3-4 |
| Figure 4-1 | Yield Strength of the Various Heats of Alloy 600 Used in Fabricating the D. C. Cook Units 1 & 2 and French Head Penetrations..... | 4-9 |
| Figure 4-2 | Carbon Content of the Various Heats of Alloy 600 Used in Fabricating the D. C. Cook Units 1 & 2 and French Head Penetration | 4-10 |
| Figure 4-3 | Screened Laboratory Data for Alloy 600 with the MRP Recommended Curve..... | 4-11 |
| Figure 4-4 | Model for PWSCC Growth Rates in Alloy 600 in Primary Water Environments (325°C), With Supporting Data from Standard Steel, Huntington, and Sandvik Materials | 4-12 |
| Figure 4-5 | Summary of Temperature Effects on PWSCC Growth Rates for Alloy 600 in Primary Water | 4-13 |
| Figure 5-1 | Finite Element Model of CRDM Penetration | 5-4 |
| Figure 5-2 | Vent Pipe Finite Element Model | 5-5 |
| Figure 5-3 | Stress Distribution at Steady State Conditions: Outermost CRDM Penetration Nozzle (50.5 Degrees) (Hoop Stress is the Top Figure, Axial Stress is the Bottom Figure) | 5-6 |
| Figure 5-4 | Stress Distribution at Steady State Conditions for the 47.0 Degrees CRDM Penetration (Hoop Stress is the Top Figure; Axial Stress is the Bottom Figure) | 5-7 |
| Figure 5-5 | Stress Distribution at Steady State Conditions for the 45.8 Degrees CRDM Penetration (Hoop Stress is the Top Figure; Axial Stress is the Bottom Figure) | 5-8 |
| Figure 5-6 | Stress Distribution at Steady State Conditions for the 27.0 Degrees CRDM Penetration (Hoop Stress is the Top Figure; Axial Stress is the Bottom Figure) | 5-9 |

| | | |
|-------------|---|------|
| Figure 5-7 | Stress Distribution at Steady State Conditions for the Center CRDM Penetration (Hoop Stress is the Top Figure; Axial Stress is the Bottom Figure)..... | 5-10 |
| Figure 5-8 | Stress Contours in the Head Vent Nozzle as a Result of Residual Stresses and Operating Pressure (Hoop Stress is the Top Figure; Axial Stress is the Bottom Figure)..... | 5-11 |
| Figure 5-9 | Axial Stress Distribution at Steady State Conditions for the Outermost CRDM Penetration (50.5 Degrees), Along a Plane Oriented Parallel to, and Just Above, the Attachment Weld | 5-12 |
| Figure 6-1 | Stress Intensity Factor for a Through-Wall Circumferential Flaw in a Head Penetration..... | 6-11 |
| Figure 6-2 | Inside, Axial Surface Flaws, .5" Below the Attachment Weld, Nozzle Uphill Side - Crack Growth Predictions for D. C. Cook Unit 1 | 6-13 |
| Figure 6-3 | Inside, Axial Surface Flaws, .5" Below the Attachment Weld, Nozzle Downhill Side - Crack Growth Predictions for D. C. Cook Unit 1..... | 6-14 |
| Figure 6-4 | Inside, Axial Surface Flaws, At the Attachment Weld, Nozzle Uphill Side - Crack Growth Predictions for D. C. Cook Unit 1..... | 6-15 |
| Figure 6-5 | Inside, Axial Surface Flaws, At the Attachment Weld, Nozzle Downhill Side - Crack Growth Predictions for D. C. Cook Unit 1 | 6-16 |
| Figure 6-6 | Inside, Axial Surface Flaws, .5" Above the Attachment Weld, Nozzle Uphill Side - Crack Growth Predictions for D. C. Cook Unit 1 | 6-17 |
| Figure 6-7 | Inside, Axial Surface Flaws, .5" Above the Attachment Weld, Nozzle Downhill Side - Crack Growth Predictions for D. C. Cook Unit 1..... | 6-18 |
| Figure 6-8 | Inside, Axial Surface Flaws, At the Attachment Weld, Head Vent, Nozzle Downhill Side - Crack Growth Predictions for D.C. Cook Unit 1..... | 6-19 |
| Figure 6-9 | Outside, Axial Surface Flaws, Below the Attachment Weld, Nozzle Uphill Side - Crack Growth Predictions for D. C. Cook Unit 1 | 6-20 |
| Figure 6-10 | Outside, Axial Surface Flaws, Below the Attachment Weld, Nozzle Downhill Side - Crack Growth Predictions for D. C. Cook Unit 1 | 6-21 |
| Figure 6-11 | Outside, Circumferential Surface Flaws, Along the Top of the Attachment Weld - Crack Growth Predictions for D. C. Cook Unit 1 (MRP Factor of 2.0 Included)..... | 6-22 |
| Figure 6-12 | Through-Wall Axial Flaws Located in the Center CRDM (0.0 Degrees) Penetration, Uphill and Downhill Side - Crack Growth Predictions for D. C. Cook Unit 1..... | 6-23 |

| | | |
|-------------|---|------|
| Figure 6-13 | Through-Wall Axial Flaws Located in the 26.2 Degrees Row of Penetrations, Uphill Side - Crack Growth Predictions for D.C. Cook Unit 1..... | 6-24 |
| Figure 6-14 | Through-Wall Axial Flaws Located in the 26.2 Degrees Row of Penetrations, Downhill Side - Crack Growth Predictions for D.C. Cook Unit 1 | 6-25 |
| Figure 6-15 | Through-Wall Axial Flaws Located in the 38.6 Degrees Row of Penetrations, Uphill Side - Crack Growth Predictions for D.C. Cook Unit 1..... | 6-26 |
| Figure 6-16 | Through-Wall Axial Flaws Located in the 38.6 Degrees Row of Penetrations, Downhill Side - Crack Growth Predictions for D. C. Cook Unit 1 | 6-27 |
| Figure 6-17 | Through-Wall Axial Flaws Located in the 44.3 Degrees Row of Penetrations, Uphill Side - Crack Growth Predictions for D.C. Cook Unit 1..... | 6-28 |
| Figure 6-18 | Through-Wall Axial Flaws Located in the 44.3 Degrees Row of Penetrations, Downhill Side - Crack Growth Predictions for D. C. Cook Unit 1 | 6-29 |
| Figure 6-19 | Through-Wall Axial Flaws Located in the 48.7 Degrees Row of Penetrations, Uphill Side - Crack Growth Predictions for D.C. Cook Unit 1..... | 6-30 |
| Figure 6-20 | Through-Wall Axial Flaws Located in the 48.7 Degrees Row of Penetrations, Downhill Side - Crack Growth Predictions for D. C. Cook Unit 1 | 6-31 |
| Figure 6-21 | Through-Wall Circumferential Flaws Near the Top of the Attachment Weld for CRDM Nozzle - Crack Growth Predictions for D. C. Cook Unit 1 (MRP Factor of 2.0 Included) | 6-32 |
| Figure 6-22 | Inside, Axial Surface Flaws, .5" Below the Attachment Weld, Nozzle Uphill Side - Crack Growth Predictions for D. C. Cook Unit 2 | 6-34 |
| Figure 6-23 | Inside, Axial Surface Flaws, .5" Below the Attachment Weld, Nozzle Downhill Side - Crack Growth Predictions for D. C. Cook Unit 2..... | 6-35 |
| Figure 6-24 | Inside, Axial Surface Flaws, At the Attachment Weld, Nozzle Uphill Side - Crack Growth Predictions for D. C. Cook Unit 2..... | 6-36 |
| Figure 6-25 | Inside, Axial Surface Flaws, At the Attachment Weld, Nozzle Downhill Side - Crack Growth Predictions for D. C. Cook Unit 2 | 6-37 |
| Figure 6-26 | Inside, Axial Surface Flaws, .5" Above the Attachment Weld, Nozzle Uphill Side - Crack Growth Predictions for D. C. Cook Unit 2 | 6-38 |
| Figure 6-27 | Inside, Axial Surface Flaws, .5" Above the Attachment Weld, Nozzle Downhill Side - Crack Growth Predictions for D. C. Cook Unit 2..... | 6-39 |

| | | |
|-------------|--|------|
| Figure 6-28 | Inside, Axial Surface Flaws, At the Attachment Weld, Head Vent, Nozzle Downhill Side - Crack Growth Predictions for D.C. Cook Unit 2..... | 6-40 |
| Figure 6-29 | Outside, Axial Surface Flaws, Below the Attachment Weld, Nozzle Uphill Side - Crack Growth Predictions for D. C. Cook Unit 2 | 6-41 |
| Figure 6-30 | Outside, Axial Surface Flaws, Below the Attachment Weld, Nozzle Downhill Side - Crack Growth Predictions for D. C. Cook Unit 2 | 6-42 |
| Figure 6-31 | Outside, Circumferential Surface Flaws, Along the Top of the Attachment Weld - Crack Growth Predictions for D. C. Cook Unit 2 (MRP Factor of 2.0 Included) | 6-43 |
| Figure 6-32 | Through-Wall Axial Flaws Located in the Center CRDM (0.0 Degrees) Penetration, Uphill and Downhill Side - Crack Growth Predictions for D. C. Cook Unit 2..... | 6-44 |
| Figure 6-33 | Through-Wall Axial Flaws Located in the 27.0 Degrees Row of Penetrations, Uphill Side - Crack Growth Predictions for D.C. Cook Unit 2..... | 6-45 |
| Figure 6-34 | Through-Wall Axial Flaws Located in the 27.0 Degrees Row of Penetrations, Downhill Side - Crack Growth Predictions for D.C. Cook Unit 2..... | 6-46 |
| Figure 6-35 | Through-Wall Axial Flaws Located in the 45.8 Degrees Row of Penetrations, Uphill Side - Crack Growth Predictions for D.C. Cook Unit 2..... | 6-47 |
| Figure 6-36 | Through-Wall Axial Flaws Located in the 45.8 Degrees Row of Penetrations, Downhill Side - Crack Growth Predictions for D. C. Cook Unit 2 | 6-48 |
| Figure 6-37 | Through-Wall Axial Flaws Located in the 47.0 Degrees Row of Penetrations, Uphill Side - Crack Growth Predictions for D.C. Cook Unit 2..... | 6-49 |
| Figure 6-38 | Through-Wall Axial Flaws Located in the 47.0 Degrees Row of Penetrations, Downhill Side - Crack Growth Predictions for D. C. Cook Unit 2 | 6-50 |
| Figure 6-39 | Through-Wall Axial Flaws Located in the 50.5 Degrees Row of Penetrations, Uphill Side - Crack Growth Predictions for D.C. Cook Unit 2..... | 6-51 |
| Figure 6-40 | Through-Wall Axial Flaws Located in the 50.5 Degrees Row of Penetrations, Downhill Side - Crack Growth Predictions for D. C. Cook Unit 2 | 6-52 |
| Figure 6-41 | Through-Wall Circumferential Flaws Near the Top of the Attachment Weld for CRDM Nozzle - Crack Growth Predictions for D. C. Cook Unit 2 (MRP Factor of 2.0 Included) ... | 6-53 |
| Figure 6-42 | Section XI Flaw Proximity Rules for Surface Flaws (Figure IWA-3400-1)..... | 6-54 |
| Figure 6-43 | Definition of "Circumferential" | 6-55 |

| | | |
|--------------|---|------|
| Figure 6-44 | Schematic of Head Penetration Geometry | 6-56 |
| Figure 6-45 | Example Problem 1 | 6-57 |
| Figure 6-46 | Example Problem 2 | 6-58 |
| Figure 6-47 | Example Problem 3 | 6-59 |
| Figure 6-48a | Example Problem 4 | 6-60 |
| Figure 6-48b | Example Problem 4 | 6-61 |
| Figure 6-49 | Example Problem 5 | 6-62 |
| Figure A-1 | Typical Head Penetration | A-3 |
| Figure A-2 | Allowable Regions of Lack of Fusion for the Outermost Penetration Tube to Weld Fusion Zone: Detailed View | A-4 |
| Figure A-3 | Allowable Regions of Lack of Fusion for the Outermost Penetration Tube to Weld Fusion Zone | A-5 |
| Figure A-4 | Allowable Regions of Lack of Fusion for all Penetrations: Weld to Vessel Fusion Zone..... | A-6 |
| Figure A-5 | Allowable Regions of Lack of Fusion for the Weld to Vessel Fusion Zone | A-7 |
| Figure B-1 | Hoop Stress Vs Distance from Bottom of Weld Plot for the Center CRDM Penetration. B-2 | |
| Figure B-2 | Hoop Stress Vs Distance from Bottom of Weld Plot for the 27.0 Degrees Row of Penetration (Uphill Side)..... | B-3 |
| Figure B-3 | Hoop Stress Vs Distance from Bottom of Weld Plot for the 27.0 Degrees Row of Penetration (Downhill Side)..... | B-4 |
| Figure B-4 | Hoop Stress Vs Distance from Bottom of Weld Plot for the 45.8 Degrees Row of Penetration (Uphill Side)..... | B-5 |
| Figure B-5 | Hoop Stress Vs Distance from Bottom of Weld Plot for the 45.8 Degrees Row of Penetration (Downhill Side)..... | B-6 |
| Figure B-6 | Hoop Stress Vs Distance from Bottom of Weld Plot for the 47.0 Degrees Row of Penetration (Uphill Side)..... | B-7 |
| Figure B-7 | Hoop Stress Vs Distance from Bottom of Weld Plot for the 47.0 Degrees Row of Penetration (Downhill Side)..... | B-8 |

| | | |
|------------|---|------|
| Figure B-8 | Hoop Stress Vs Distance from Bottom of Weld Plot for the 50.5 Degrees Row of Penetration (Uphill Side)..... | B-9 |
| Figure B-9 | Hoop Stress Vs Distance from Bottom of Weld Plot for the 50.5 Degrees Row of Penetration (Downhill Side)..... | B-10 |

1 INTRODUCTION

In September of 1991, a leak was discovered in the Reactor Vessel Control Rod Drive Mechanism (CRDM) head penetration region of an operating plant. This has led to the question of whether such a leak could occur at the D. C. Cook Units 1 and 2 CRDM or head vent nozzle penetrations. The geometry of interest is shown in Figure 1-1. Throughout this report, the penetration rows have been identified by their angle of intersection with the head. The locations of the Unit 1 and Unit 2 head penetrations are shown in Figures 1-2 and 1-3 respectively and the angles for each penetration are identified for Unit 1 and Unit 2 respectively in Tables 1-1 and 1-2.

The CRDM leak resulted from cracking in Alloy 600 base metal, which occurred in the outermost penetrations of a number of operating plants as discussed in Section 2. This outermost CRDM location, as well as a number of intermediate CRDM locations and the head vent were chosen for fracture mechanics analyses to support continued safe operation of D. C. Cook Units 1 and 2 if such cracking were to be found. The dimensions of the CRDM penetrations are identical for both Units, with a 4.00 inch Outside Diameter (OD) and a wall thickness of 0.625 inch [11A, 12A]. The head vent OD for Unit 1 is 1.050 inch and the wall thickness is 0.154 inch [11B]. The head vent OD for Unit 2 is 1.050 inch and the wall thickness is 0.218 inch [12B]. All of these dimensions are summarized in Table 6-2.

The basis of the analysis was a detailed three-dimensional elastic-plastic finite element stress analysis of several penetration locations, as described in detail in Section 5 and a fracture analysis as described in Section 6. The fracture analysis was carried out using crack growth rates recommended by the EPRI Materials Reliability Program (MRP-55 [4H]). These rates are consistent with service experience. The results are presented in the form of flaw tolerance charts for both surface and through wall flaws. If indications are found, the charts will determine the allowable service life of safe operation. The service life calculated in the flaw tolerance charts are all in Effective Full Power Years (EFPY). For the purposes of this report, a flaw is considered to be a linear indication attributed to Primary Water Stress Corrosion Cracking (PWSCC).

Note that there are several locations in this report where proprietary information has been bracketed and deleted. For each of the bracketed locations, reasons for proprietary classifications are given using a standardized system. The proprietary brackets are labeled with three different letters to provide this information. The explanation for each letter is given below:

- a. The information reveals the distinguishing aspects of a process or component, structure, tool, method, etc., and the prevention of its use by Westinghouse's competitors, without license from Westinghouse, gives Westinghouse a competitive economic advantage.
- c. The information, if used by a competitor, would reduce the competitor's expenditure of resources or improve the competitor's advantage in the design, manufacture, shipment, installation, assurance of quality, or licensing of a similar product.
- e. The information reveals aspects of past, present, or future Westinghouse or customer funded development plans and programs of potential commercial value to Westinghouse.

Two non-proprietary versions of WCAP-14118 were previously published as WCAP-15753. WCAP-15753 Rev. 0 and Rev. 1 were published as the non-proprietary versions of WCAP-14118 Rev. 4 and Rev. 5 respectively. No Prior versions of WCAP-14118-NP were published. This report, WCAP-14118-NP Rev. 1 is the first issue of WCAP-14118-NP and represents the non-proprietary version of WCAP-14118-P Rev. 7.

Record of Revisions

| Rev | Description |
|------------|--|
| 0 | The report was never published. |
| 1 | The report was never published. |
| 2 | The report was never published. |
| 3 | The report was never published. |
| 4 | The report was never published. |
| 5 | The report was never published. |
| 6 | The report was never published. |
| 7 | This is the first issue of WCAP-14118-NP based on WCAP-14118-P Revision 7. |

Table 1-1 D. C. Cook Unit 1 Head Penetration Nozzles with the Intersection Angles Identified

| Nozzle No. | Type [14A] | Angle (Degrees) | Nozzle No. | Type [14A] | Angle (Degrees) | Nozzle No. | Type [14A] | Angle (Degrees) |
|------------|------------|-----------------|------------|------------|-----------------|------------|------------|-----------------|
| 1 | TS | 0.0 | 28 | NS | 24.8 | 55 | TS | 35.1 |
| 2 | NS | 8.0 | 29 | NS | 24.8 | 56 | TS | 35.1 |
| 3 | NS | 8.0 | 30 | PL | 26.2 | 57 | TS | 35.1 |
| 4 | NS | 8.0 | 31 | PL | 26.2 | 58 | TS | 36.3 |
| 5 | NS | 8.0 | 32 | PLR | 26.2 | 59 | TS | 36.3 |
| 6 | TS | 11.4 | 33 | PL | 26.2 | 60 | TS | 36.3 |
| 7 | TS | 11.4 | 34 | PL | 26.2 | 61 | TS | 36.3 |
| 8 | TS | 11.4 | 35 | PL | 26.2 | 62 | TS | 38.6 |
| 9 | TS | 11.4 | 36 | PL | 26.2 | 63 | TS | 38.6 |
| 10 | TS | 16.2 | 37 | PL | 26.2 | 64 | TS | 38.6 |
| 11 | TS | 16.2 | 38 | TS | 30.2 | 65 | TS | 38.6 |
| 12 | TS | 16.2 | 39 | TS | 30.2 | 66 | TS | 38.6 |
| 13 | TS | 16.2 | 40 | TS | 30.2 | 67 | TS | 38.6 |
| 14 | TS | 18.2 | 41 | TS | 30.2 | 68 | TS | 38.6 |
| 15 | NS | 18.2 | 42 | TS | 30.2 | 69 | TS | 38.6 |
| 16 | TS | 18.2 | 43 | TS | 30.2 | 70 | TS | 44.3 |
| 17 | NS | 18.2 | 44 | TS | 30.2 | 71 | TS | 44.3 |
| 18 | TS | 18.2 | 45 | TS | 30.2 | 72 | TS | 44.3 |
| 19 | NS | 18.2 | 46 | TS | 33.9 | 73 | TS | 44.3 |
| 20 | TS | 18.2 | 47 | TS | 33.9 | 74 | TC | 48.7 |
| 21 | NS | 18.2 | 48 | TS | 33.9 | 75 | TC | 48.7 |
| 22 | TS | 23.3 | 49 | TS | 33.9 | 76 | TC | 48.7 |
| 23 | TS | 23.3 | 50 | TS | 35.1 | 77 | TC | 48.7 |
| 24 | TS | 23.3 | 51 | TS | 35.1 | 78 | TC | 48.7 |
| 25 | TS | 23.3 | 52 | TS | 35.1 | 79 | TC | 48.7 |
| 26 | NS | 24.8 | 53 | TS | 35.1 | | | |
| 27 | NS | 24.8 | 54 | TS | 35.1 | | | |

TS CRDM Penetration with Thermal Sleeve
 NS Non Sleeved Location
 PL Part Length Drive Location
 PLR Part length Removed Location
 TC Thermocouple Penetration

Table 1-2 D. C. Cook Unit 2 Head Penetration Nozzles with the Intersection Angles Identified

| Nozzle No. | Type [14B] | Angle (Degrees) | Nozzle No. | Type [14B] | Angle (Degrees) | Nozzle No. | Type [14B] | Angle (Degrees) |
|------------|------------|-----------------|------------|------------|-----------------|------------|------------|-----------------|
| 1 | TS | 0.0 | 27 | PL | 27.0 | 53 | TS | 37.5 |
| 2 | TS | 11.7 | 28 | PL | 27.0 | 54 | TS | 39.9 |
| 3 | TS | 11.7 | 29 | PL | 27.0 | 55 | TS | 39.9 |
| 4 | TS | 11.7 | 30 | TS | 31.1 | 56 | TS | 39.9 |
| 5 | TS | 11.7 | 31 | TS | 31.1 | 57 | TS | 39.9 |
| 6 | TS | 16.7 | 32 | TS | 31.1 | 58 | TS | 39.9 |
| 7 | TS | 16.7 | 33 | TS | 31.1 | 59 | TS | 39.9 |
| 8 | TS | 16.7 | 34 | TS | 31.1 | 60 | TS | 39.9 |
| 9 | TS | 16.7 | 35 | TS | 31.1 | 61 | TS | 39.9 |
| 10 | NS | 18.7 | 36 | TS | 31.1 | 62 | NS | 45.8 |
| 11 | NS | 18.7 | 37 | TS | 31.1 | 63 | NS | 45.8 |
| 12 | NS | 18.7 | 38 | TS | 35.0 | 64 | NS | 45.8 |
| 13 | NS | 18.7 | 39 | TS | 35.0 | 65 | NS | 45.8 |
| 14 | TS | 23.9 | 40 | TS | 35.0 | 66 | TS | 47.0 |
| 15 | TS | 23.9 | 41 | TS | 35.0 | 67 | TS | 47.0 |
| 16 | TS | 23.9 | 42 | TS | 36.2 | 68 | TS | 47.0 |
| 17 | TS | 23.9 | 43 | TS | 36.2 | 69 | TS | 47.0 |
| 18 | NS | 25.5 | 44 | TS | 36.2 | 70 | TS | 47.0 |
| 19 | NS | 25.5 | 45 | TS | 36.2 | 71 | TS | 47.0 |
| 20 | NS | 25.5 | 46 | TS | 36.2 | 72 | TS | 47.0 |
| 21 | NS | 25.5 | 47 | TS | 36.2 | 73 | TS | 47.0 |
| 22 | PL | 27.0 | 48 | TS | 36.2 | 74 | TC | 50.5 |
| 23 | PL | 27.0 | 49 | TS | 36.2 | 75 | TC | 50.5 |
| 24 | PLR | 27.0 | 50 | TS | 37.5 | 76 | TC | 50.5 |
| 25 | PL | 27.0 | 51 | TS | 37.5 | 77 | TC | 50.5 |
| 26 | PL | 27.0 | 52 | TS | 37.5 | 78 | TC | 50.5 |

TS CRDM Penetration with Thermal Sleeve
 NS Non Sleeved Location
 PL Part Length Drive Location
 PLR Part length Removed Location
 TC Thermocouple Penetration

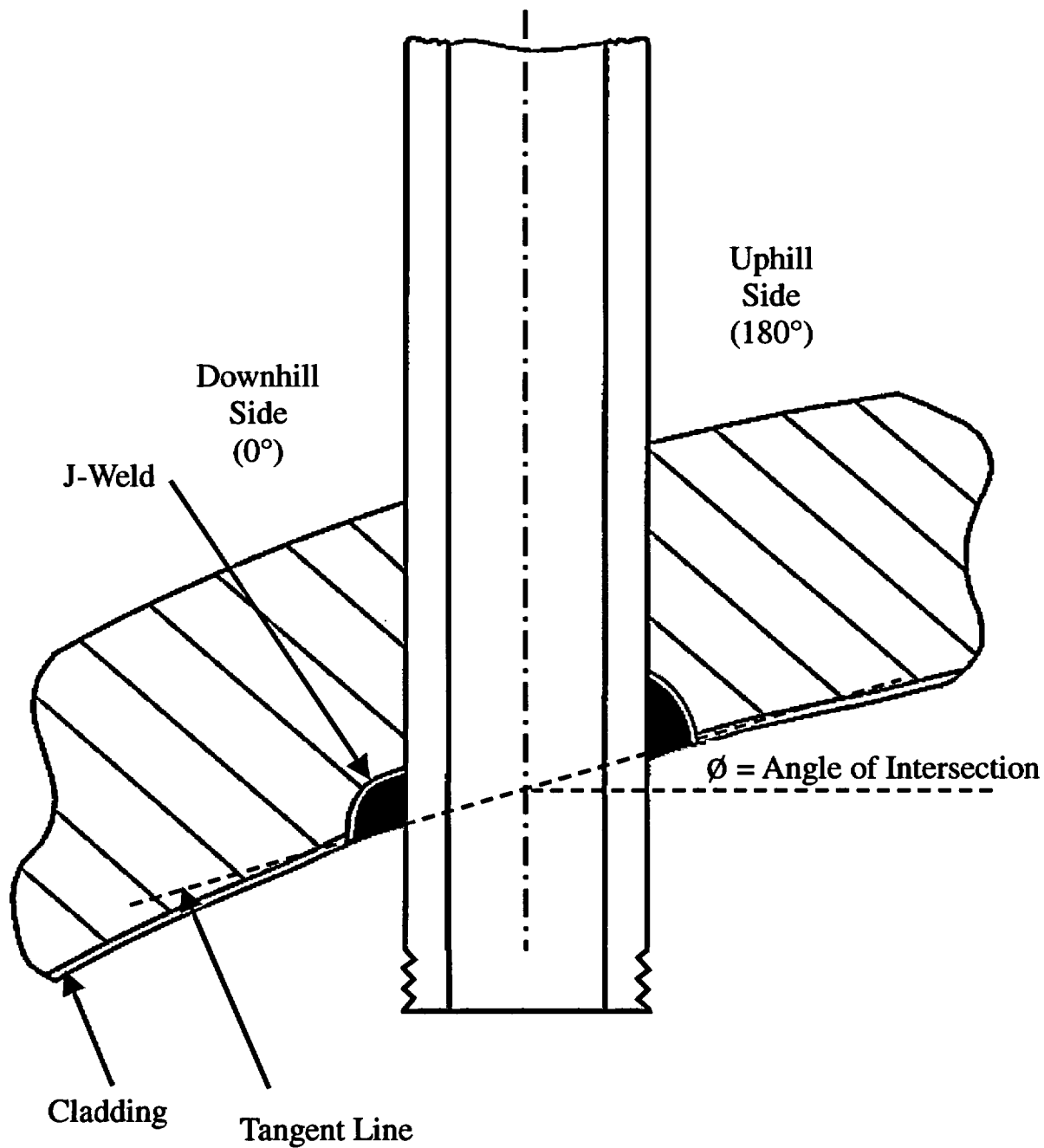


Figure 1-1 Reactor Vessel Control Rod Drive Mechanism (CRDM) Penetration

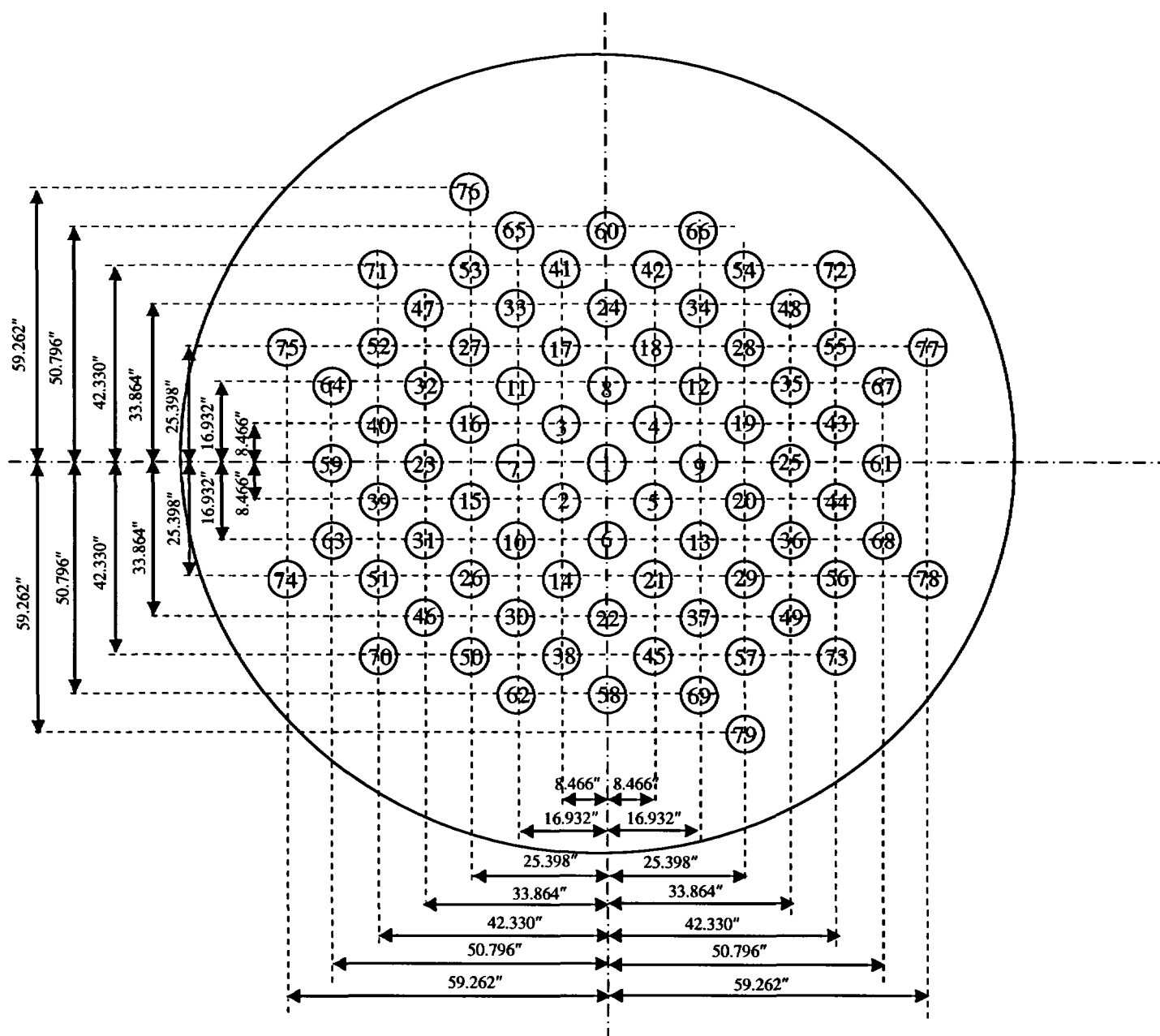


Figure 1-2 Location of Head Penetrations for D. C. Cook Unit 1 [11C]

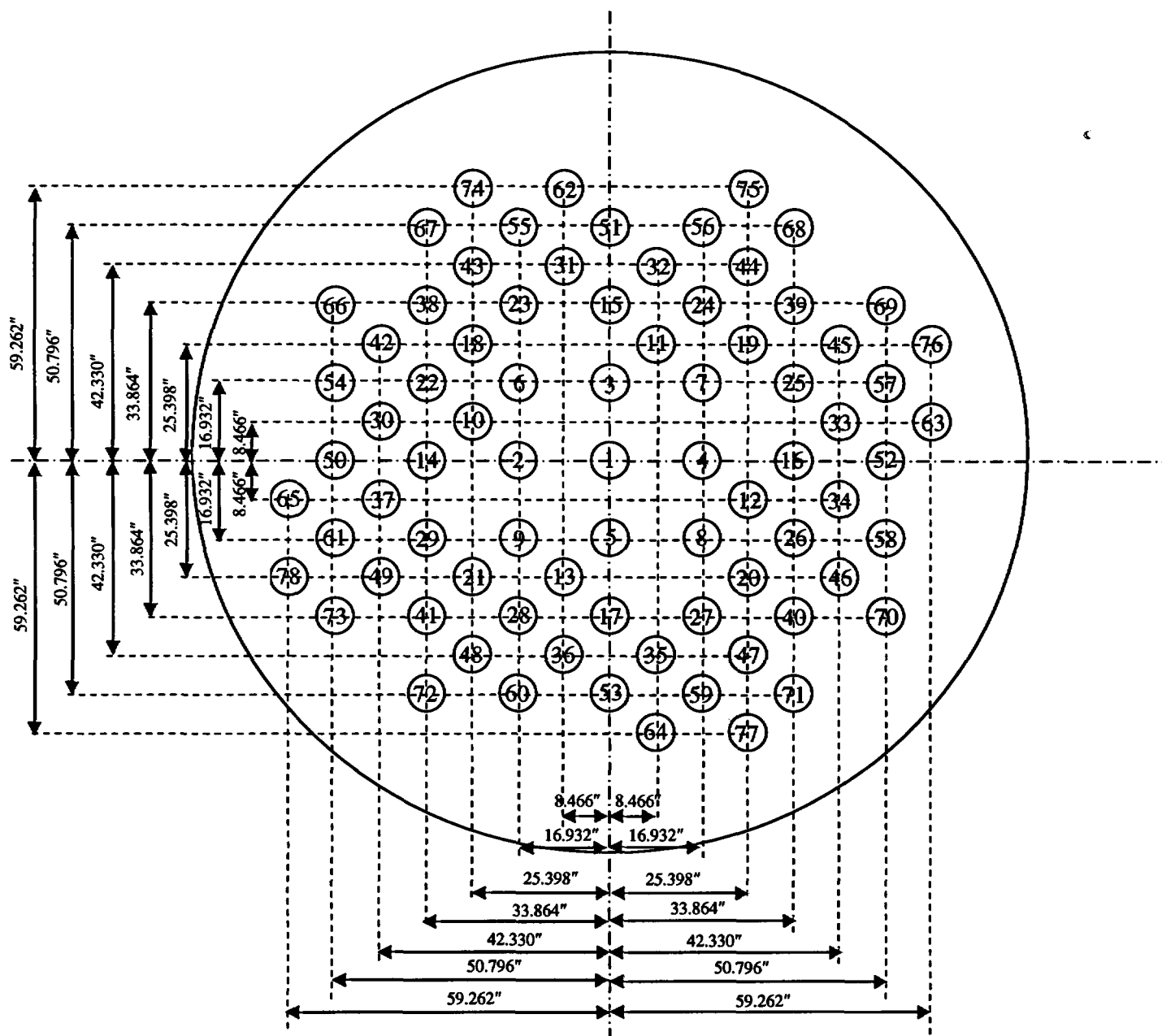


Figure 1-3 Location of Head Penetrations for D. C. Cook Unit 2 [12C]

2 HISTORY OF CRACKING IN HEAD PENETRATIONS

In September of 1991, leakage was reported from the reactor vessel CRDM head penetration region of a French plant, Bugey Unit 3. Bugey 3 is a 920 megawatt three-loop Pressurized Water Reactor (PWR) plant which had just completed its tenth fuel cycle. The leak occurred during a post ten year hydrotest conducted at a pressure of approximately 3000 psi (204 bar) and a temperature of 194°F (90°C). The leak was detected by metal microphones, which are located on the top and bottom heads. The leak rate was estimated to be approximately 0.7 liter/hour. The location of the leak was subsequently established on a peripheral penetration with an active control rod (H-14), as seen in Figure 2-1.

The control rod drive mechanism and thermal sleeve were removed from this location to allow further examination. A study of the head penetration revealed the presence of longitudinal cracks near the head penetration attachment weld. Penetrant and ultrasonic testing confirmed the cracks. The cracked penetration was fabricated from Alloy 600 bar stock (SB-166), and has an outside diameter of 4 inches (10.16 cm) and an inside diameter of 2.75 inches (7.0 cm).

As a result of this finding, all of the control rod drive mechanisms and thermal sleeves at Bugey 3 were removed for inspection of the head penetrations. Only two penetrations were found to have cracks, as shown in Figure 2-1.

An inspection of a sample of penetrations at three additional plants were planned and conducted during the winter of 1991-92. These plants were Bugey 4, Fessenheim 1, and Paluel 3. The three outermost rows of penetrations at each of these plants were examined, and further cracking was found in two of the three plants.

At Bugey 4, eight of the 64 penetrations examined were found to contain axial cracks, while only one of the 26 penetrations examined at Fessenheim 1 was cracked. The locations of all the cracked penetrations are shown in Figure 2-1. At the time, none of the 17 CRDM penetrations inspected at Paluel 3 showed indications of cracking, however subsequent inspections of the French plants have confirmed at least one crack in each operating plant.

Thus far, the cracking in reactor vessel heads not designed by Babcock and Wilcox (B&W) has been consistent in both its location and extent. All cracks discovered by nondestructive examination have been oriented axially, and have been located in the bottom portion of the penetration in the vicinity of the partial penetration attachment weld to the vessel head as shown schematically in Figure 1-1.

One small, outside diameter initiated, circumferential flaw was found during destructive examination at Bugey 3. The flaw was found to have resulted from Primary Water Stress Corrosion Cracking (PWSCC) as a consequence of leakage of the PWR water from an axial through-wall crack into the annulus between the penetration and head.

From the years 2000 through 2002, leaks were discovered in a total of 29 CRDM nozzles at seven Babcock & Wilcox designed plants:

- Oconee 1 (1 leaking nozzle)
- Oconee 2 (4 leaking nozzles)
- Oconee 3 (9 leaking nozzles)
- ANO-1 (1 leaking nozzle)
- Crystal River Unit 3 (1 leaking nozzle)
- Three Mile Island 1 (5 leaking nozzles)
- Davis Besse (8 leaking nozzles)

In addition, five of the eight smaller diameter thermocouple nozzles at Oconee 1, and all eight at Three Mile Island 1, were discovered to have leaks. All of these leaks were first detected during visual inspections of the top surface of the vessel heads for boric acid crystal deposits. In all cases, except Davis Besse, the quantity of boric acid crystals at each nozzle location was small ($<1 \text{ in}^3$).

Destructive examinations of several specimens from cracked Oconee 1 and 3 nozzles showed that the leaks were the result of Primary Water Stress Corrosion Cracking (PWSCC).

Non-destructive examinations of the leaking CRDM nozzles showed that most of the cracks were axially oriented, originating on the outside surface of the nozzles below the J-groove weld and propagating primarily in the nozzle base material to an elevation above the top of the J-groove weld. Leakage could then pass through the annulus to the top of the head where it was detected by visual inspection. In some cases the cracks initiated in the weld metal or propagated into the weld metal, and in a few cases the cracks propagated through the nozzle wall thickness to the inside surface.

In addition to the predominantly axial cracks, several nozzles had cracks on the outside surface of the nozzle approximately following the weld contour above or below the J-groove weld. At least eight of these nozzles (three in Oconee 3, one in Oconee 2, one in Crystal River 3, and three in Davis Besse) were found to have cracks approximately following the weld contour just above the J-groove weld. Two of the nozzles had relatively short and shallow cracks. Two of these nozzles had cracks either through-wall or essentially through-wall over an arc length of about 165° around the nozzle centered approximately about the nozzle uphill side. Cracks which follow the weld contour are a greater concern than axial cracks because there is a potential for a control rod to be ejected if a circumferential crack extends completely around the nozzle above the attachment weld. Plastic limit load failure would be the failure mode if the circumferential crack extends more than about 92% around the nozzle circumference.

Seventeen additional non-leaking Oconee 1 and nine non-leaking Oconee 3 CRDM nozzles were inspected by eddy current, ultrasonic testing, or eddy current and ultrasonic testing to assess the extent of the condition of non-leaking nozzles in the vessel head. No significant cracking was found in any of these additional nozzles.

The recent experience at Oconee, Three Mile Island, Crystal River, Davis Besse, and ANO-1 differs from previous industry experience in that the cracking appears to initiate primarily on the outside surface of the nozzle below the weld rather than on the nozzle Inside Diameter (ID) surface. Five of the nozzles had also developed OD-initiated flaws approximately following the contour of the top of the J-groove weld. These CRDM tubes have shown no pattern of cracking, whereas the previous CRDM tubes were cracking only in the outermost three rows.

The cracking has now been confirmed to be primary water stress corrosion cracking. Relatively high residual stresses are produced in the outermost CRDM penetrations due to the welding process. Other important factors which affect this process are temperature and time, with higher temperatures and longer times being more detrimental. The inspection findings for the plants examined through April 30th, 2002 are summarized in Table 2-1.

Table 2-1 Operational Information and Inspection Results for Units Examined (Results through April 30, 2002)

| Country | Plant Type | Units Inspected | K Hours | Head Temp. (°F) | Total Penetrations | Penetrations Inspected | Penetrations With Indications |
|--------------|------------|-----------------|---------|-----------------|--------------------|------------------------|-------------------------------|
| France | CPO | 6 | 80-107 | 596-599 | 390 | 390 | 23 |
| | CPY | 28 | 42-97 | 552 | 1820 | 1820 | 126 |
| | 1300MW | 20 | 32-51 | 558-597 | 1542 | 1542 | 95 |
| Sweden | 3 Loop | 3 | 75-115 | 580-606 | 195 | 190 | 8 |
| Switzerland | 2 Loop | 2 | 148-154 | 575 | 72 | 72 | 2 |
| Japan | 2 Loop | 7 | 105-108 | 590-599 | 276 | 243 | 0 |
| | 3 Loop | 7 | 99 | 610 | 455 | 398 | 0 |
| | 4 Loop | 3 | 46 | 590 | 229 | 193 | 0 |
| Belgium | 2 Loop | 2 | 115 | 588 | 98 | 98 | 0 |
| | 3 Loop | 5 | 60-120 | 554-603 | 337 | 337 | 6 |
| Spain | 3 Loop | 5 | 65-70 | 610 | 325 | 102 | 0 |
| Brazil | 2 Loop | 1 | 25 | NA | 40 | 40 | 0 |
| South Africa | 3 Loop | 1 | NA | NA | 65 | 65 | 6 |
| Slovenia | 2 Loop | 1 | NA | NA | 49 | 49 | 0 |
| South Korea | 2 Loop | 3 | NA | NA | 49 | 49 | 3 |
| | 3 Loop | 2 | NA | NA | 130 | 130 | 2 |
| US | 2 Loop | 2 | 170 | 590 | 98 | 98 | 0 |
| | 3 Loop | 1 | NA | NA | 65 | 20 | 12 |
| | 4 Loop | 18 | NA | NA | 1149 | 537 | 35 |
| TOTALS | | 117 | – | – | 7384 | 6373 | 318 |

NA = Not Available.

Note: CPY and CPO are both 900 MW reactors.

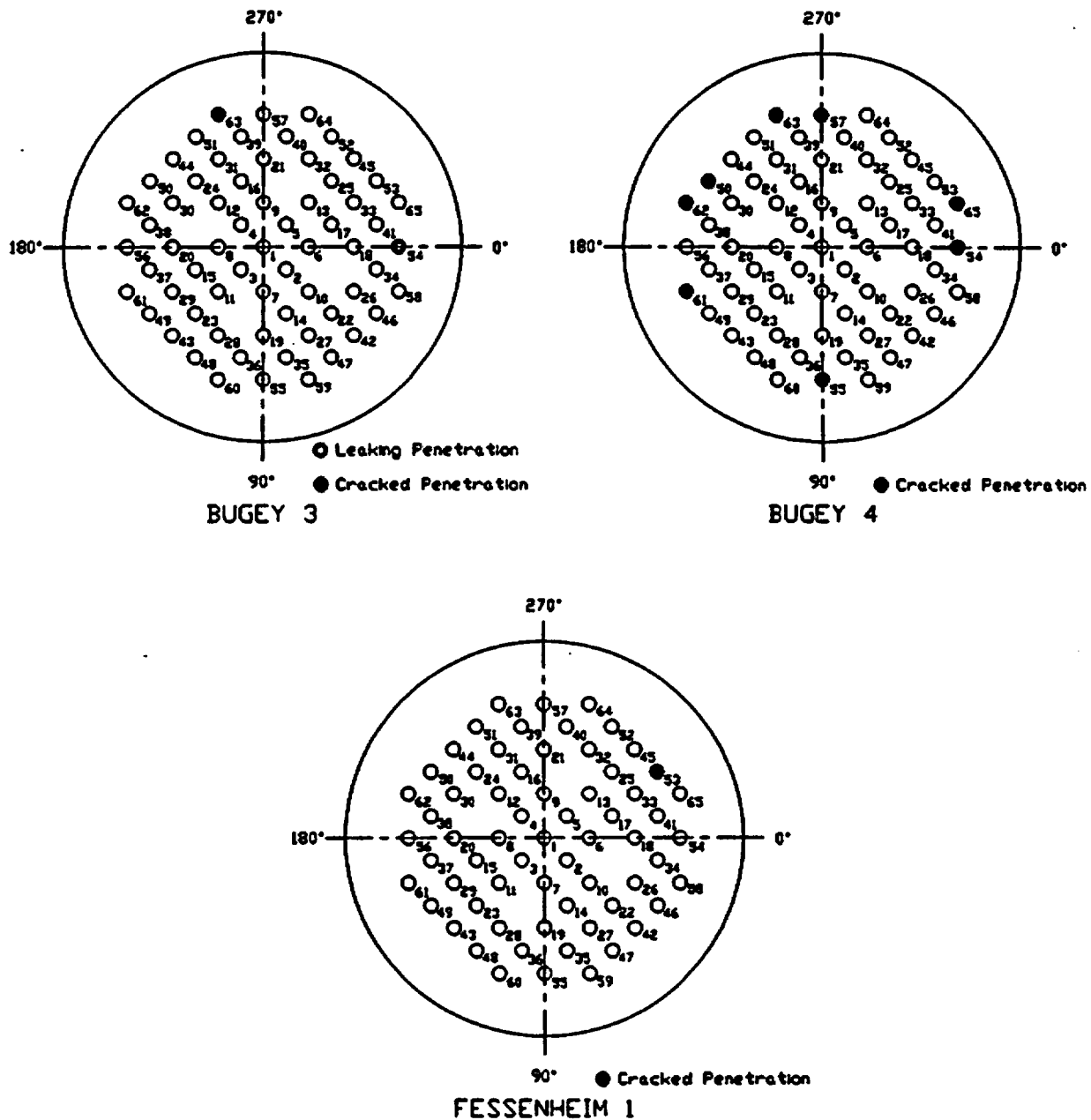


Figure 2-1 EDF Plant R/V Closure Head CRDM Penetrations – Penetrations with Cracking

3 OVERALL TECHNICAL APPROACH

The primary goal of this work is to provide technical justification for the continued safe operation of D. C. Cook Units 1 and 2 in the event that cracking is discovered during in-service inspections of the Alloy 600 reactor vessel upper head penetrations.

3.1 PENETRATION STRESS ANALYSIS

Three-dimensional elastic-plastic finite element stress analyses were performed using ANSYS computer code to determine the stresses in the head penetration region [6A, 6B]. These analyses have considered the normal operating temperature and pressure loads associated with normal operation, as well as the residual stresses that are produced by the fabrication process.

Detailed finite element stress analyses have been carried out for a number of rows of penetrations, including those nearest the head flange, which is the region where cracking has been discovered in other non-B&W design plants. In addition, an analysis has been completed for several other rows of penetrations and the center CRDM penetrations to provide additional results, so a trend can be established as a function of radial location. The head vent was also analyzed. The calculated stresses as well as field-measured deformation have been found to be more severe at the outermost location. The stress analysis will be used to provide input directly to the crack growth analysis.

The stress analysis provides the key input to the flaw tolerance evaluation, which is described below.

3.2 FLAW TOLERANCE APPROACH

A flaw tolerance approach has been developed to allow continued safe operation until an appropriate time for repair, or the end of plant life. The approach is based on the prediction of future growth of detected flaws, to ensure that such flaws would remain stable.

If an indication is discovered during in-service inspection, its size can be compared with the flaw size considered as allowable for continued service. This "allowable" flaw size is determined from the actual loading (including mechanical and residual loads) on the head penetration for D.C. Cook Units 1 and 2. Acceptance criteria are discussed in Section 6.5.

The time for the observed crack to reach the allowable crack size determines the length of time the plant can remain online before repair, if required. For the crack growth calculation, a best estimate is needed and no additional margins are necessary.

The results of the evaluation are presented in terms of simple flaw tolerance charts. The charts graphically show the time required to reach the allowable length or depth, which represents additional service life before repair. This result is a function of the loading on the particular head penetration as well as the circumferential location of the crack in the penetration nozzle.

Schematic drawings of the head penetration flaw tolerance charts are presented as Figures 3-1 and 3-2. These two types of charts can be used to provide estimates of the remaining service life before a leak would develop from an observed crack. For example, if a part-through flaw was discovered, the user would first refer to Figure 3-1, to determine the time (t_p) which would be remaining before the crack would penetrate the wall or reach the allowable depth (t_a) (e.g. $a/t = 0.75$). Once the crack penetrates the wall, the time (t_B) required to reach an allowable crack length would be determined from Figure 3-2. The total time remaining would then be the simple sum:

$$\text{Time remaining} = t_p + t_B$$

Another way to determine the allowable time of operation with a part-through flaw would be to use Figure 3-2 directly, in effect assuming the part-through flaw is a through-wall flaw. This approach would be more conservative than that above, and the time remaining would then be:

$$\text{Time remaining} = t_B$$

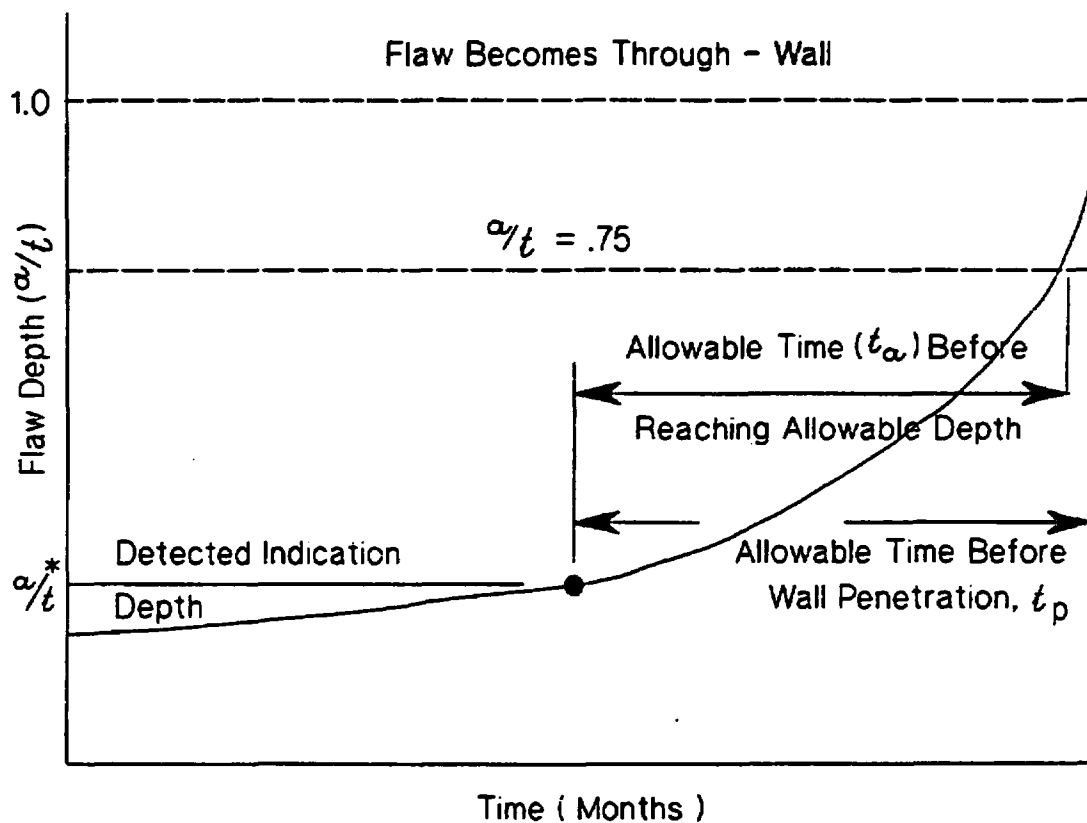


Figure 3-1 Schematic of a Head Penetration Flaw Growth Chart for Part-Through Flaws

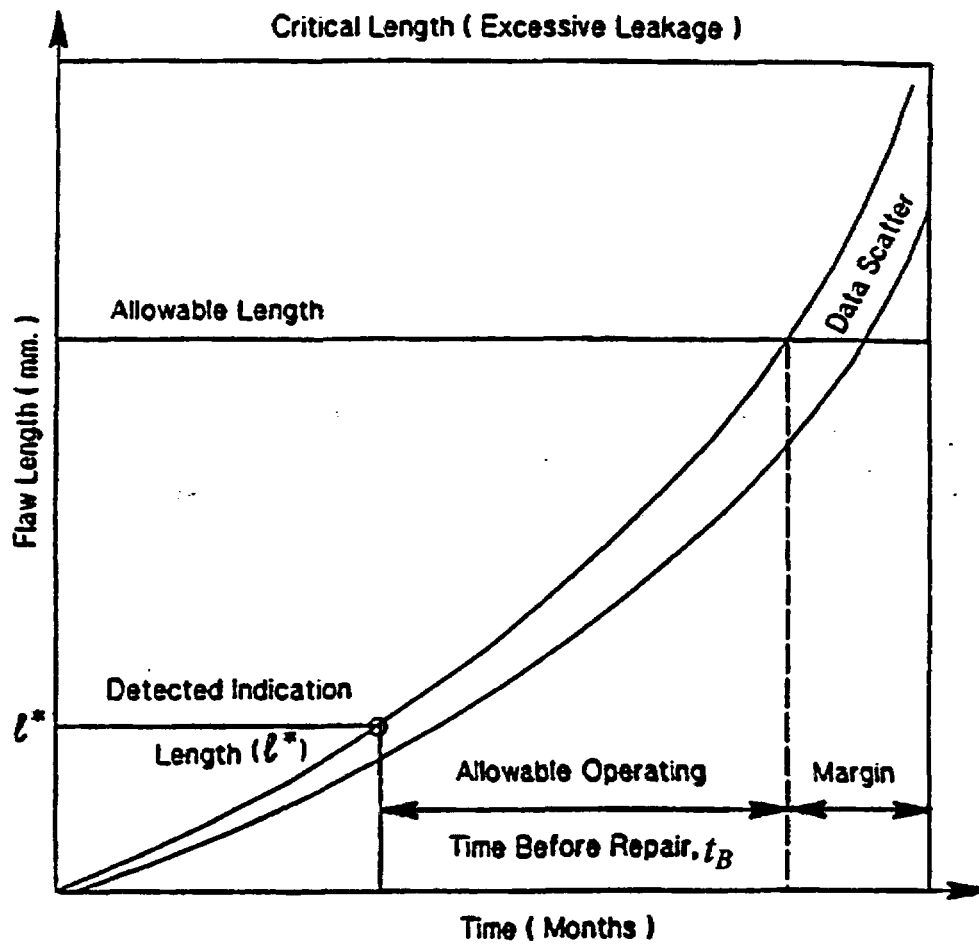


Figure 3-2 Schematic of a Head Penetration Flaw Tolerance Chart for Through-Wall Flaws

4 MATERIAL PROPERTIES, FABRICATION HISTORY AND CRACK GROWTH PREDICTION

4.1 MATERIALS AND FABRICATION

The head adapters for D. C. Cook Units 1 & 2 were manufactured by Westinghouse from material produced by Huntington Alloys in the USA. The carbon content and mechanical properties of the Alloy 600 material used to fabricate the D.C. Cook Units 1 & 2 vessels are provided in Tables 4-1 and 4-2. The material CMTRs were used to obtain the chemistry and mechanical properties for the vessel head penetrations. The CMTRs for the material do not indicate the heat treatment of the material. However, Westinghouse records indicate that the materials were annealed for one hour at a temperature of 1700°F-1800°F, followed by a water quench. Note that all Unit 1 CRDMs were air-cooled and water quenching was for Unit 2 only. Figures 4-1 and 4-2 illustrate the yield strengths and carbon content based on percent of heats of the head adapter penetrations in the D. C. Cook Units 1 & 2 vessels relative to a sample of the French head adapters that have experienced cracking. The general trend for the head adapter penetrations in D. C. Cook Units 1 & 2 is of a higher carbon content, higher mill annealing temperature, and lower yield strength relative to those on the French vessels. These factors should all have a beneficial effect on the material resistance to PWSCC in the head penetrations.

4.2 CRACK GROWTH PREDICTION

The cracks in the penetration region have been determined to result from primary water stress corrosion cracking in the Alloy 600 base metal and, in some cases, the Alloy 182 weld metal. There are a number of available measurements of static load crack growth rates in primary water environment, and in this section the available results will be compared and a representative growth rate established.

Direct measurements of Stress Corrosion Cracking (SCC) growth rates in Alloy 600 are relatively rare. Also, care should be used when interpreting the results because the materials may be excessively cold worked, or the loading applied may be near or exceeding the limit load of the penetration nozzle, meaning there will be an interaction between tearing and crack growth. In these cases the crack growth rates may not be representative of service conditions.

The effort to develop a reliable crack growth rate model for Alloy 600 began in the spring of 1992, when the Westinghouse Owners Group began to develop a safety case to support continued operation of plants. At the time, there was no available crack growth rate data for head penetration materials, and only a few publications existed on growth rates of Alloy 600 in any product form.

The best available publication at that time was that of Peter Scott of Framatome, who had developed a growth rate model for PWR steam generator materials [1]. His model was based on a study of results obtained by McIlree, Rebak and Smialowska [2] who had tested short steam generator tubes which had been flattened into thin compact specimens.

An equation was fitted to the data of reference [2] for the results obtained in water chemistries that fell within the standard specification for PWR primary water. Results for chemistries outside the specification were not used. The following equation was fitted to the data at 330°C (626°F):

$$\frac{da}{dt} = 2.8 \times 10^{-11} (K - 9)^{1.16} \text{ m/sec} \quad (4-1)$$

where:

K is in MPa $\sqrt{\text{m}}$

The next step was to correct these results for the effects of cold work. Based on work by Cassagne and Gelpi [3], Scott concluded that dividing the above equation by a factor of 10 would be appropriate to account for the effects of cold work. The crack growth law for 330°C (626°F) then becomes:

$$\frac{da}{dt} = 2.8 \times 10^{-12} (K - 9)^{1.16} \text{ m/sec} \quad (4-2)$$

Scott further corrected this law for the effects of temperature. This forms the basis for the PWR Materials Reliability Program (MRP) recommended crack growth rate (CGR) curve for the evaluation of SCC where a power-law dependence on stress intensity factor was assumed [4H]. The MRP recommended CGR curve was used in this report for determining the primary water stress corrosion crack growth rate and a brief discussion on this recommended curve is as follows:

The EPRI-MRP crack growth review team, an international panel of experts in the area of SCC crack growth, provided input to the MRP in its development of the recommended CGR curve. This group met to review the available worldwide data on October 2-4, 2001, in Airlie, Virginia. The PWR Materials Reliability Program (MRP) has developed a recommended crack growth rate (CGR) curve for primary water stress corrosion cracking (PWSCC) of Alloy 600 materials. The recommended CGR curve is based on controlled testing of fracture mechanics specimens conducted at several laboratories. Such testing allows careful control of applied load (stress intensity factor) and temperature and also allows accurate measurement of CGR. The MRP recommends that this curve be applied to the growth evaluations of SCC flaws in Alloy 600 materials exposed to the primary water environment.

The most likely environments responsible for SCC of Alloy 600 materials in the annulus between a penetration and the reactor upper head as a result of a through-wall or through-weld leak are either hydrogenated, superheated steam or normal PWR primary water. MRP recommends that a multiplicative factor of 2.0 increasing the CGR be considered for evaluating the growth of hypothetical circumferential flaws connected to the Outside Diameter (OD) of the reactor vessel head penetration nozzles above the elevation of the J-groove weld due to the uncertainties in the exact composition of the chemical environment in contact with the nozzle OD.

The MRP is continuing its review of the available data regarding SCC crack growth in Alloy 600 components exposed to the primary water environment, and revised recommendations will be provided to the industry in the future as warranted.

There is a general agreement that crack growth in Alloy 600 materials in the primary water environment can be modeled using a power-law dependence on stress intensity factor with differences in temperature accounted for by an activation energy (Arrhenius) model for thermally controlled processes. Figure 4-3 shows the recommended CGR curve along with the laboratory data from Huntington materials used to develop the curve.

[

$J^{a,c,e}$

[

 $J^{a,c,e}$

The applicability of the MRP recommended model to head penetrations was recently confirmed by two independent approaches. The first was a collection of all available data from Standard Steel and Huntington Alloys materials tested over the past ten years [4H]. The results are shown in Figure 4-3, along with the Scott model for the test temperature.

The MRP crack growth curve was structured to bound 75 percent of the 26 heats for which test results were available. Fits were done on the results for each heat, and the constant term was determined for each heat. This was done to eliminate the concern that the curve might be biased from a large number of results from a single heat. The 75th percentile was then determined from these results. The MRP expert panel on crack growth endorsed the resulting curve unanimously in a meeting on March 6th and 7th 2002. This approach is consistent with the ASME Section XI flaw evaluation philosophy, which is to make a best estimate prediction of future growth of a flaw. Margins are incorporated in the allowable flaw sizes. The entire data set is shown in Figure 4-3, where the data have been adjusted to a single temperature of 325°C.

A second independent set of data were used to validate the model, and these data were obtained from the two inspections carried out on penetration no. 75 of D. C. Cook Unit 2, which was first found to be cracked in 1994 [4G]. The plant operated for one fuel cycle before the penetration was repaired in 1996 and the flaw was measured again before being repaired. These results were used to estimate the PWSCC growth rate for both the length of the flaw and its depth. These two points are also shown in Figure 4-4, and are consistent with the laboratory data for Huntington materials. In fact, Figure 4-4 demonstrates that the MRP model is nearly an upper bound for these materials. The D. C. Cook Unit 2 penetrations were made from Huntington materials.

Since D. C. Cook Units 1 and 2 operates at a temperature of 303°C (578°F) and 316°C (601°F) in the head region [9] respectively, and the crack growth rate is strongly affected by temperature, a temperature adjustment is necessary. This temperature correction was obtained from study of both laboratory and field data for stress corrosion crack growth rates for Alloy 600 in primary water environments. The available data showing the effect of temperature are summarized in Figure 4-5. Most of the results shown here are from steam generator tube materials, with several

sets of data from operating plants, and results from two heats of materials tested in a laboratory [4A].

Study of the data shown in Figure 4-5 results in an activation energy of 31-33 Kcal/mole, which can then be used to adjust for the lower operating temperature. This value is slightly lower than the generally accepted activation energy of 44-50 Kcal/mole used to characterize the effect of temperature on crack initiation, but the trend of the actual data for many different sources is unmistakable.

[

^{a,c,e} Therefore the following crack growth rate model was used for the D. C. Cook Units 1 and 2 head penetrations for crack growth in all the cases analyzed.

$$\frac{da}{dt} = 1.00 \times 10^{-12} (K - 9)^{1.16} \text{ m/sec} \quad (\text{Unit 1})$$

$$\frac{da}{dt} = 1.80 \times 10^{-12} (K - 9)^{1.16} \text{ m/sec} \quad (\text{Unit 2})$$

where:

K = applied stress intensity factor, in $\text{MPa}\sqrt{\text{m}}$

This equation implies a threshold for cracking susceptibility, $K_{\text{ISCC}} = 9 \text{ MPa}\sqrt{\text{m}}$. The crack growth rate is applicable to propagation in both axial and circumferential directions.

Table 4-1 D. C. Cook Unit 1 R/V Head Adapter Material Information

| HT. No. | | C | Mn | Fe | S | Si | Cu | Ni | Cr | Co | YS (ksi) | UTS (ksi) | Mtl. Spec | Vendor | Heat Treatment |
|---------|-------|-------|------|------|-------|------|------|-------|-------|------|-------------|--------------|--------------|------------|-----------------------------|
| NX-7926 | Ladle | 0.07 | 0.37 | 7.51 | 0.009 | 0.3 | 0.16 | 76.18 | 15.38 | 0.05 | 35.5 | 94.5 | SB-167 | Huntington | 1725F 1.5hr – Air Cooled |
| | Check | 0.072 | 0.37 | 7.47 | 0.009 | 0.38 | 0.15 | 74.83 | 15.7 | 0.03 | | | | | |
| NX-7280 | Ladle | 0.07 | 0.13 | 8.19 | 0.007 | 0.2 | 0.11 | 76.32 | 14.95 | 0.05 | 40.5 | 98.5 | SB-167 | Huntington | 1725F 1.5hr – Air Cooled |
| | Check | 0.08 | 0.14 | 8.26 | 0.006 | 0.26 | 0.11 | 75.15 | 15.1 | 0.03 | | | | | |
| NX-8069 | Ladle | 0.06 | 0.25 | 8.1 | 0.007 | 0.29 | 0.18 | 76.1 | 14.99 | 0.08 | 58.5 | 98 | SB-167 | Huntington | 1725F 1.5hr – Air Cooled |
| | Check | 0.061 | 0.25 | 8.21 | 0.004 | 0.32 | 0.15 | 74.14 | 14.9 | 0.08 | | | | | |
| NX-8251 | Ladle | 0.06 | 0.3 | 7.69 | 0.007 | 0.28 | 0.16 | 76.16 | 15.32 | 0.05 | 35 | 94.5 | SB-167 | Huntington | 1725F 1.5hr – Air Cooled |
| | Check | 0.056 | 0.29 | 7.73 | 0.007 | 0.3 | 0.15 | 74.89 | 15.2 | 0.04 | | | | | |
| NX-7760 | Ladle | 0.06 | 0.16 | 8.2 | 0.007 | 0.3 | 0.15 | 74.83 | 16.27 | 0.06 | 38 | 97.5 | SB-167 | Huntington | 1725F 1.5hr – Air Cooled |
| | Check | 0.062 | 0.18 | 8.01 | 0.003 | 0.33 | 0.14 | 74.86 | 16.32 | 0.05 | | | | | |

Table 4-2 D. C. Cook Unit 2 R/V Head Adapter Material Information

| HT. No. | | C | Mn | Fe | S | Si | Cu | Ni | Cr | Co | YS (ksi) | UTS (ksi) | Mtl. Spec | Vendor | Heat Treatment |
|---------|-------|------|------|------|-------|------|------|-------|-------|------|-------------|-----------------|--------------|--------------|--|
| NX-0215 | Ladle | 0.07 | 0.22 | 8.64 | 0.007 | 0.25 | 0.22 | 75.21 | 15.36 | 0.07 | 51.0 | 103.0 | SB-166 | Westinghouse | 1700F or 1800F 1 hr / Water Quenched |
| | Check | 0.07 | 0.21 | 8.47 | 0.002 | 0.32 | 0.24 | 74.66 | 15.17 | 0.06 | | | | | |
| NX-0216 | Ladle | 0.09 | 0.24 | 8.53 | 0.007 | 0.21 | 0.22 | 75.11 | 15.57 | 0.06 | 57.0 | 107.0 | SB-166 | Westinghouse | 1700F or 1800F 1 hr / Water Quenched |
| | Check | 0.07 | 0.23 | 8.36 | 0.002 | 0.28 | 0.22 | 74.53 | 15.35 | 0.05 | | | | | |
| NX-0218 | Ladle | 0.08 | 0.28 | 9.02 | 0.008 | 0.19 | 0.28 | 74.31 | 15.81 | 0.06 | 51.0 | 102.0 | SB-166 | Westinghouse | 1700F or 1800F 1 hr / Water Quenched |
| | Check | 0.09 | 0.27 | 8.65 | 0.003 | 0.27 | 0.29 | 74.06 | 15.60 | 0.05 | | | | | |
| NX-0219 | Ladle | 0.06 | 0.24 | 8.76 | 0.007 | 0.18 | 0.22 | 75.0 | 15.51 | 0.07 | 41.0 | 100.0 | SB-166 | Westinghouse | 1700F or 1800F 1 hr / Water Quenched |
| | Check | 0.05 | 0.23 | 8.56 | 0.003 | 0.23 | 0.23 | 74.50 | 15.25 | 0.06 | | | | | |
| NX-0223 | Ladle | 0.07 | 0.31 | 8.5 | 0.007 | 0.29 | 0.17 | 75.29 | 15.34 | 0.07 | 63.0 | 104.0 | SB-166 | Westinghouse | 1700F or 1800F 1 hr / Water Quenched |
| | Check | 0.08 | 0.31 | 8.37 | 0.002 | 0.36 | 0.19 | 74.31 | 15.33 | 0.06 | | | | | |
| NX-0230 | Ladle | 0.06 | 0.18 | 8.69 | 0.007 | 0.18 | 0.17 | 75.5 | 15.09 | 0.04 | 58/56 | 101.0/ 100.0 | SB-166 | Westinghouse | 1700F or 1800F 1 hr / Water Quenched |
| | Check | 0.03 | 0.19 | 8.54 | 0.002 | 0.23 | 0.19 | 74.81 | 15.04 | 0.04 | | | | | |
| NX-0233 | Ladle | 0.06 | 0.18 | 7.93 | 0.007 | 0.26 | 0.14 | 76.17 | 15.23 | 0.05 | 58/44 | 101.0/ 100.0 | SB-166 | Westinghouse | 1700F or 1800F 1 hr / Water Quenched |
| | Check | 0.04 | 0.18 | 7.85 | 0.003 | 0.30 | 0.16 | 75.44 | 15.09 | 0.04 | | | | | |

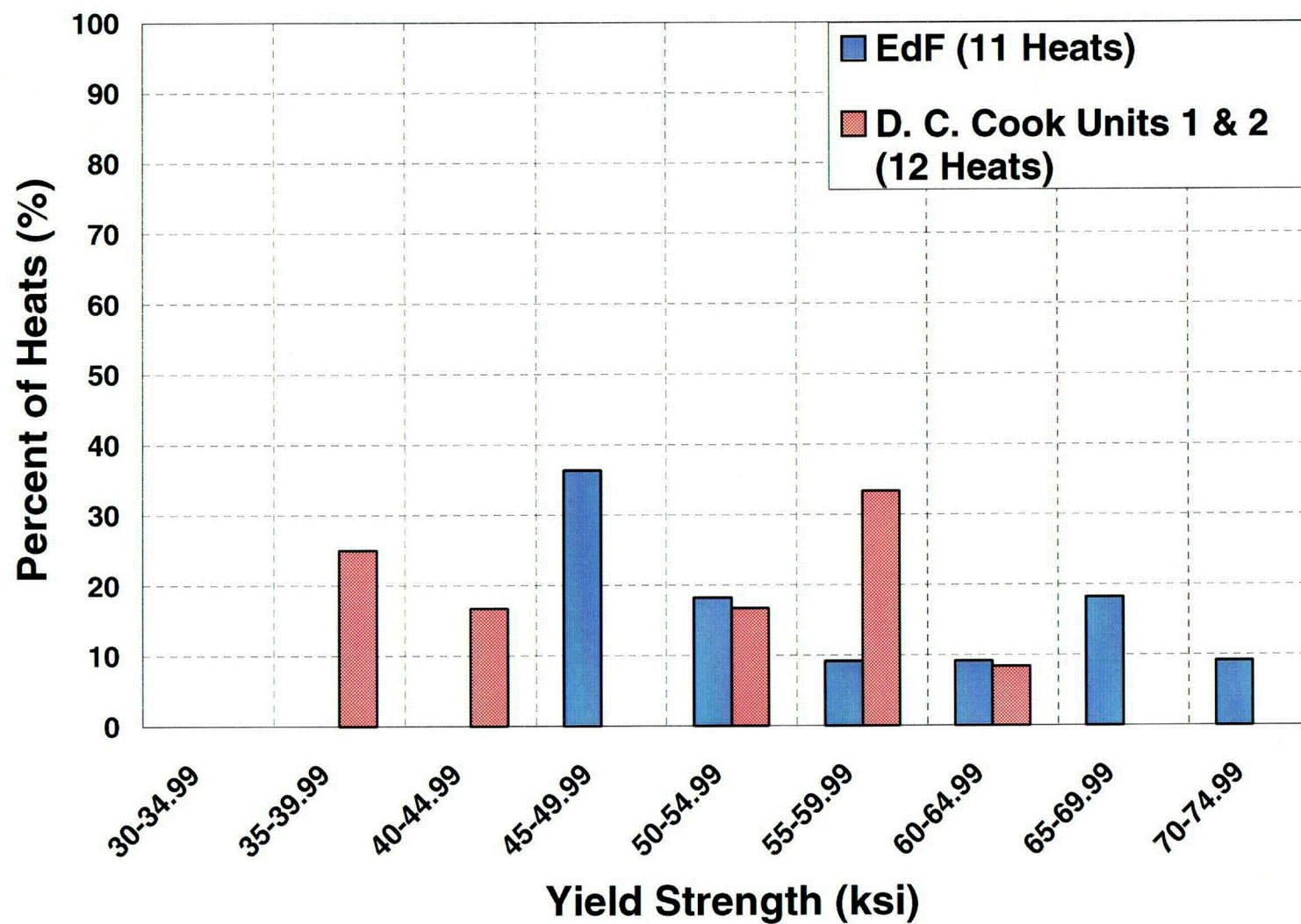


Figure 4-1 Yield Strength of the Various Heats of Alloy 600 Used in Fabricating the D. C. Cook Units 1 & 2 and French Head Penetrations

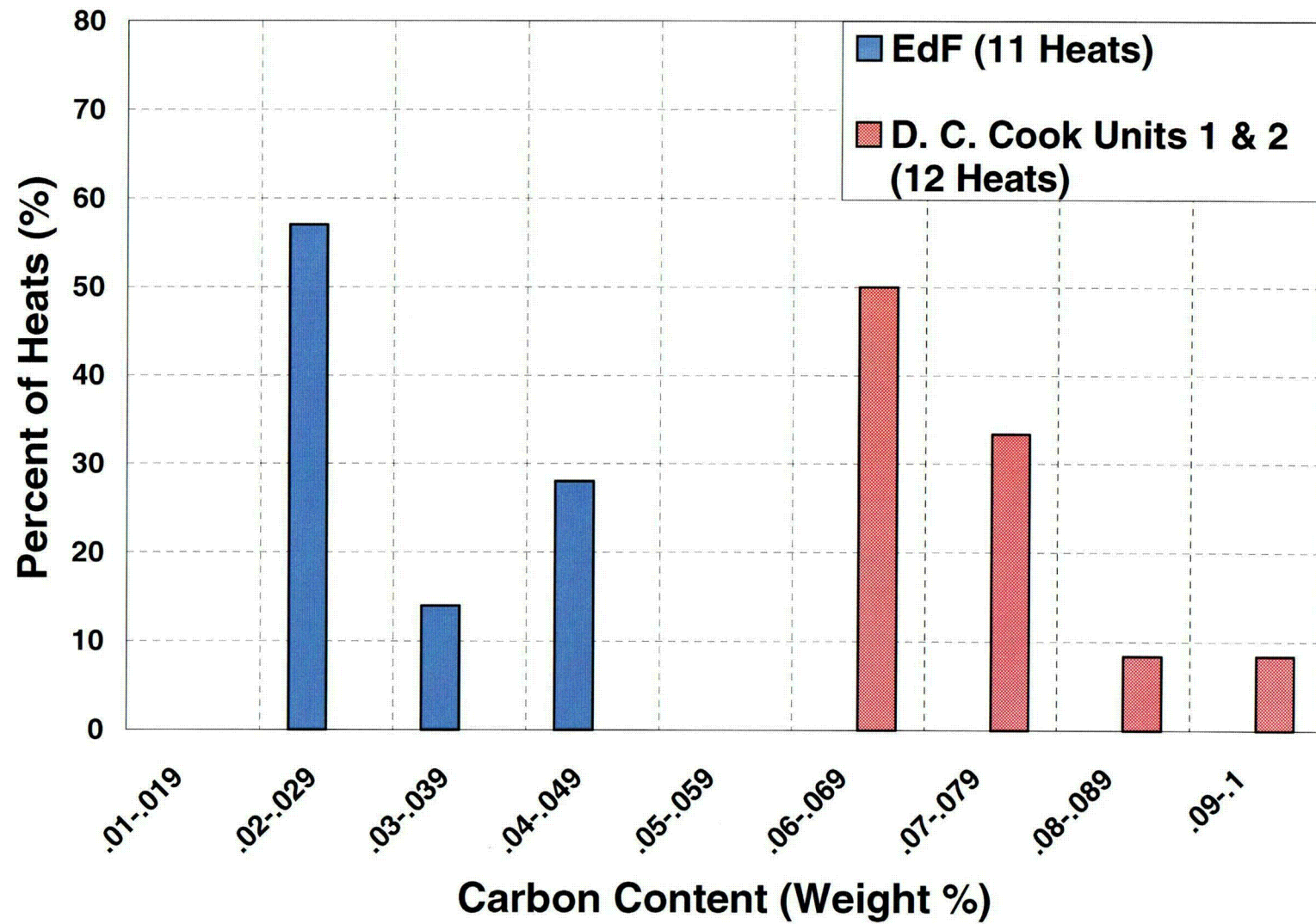


Figure 4-2 Carbon Content of the Various Heats of Alloy 600 Used in Fabricating the D. C. Cook Units 1 & 2 and French Head Penetration

a,c,e

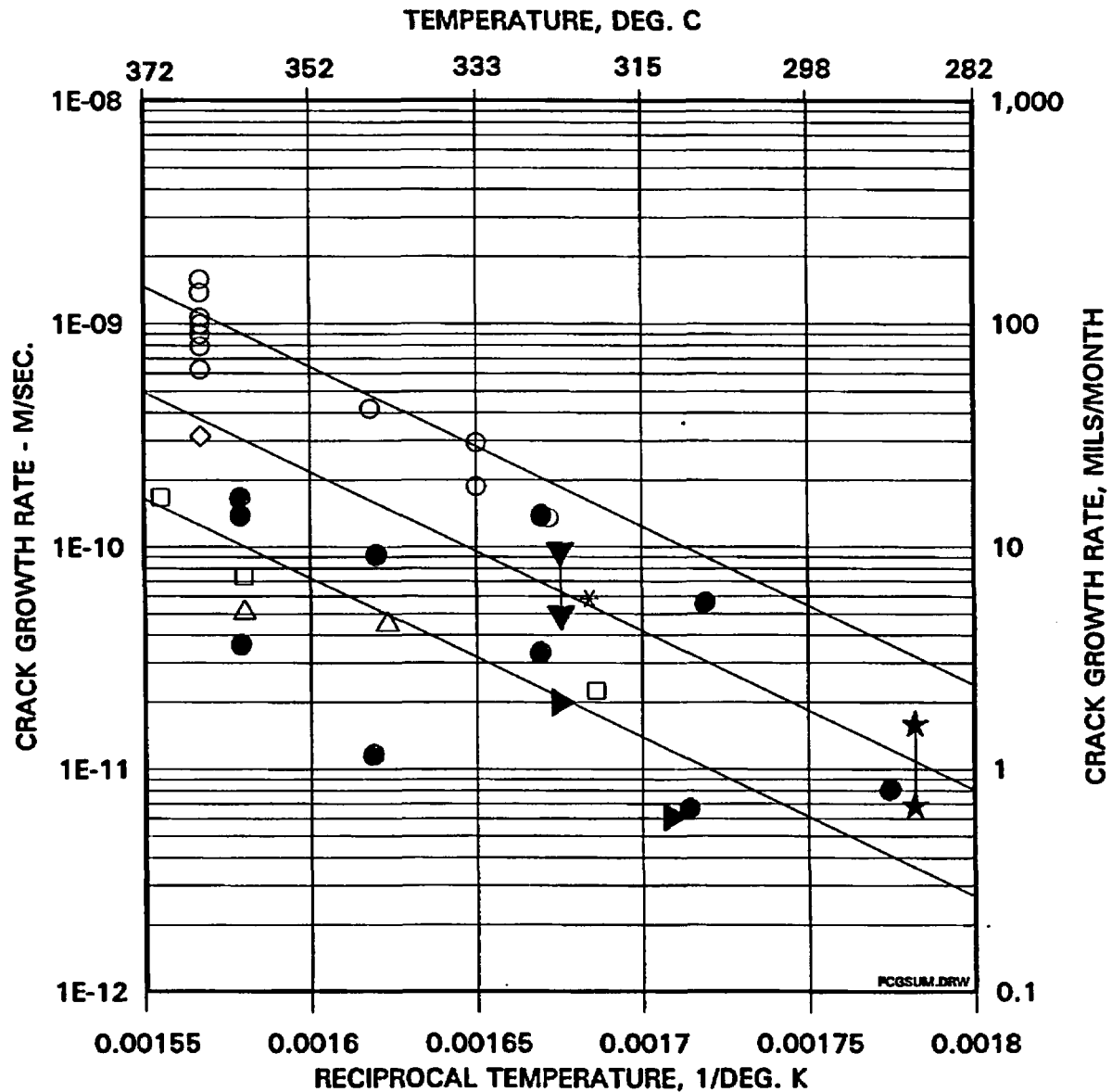


Figure 4-3 Screened Laboratory Data for Alloy 600 with the MRP Recommended Curve
(Note that the Modified Scott Model is also Shown)



Figure 4-4 Model for PWSCC Growth Rates in Alloy 600 in Primary Water Environments (325°C), With Supporting Data from Standard Steel, Huntington, and Sandvik Materials

Note that the data have been normalized to a temperature of 325°C. The actual test temperatures are listed in parenthesis after the caption. For example, the Huntington data were obtained at temperature ranging from 315°C to 331°C.



Note: All symbols are for steam generator materials, except the solid circles, which are head penetration laboratory data.

Figure 4-5 Summary of Temperature Effects on PWSCC Growth Rates for Alloy 600 in Primary Water

5 STRESS ANALYSIS

5.1 OBJECTIVES OF THE ANALYSIS

The objective of this analysis was to obtain accurate stresses in each of the CRDM and head vent penetrations as well as the immediate vicinity. To do so requires a three-dimensional finite element analysis which considers all the pertinent loading on the penetration [6]. The stress analysis for the CRDM penetration is documented in [6A] while the head vent analysis is documented in [6B]. One analysis based on D. C. Cook Unit 2 parameters was performed to envelop both units, with the assumption that Unit 2 stresses are higher due to larger weld sizes. An investigation of deformations at the lower end of the housing was also performed using the same model.

Five CRDM locations were considered for each unit: the outermost row (48.7° for Unit 1 and 50.5° for Unit 2), the intermediate rows (44.3° , 38.6° , 26.2° for Unit 1 and 47.0° , 45.8° , 27.0° for Unit 2), and the center location (0° for both units). These locations cover the whole range of all of the CRDM penetration angles in the D.C. Cook Units 1 & 2 reactor vessel head. It shall be noted that since the analysis was done based on Unit 2 parameters, the three outermost nozzle angles used (50.5° , 47.0° , and 45.8° of Unit 2) were correlated to Unit 1 by matching them to the three outermost angles of Unit 1 respectively (see Table B). For the center (0°) and 27.0° rows, the angles were matched to the nearest location of Unit 1 angle (see Table B). In addition, the head vent was analyzed.

The analyses were used to provide information for the flaw tolerance evaluation in Section 6. Also, the results of the stress analysis were compared to the findings from service experience to help assess the causes of the observed cracking. The hoop stress distribution below the attachment weld for all five CRDM penetration nozzles analyzed are included in Appendix B.

5.2 MODEL

A three-dimensional finite element model comprised of iso-parametric brick and wedge elements with mid-side nodes on each face was used to obtain the stresses and deflections. Views of the head penetrations and head vent models are shown in Figures 5-1 and 5-2 respectively. Taking advantage of the symmetry of the vessel head, only half of the head penetrations were modeled. Similarly, only half of the center penetration was modeled.

In the models, the lower portion of the head penetration nozzle, the head vent, the adjacent section of the vessel closure head, and the attachment weld were modeled. The vessel to penetration nozzle weld was simulated with two weld passes. The penetration nozzle, weld metal, cladding and the vessel head shell were modeled in accordance with the relevant materials.

Loading

The only loads used in the analysis are the steady state condition loads. The steady state condition loads considered in the penetration stress analysis of this report consist of the residual stress resulting from the welding process, effect of hydrostatic testing and the normal operating

condition loads. Three basic loading steps: (a) welding, (b) hydrostatic testing and (c) normal operating condition are considered in the stress analysis. The welding process is simulated by combined thermal and structural analysis to determine the thermally induced residual stress. Once welding is completed, a hydrostatic pressure load is applied to and then removed from the wetted regions of the model at ambient temperature. Finally, the model is loaded with normal operating temperature and pressure. The stresses under steady state condition are shown in Figure 5-3 through Figure 5-9.

External loads, such as seismic loads, have been studied and have no impact since the penetration nozzles are captured by the full thickness of the reactor vessel head (about 7 inches for Unit 1 [11D] and 6-1/2 inches for Unit 2 [12D]) into which the penetrations are shrunk fit during construction. The area of interest is in the penetration near the attachment weld, which is unaffected by these external loads.

Material Properties

Four materials were used in the reactor vessel head penetration model. The vessel head is alloy steel, the nozzle is nickel-chrome-iron Alloy 600, the cladding on the inside surface of the vessel head is stainless steel, and the weld buttering layer is Inconel. The stress strain values for Alloy 600 are based on the cyclic stress-strain curves data obtained in [15] at 600°F. Scaling factors for higher temperatures were applied to the Alloy 600 multi-linear isotropic hardening curve based on high temperature yield strength data for Alloy 600. The nozzle yield strength at 600°F is 39.3 ksi. While material properties used for the nozzle material make use of multi-linear isotropic hardening, the material properties for the weld and weld buttering, head shell and stainless steel cladding are modeled using elastic-perfectly plastic hardening laws.

Assumptions

The nozzle was assumed to be flush with the penetration. No clearance or interference fit was assumed. It has been shown that the assumption of no interference fit would produce conservative nozzle stresses as compared to stresses calculated with interference fits typically specified for CRDM nozzles.

Two passes of welding were performed for the head penetration nozzle: an inner pass and an outer pass. For the simulated welds, the model geometry was designed such that each weld pass is approximately the same volume. The results of this modeling methodology have been correlated with the experimental and field data in Reference 16.

The model geometry is based on the nominal drawing dimensions of D. C. Cook Unit 2 reactor vessel head and nozzles to envelop both Unit 1 and 2.

5.3 STRESS ANALYSIS RESULTS – OUTERMOST CRDM PENETRATION (50.5°)

Figure 5-3 presents the hoop and axial stresses for the steady state condition for the outermost CRDM penetration.

The hoop stresses for steady state operation are much greater than the axial stresses. This is consistent with the field findings, where the cracks discovered are generally oriented axially. Typically, in-service cracks will orient themselves perpendicular to the largest stress component. Also it should be noted from Figure 5-3 that the highest tensile hoop stresses are at the uphill side and downhill side locations rather than midway around the penetration, where they are compressive. This is consistent with finding the axial cracks only at the uphill side and downhill side locations. It is these steady state stresses that will be used to predict crack extension in the penetrations, as will be discussed further in Section 6.

These stress findings also support the safety argument that cracks are unlikely to propagate in the circumferential direction, because the axial stresses are relatively low. This is illustrated in a cut taken along the plane of the top of the attachment weld, as shown in Figure 5-9. Note the area of compressive axial stress near mid-wall of the penetration, which extends for nearly the entire circumference.

5.4 STRESS ANALYSIS RESULTS – INTERMEDIATE CRDM PENETRATIONS

The stresses in these penetrations are similar in character. Figures 5-4, 5-5, and 5-6 show the results for the 47.0 degree, 45.8 degree, and 27.0 degree CRDM penetrations respectively. As with the outermost housing, the hoop stresses for steady state operation are greater than the axial stresses.

5.5 STRESS ANALYSIS RESULTS – CENTER CRDM PENETRATION

Figure 5-7 shows the hoop and axial stresses at steady state for the center CRDM penetration. The tube hoop stresses near the weld are generally lower than the tube hoop stresses at the downhill side or uphill side locations of the outer head penetration.

5.6 STRESS ANALYSIS RESULTS – HEAD VENT

The head vent is a smaller penetration than the CRDM head penetration, but is also constructed of Alloy 600 material, with a partial penetration weld at the inside of the reactor vessel head. The head vent was evaluated using a three-dimensional finite element model as shown in Figure 5-2.

The critical stress location in the head vent is in the vicinity of the attachment weld, where residual and pressure stresses have the most impact. As with the CRDM penetrations, the residual stresses dominate. Also similar to the CRDM head penetrations, the stresses in the pipe decrease quickly as a function of distance up the pipe away from the weld. The hoop and axial stresses are shown as contours in Figure 5-8.

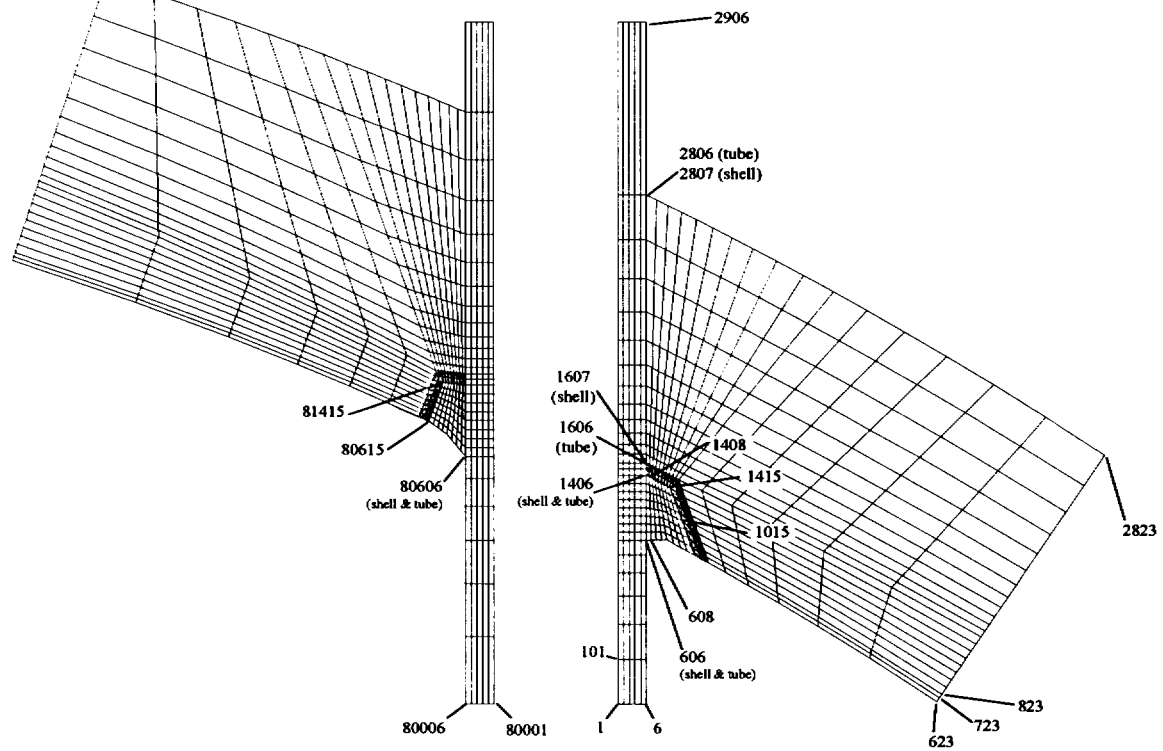


Figure 5-1 Finite Element Model of CRDM Penetration

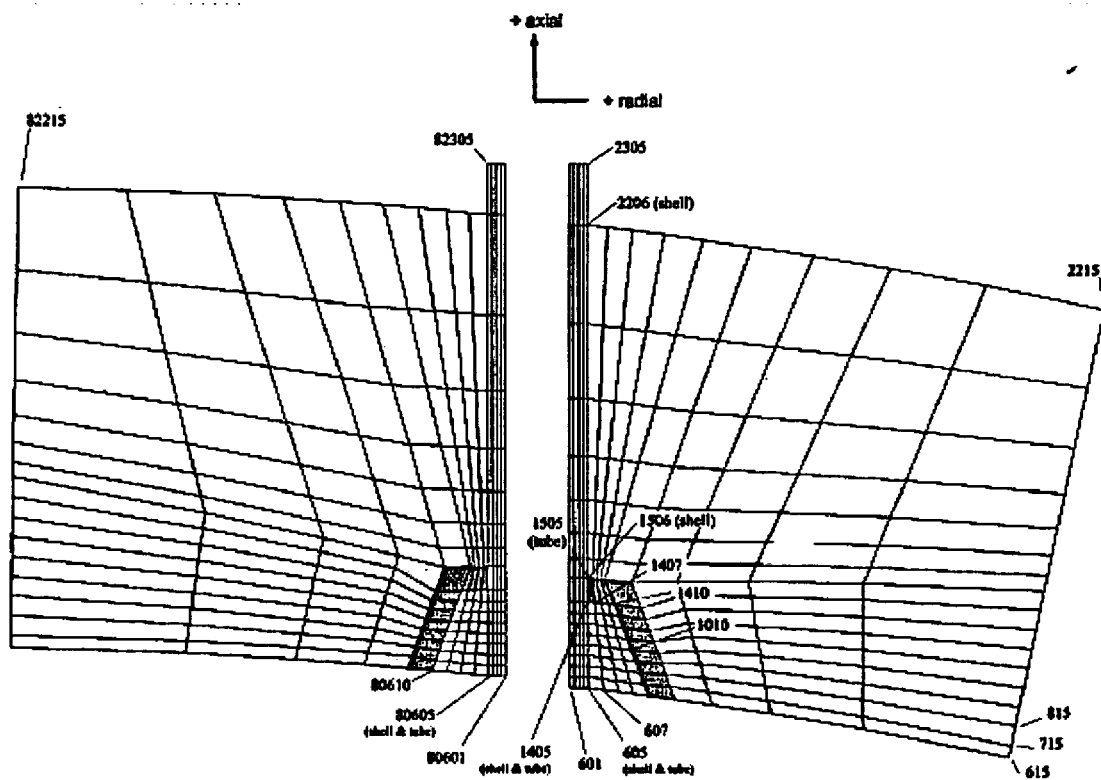


Figure 5-2 Vent Pipe Finite Element Model

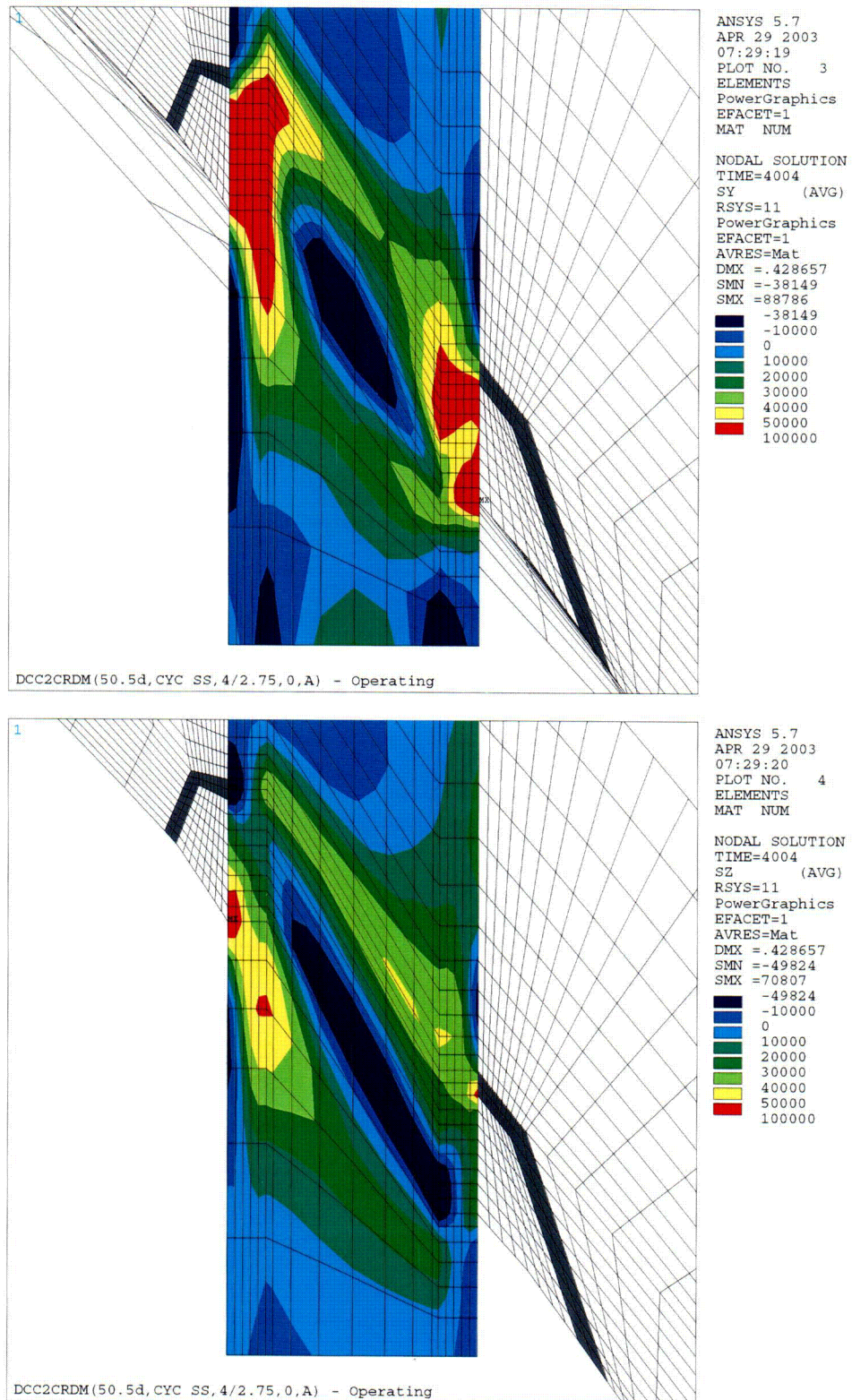


Figure 5-3 Stress Distribution at Steady State Conditions: Outermost CRDM Penetration Nozzle (50.5 Degrees) (Hoop Stress is the Top Figure, Axial Stress is the Bottom Figure)

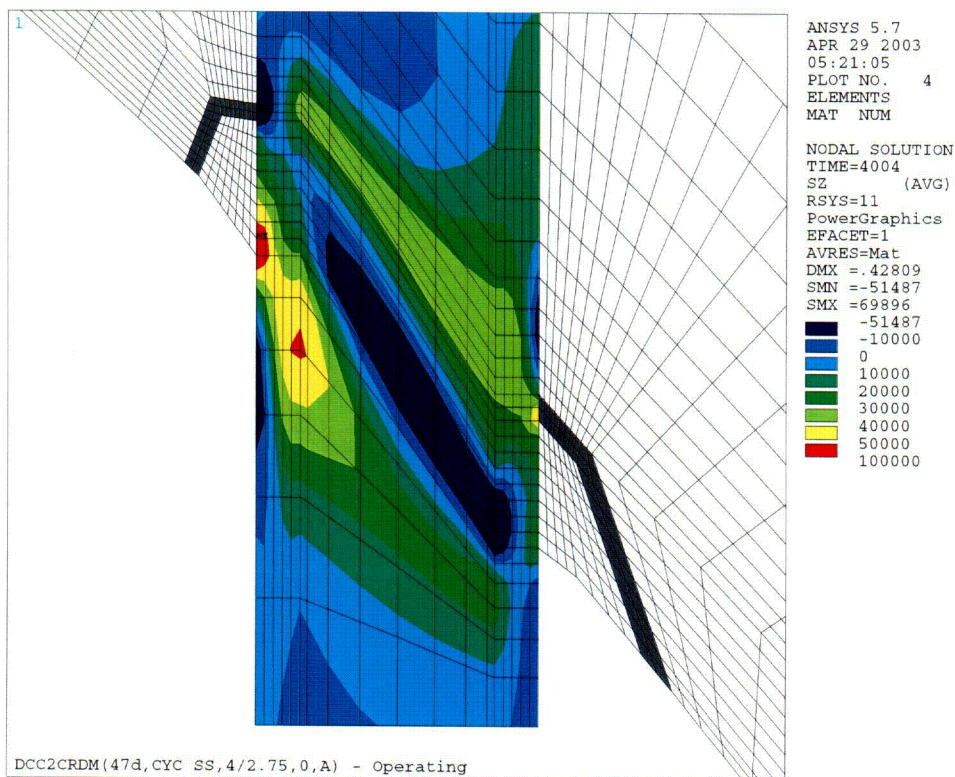
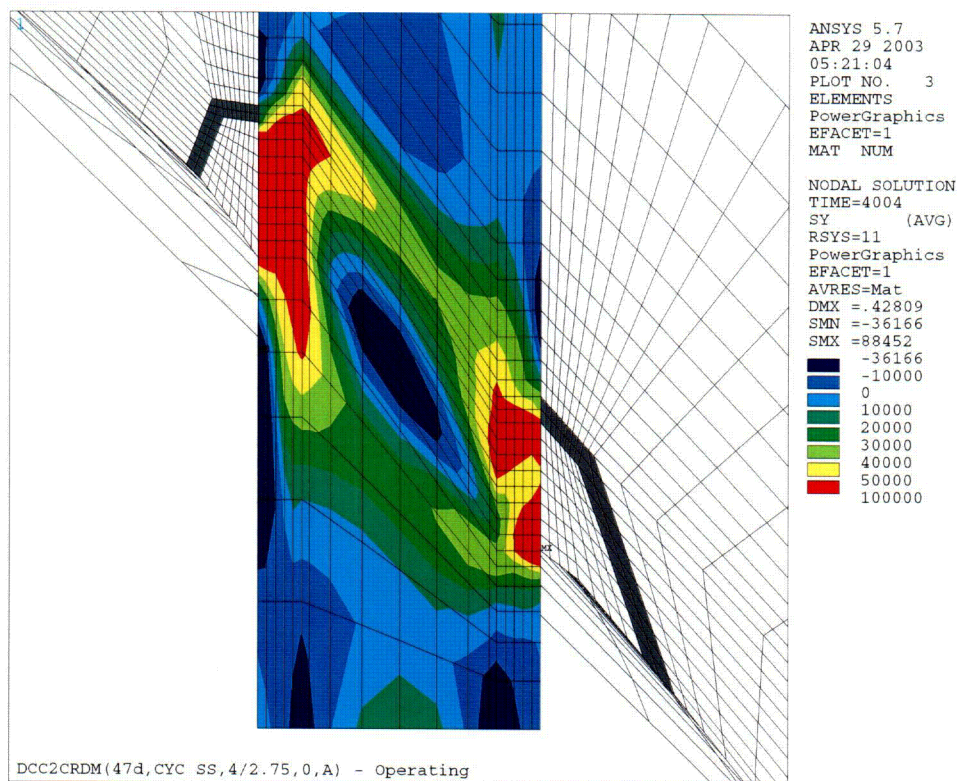


Figure 5-4 Stress Distribution at Steady State Conditions for the 47.0 Degrees CRDM Penetration (Hoop Stress is the Top Figure; Axial Stress is the Bottom Figure)

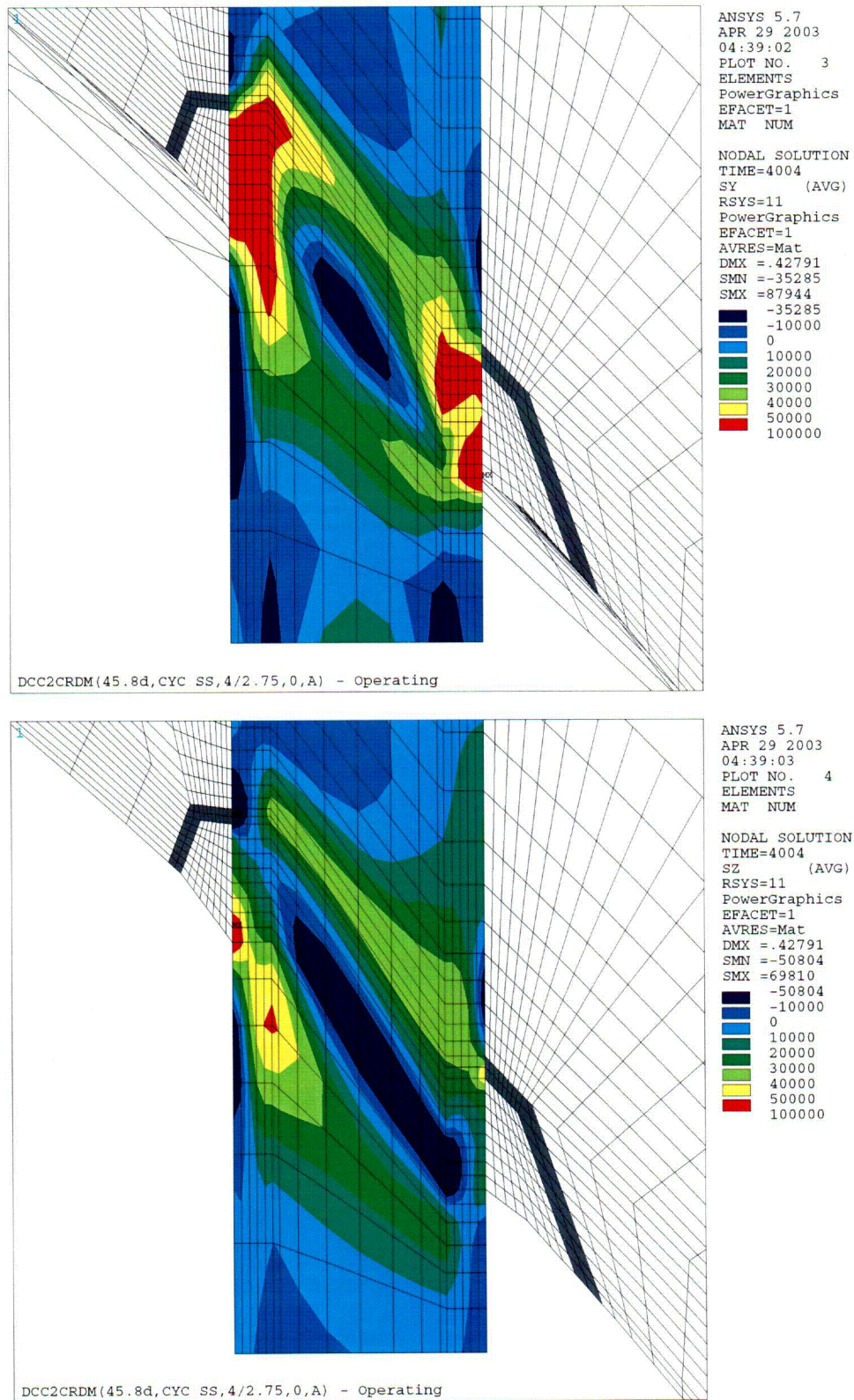


Figure 5-5 Stress Distribution at Steady State Conditions for the 45.8 Degrees CRDM Penetration (Hoop Stress is the Top Figure; Axial Stress is the Bottom Figure)

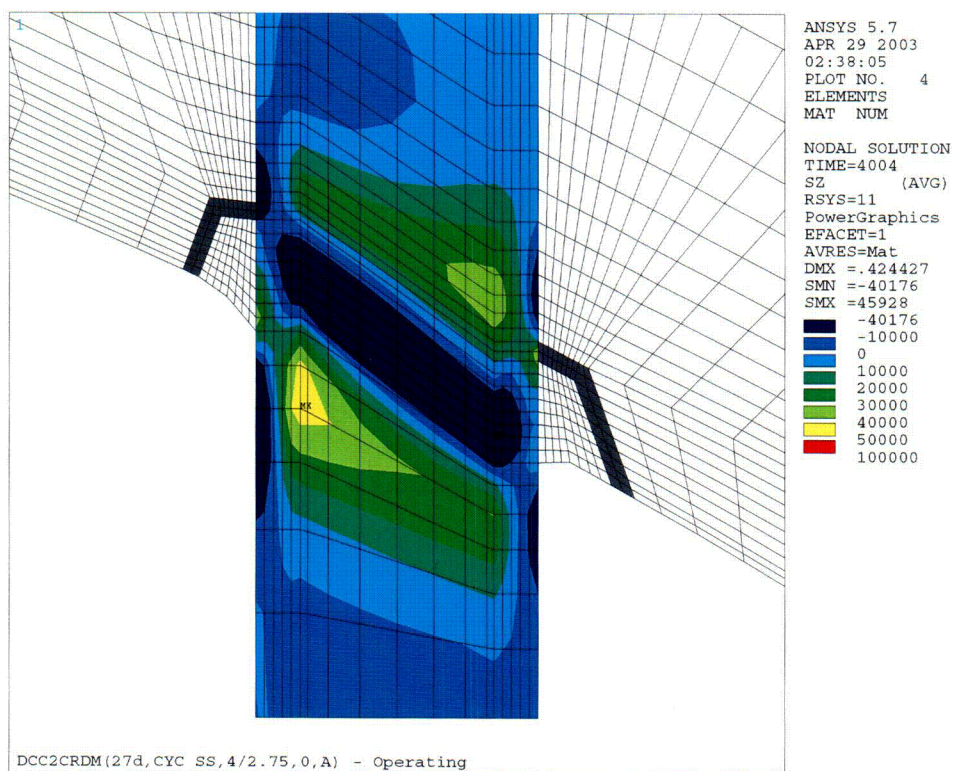
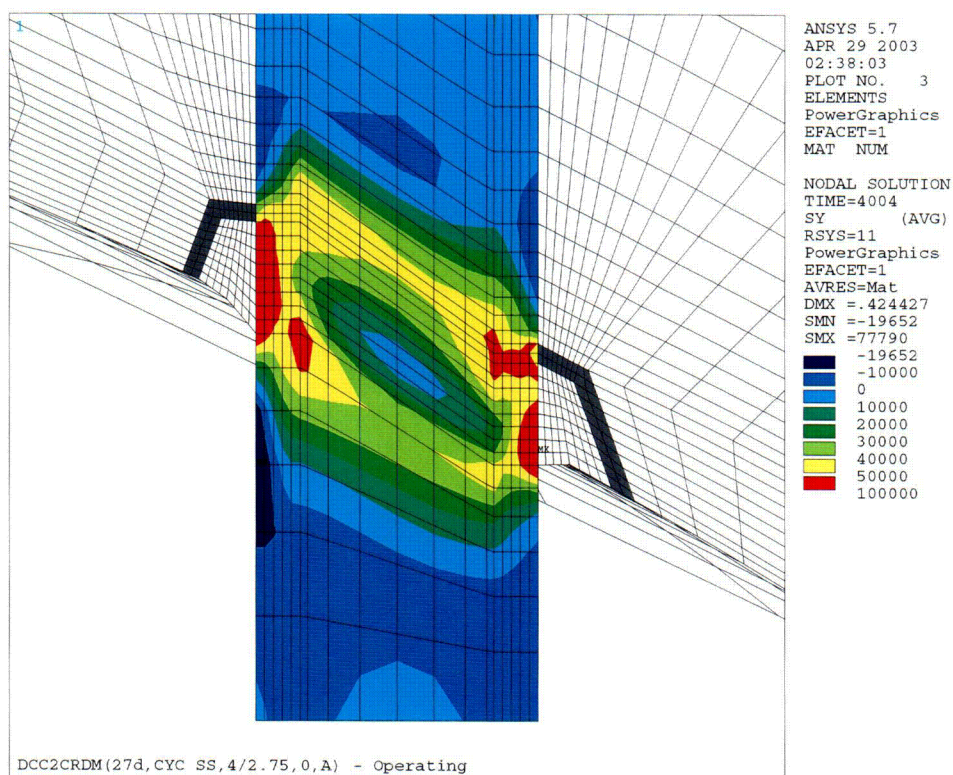


Figure 5-6 Stress Distribution at Steady State Conditions for the 27.0 Degrees CRDM Penetration (Hoop Stress is the Top Figure; Axial Stress is the Bottom Figure)

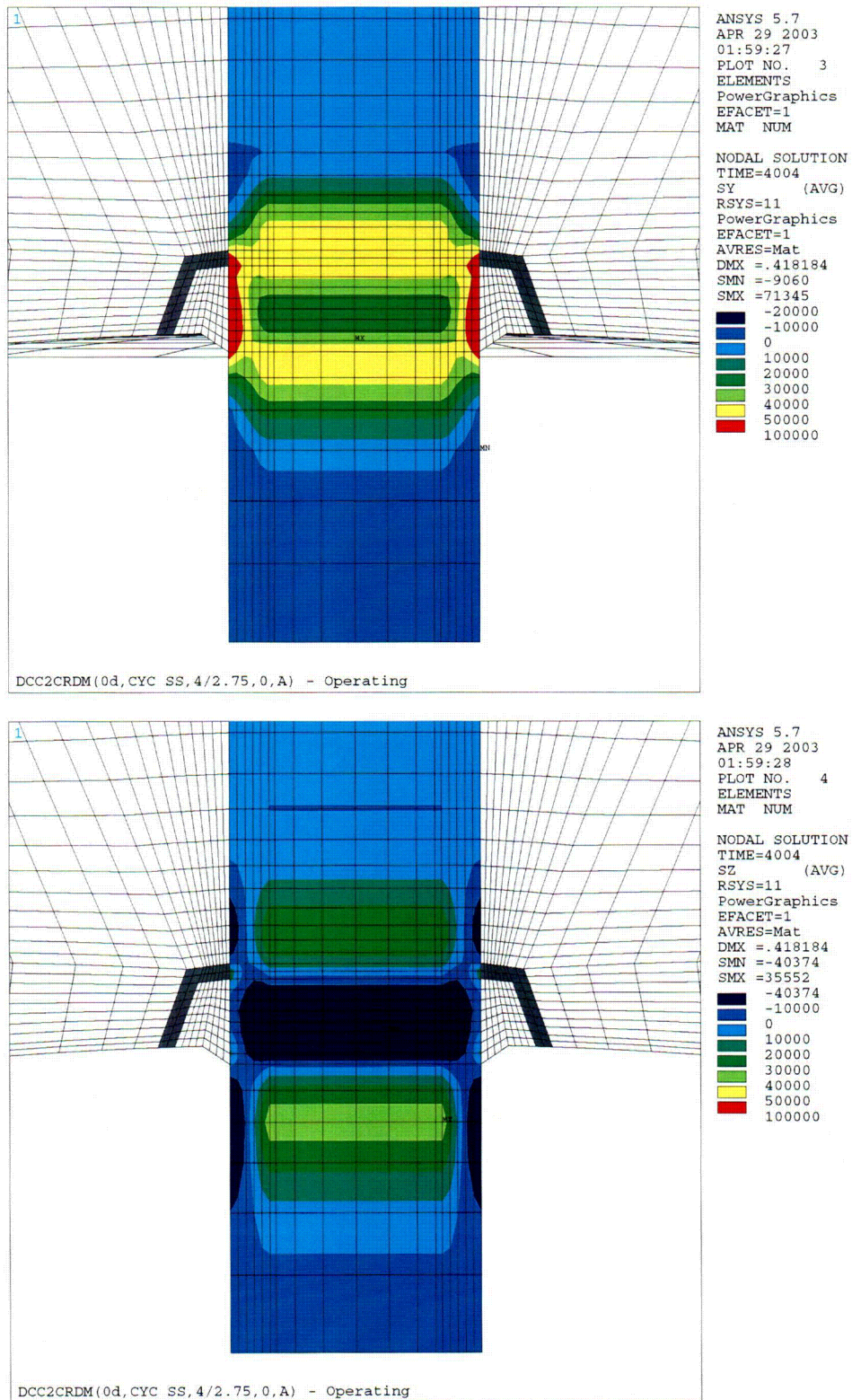


Figure 5-7 Stress Distribution at Steady State Conditions for the Center CRDM Penetration (Hoop Stress is the Top Figure; Axial Stress is the Bottom Figure)

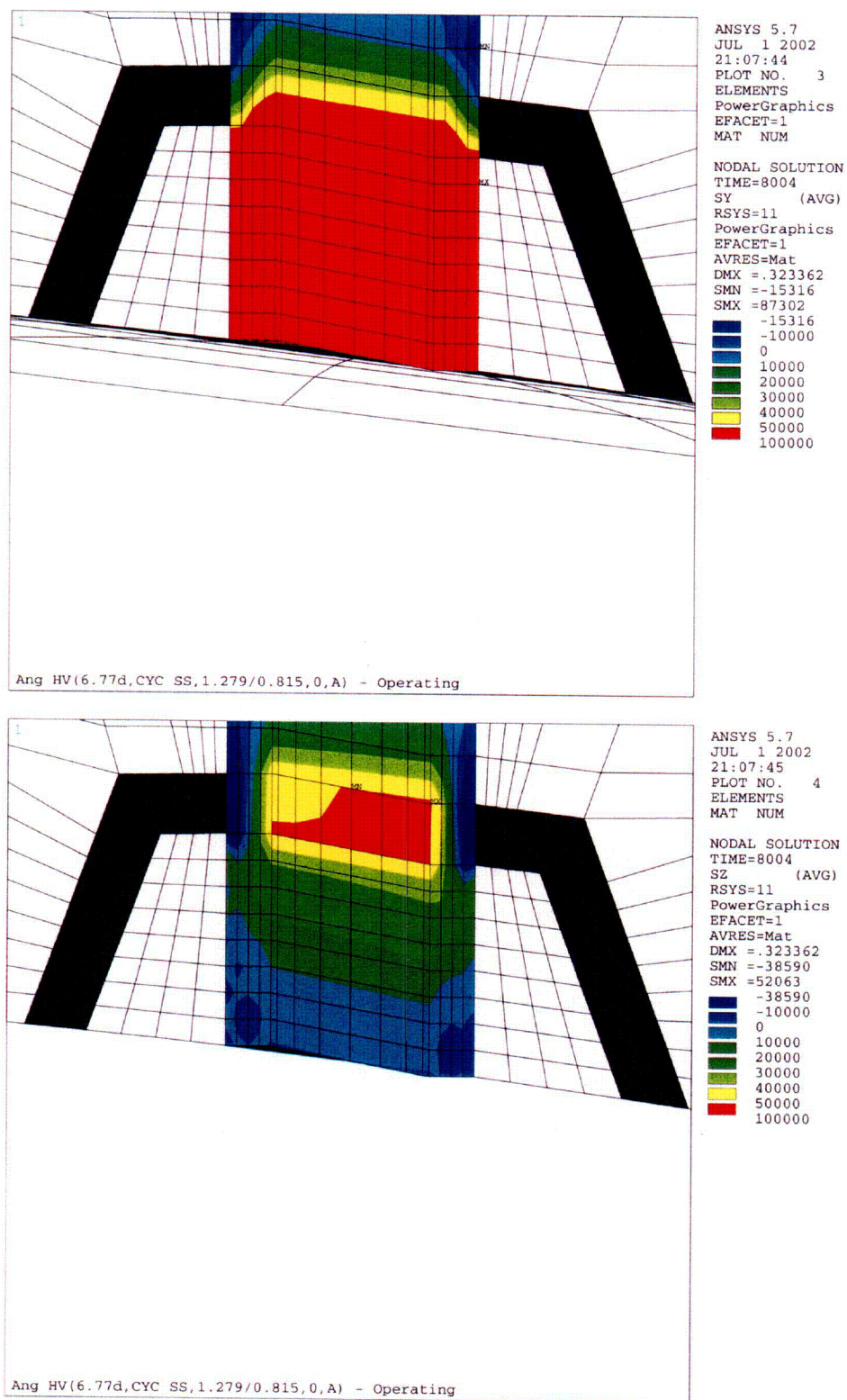


Figure 5-8 Stress Contours in the Head Vent Nozzle as a Result of Residual Stresses and Operating Pressure (Hoop Stress is the Top Figure; Axial Stress is the Bottom Figure)

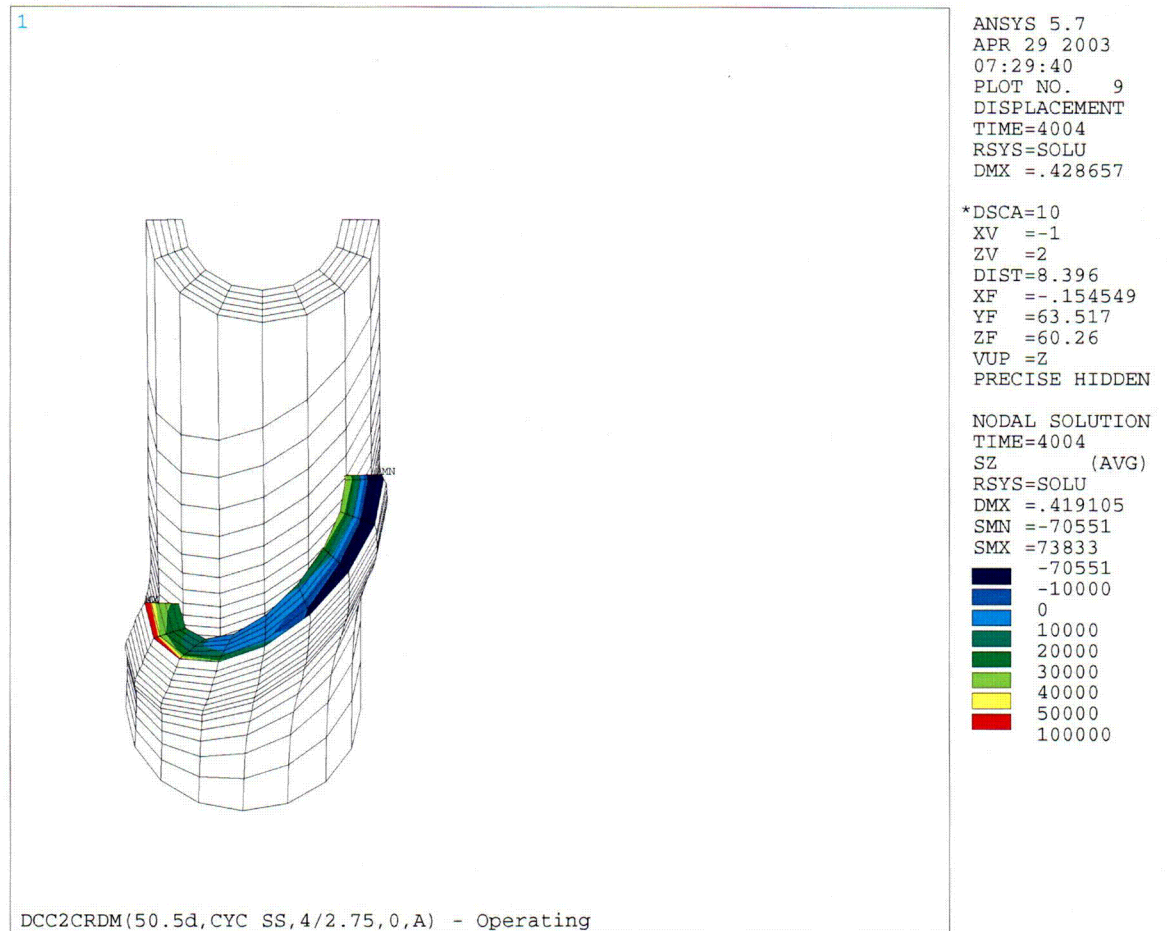


Figure 5-9 Axial Stress Distribution at Steady State Conditions for the Outermost CRDM Penetration (50.5 Degrees), Along a Plane Oriented Parallel to, and Just Above, the Attachment Weld

6 FLAW TOLERANCE CHARTS

6.1 INTRODUCTION

The flaw tolerance charts were developed using the stress analysis of each of the penetration locations as discussed in Section 5. The crack growth law developed for D. C. Cook Units 1 & 2 in Section 4.2 was used for each case, and several flaw tolerance charts were developed for each penetration location. The first series of charts characterizes the growth of a part through flaw, and the second series of charts characterizes the growth of a through-wall flaw in the length direction. The allowable safe operating life of the penetration nozzle may then be directly determined, using the combined results of the two charts. All times resulting from these calculations are effective full power years, since crack growth will only occur at operating temperatures.

6.2 OVERALL APPROACH

The results of the three-dimensional stress analysis of the penetration locations were used directly in the flaw tolerance evaluation.

The crack growth evaluation for the part-through flaws was based on the worst stress distribution through the penetration wall at the location of interest of the penetration. The highest stressed location was found to be in the immediate vicinity of the weld for both the center and outermost penetrations.

The stress profile was represented by a cubic polynomial:

$$\sigma(x) = A_0 + A_1x + A_2x^2 + A_3x^3 \quad (6-1)$$

where:

- x = the coordinate distance into the nozzle wall
- σ = stress perpendicular to the plane of the crack
- A_i = coefficients of the cubic polynomial fit

For the surface flaw with length six times its depth, the stress intensity factor expression of Raju and Newman [5A] was used. The stress intensity factor $K_I(\Phi)$ can be calculated anywhere along the crack front. The point of maximum crack depth is represented by $\Phi = 0$, and this location was also found to be the point of maximum K_I for the cases considered here. The following expression is used for calculating $K_I(\Phi)$, where Φ is the angular location around the crack. The units of $K_I(\Phi)$ are $\text{ksi}\sqrt{\text{in}}$.

$$K_I(\Phi) = \left[\frac{\pi a}{Q} \right]^{0.5} \sum_{j=0}^3 G_j(a/c, a/t, t/R, \Phi) A_j a^j \quad (6-2)$$

The boundary correction factors $G_0(\Phi)$, $G_1(\Phi)$, $G_2(\Phi)$ and $G_3(\Phi)$ are obtained by the procedure outlined in reference [5A]. The dimension "a" is the crack depth, and "c" is the semi crack length, while "t" is the wall thickness. "R" is the inside radius of the tube, and "Q" is the shape

factor. It should be noted that the stress profile in Equation (6-1) is embedded in Equation (6-2) in the form of the cubic polynomial coefficients, A_i .

[

$]^{a,c,e}$

For the prediction of crack growth for a circumferential through-wall flaw in the head penetration along a plane above the attachment weld, an expression first presented by Hiser [5B] was used. The stress intensity factor for a through-wall flaw was developed using finite element modeling by Structural Integrity Associates (SIA), and these results were merged with results obtained by Richard Bass of Oak Ridge National Labs (ORNL), as shown in Figure 6-1. The equation of the stress intensity factor is simply a function of the crack half angle, and is given below:

$$K_I = 3.476x - 6.619 \times 10^{-2} x^2 + 4.733 \times 10^{-4} x^3 - 1.445 \times 10^{-6} x^4 + 1.790 \times 10^{-9} x^5 \quad (6-4)$$

In this equation, x is the crack half angle in degrees and K_I is in $\text{ksi}\sqrt{\text{in}}$.

[

$]^{a,c,e}$

Because of the assumed 6:1 aspect ratio, the use of the flaw tolerance charts is restricted to flaws with aspect ratios less than or equal to 6:1. For flaws with aspect ratios greater than 6:1, additional evaluation will need to be performed. The flaw tolerance charts are conservative for aspect ratios less than 6:1.

6.3 AXIAL FLAW PROPAGATION

CRDM Surface Flaws

The results of the calculated growth for inside surface flaws growing through the wall thickness of the CRDM penetration nozzles for inside surface flaws are shown in Figures 6-2 through 6-7 for Unit 1 and Figures 6-22 through 6-27 for Unit 2. For outside surface flaws the results are shown in Figures 6-9 and 6-10 for Unit 1 and Figures 6-29 and 6-30 for Unit 2. Based on the discussion in MRP-55 report [4H], the use of stress intensity factors less than $15\text{MPa}\sqrt{\text{m}}$ involves assumption not currently substantiated by actual CGR data for CRDM nozzle materials. Therefore, these crack growth curves begin at a flaw depth resulting in a stress intensity factor of $15\text{MPa}\sqrt{\text{m}}$, which exceeds the threshold value of $9\text{MPa}\sqrt{\text{m}}$. This may result in curves with different initial flaw sizes, as seen for example in Figure 6-3. Note that results are only provided for the uphill and downhill sides of each penetration nozzle; the stresses for the regions 90 degrees from these locations are compressive. If flaws are found in such a location, the results for either the uphill or downhill location, whichever is closer, can be used.

Each of these figures allows the future allowable service time to be estimated graphically, as discussed in Section 3. Results are shown for each of the penetration nozzles analyzed in each of these figures. The stresses are much higher near the attachment weld than at 0.5 inch below or above it, so separate figures have been provided for these three regions. For more than 0.5 inch below the weld, the crack growth will eventually come to rest since the stresses are compressive as shown for the CRDM nozzles in Appendix B. It should be noted that the flaw tolerance charts generated for 0.5" below the weld are applicable and conservative for evaluating flaws located more than 0.5" below the weld. Similarly, for the flaw tolerance charts generated for 0.5" above the weld, they are applicable and conservative for evaluating flaws located more than 0.5" above the weld. Also, the stresses are different on the downhill side of the penetration as opposed to the uphill side, so these two cross sections have also been treated separately.

Example problems are provided in section 6.6 for a range of possible flaw types.

CRDM Through-Wall Flaws

The projected crack growth of a through-wall flaw in the CRDM penetration nozzles are the primary concern in evaluating the structural integrity of head penetrations. In some cases, the through-wall flaw may be located sufficiently below the attachment weld that additional time may be required for the flaw to grow to the attachment weld. To provide a means to evaluate the duration of this additional time, a series of flaw tolerance charts for through-wall flaws were prepared.

Charts were prepared for each of the penetrations evaluated, for both the uphill and downhill locations, as shown in Figures 6-12 through 6-20 for Unit 1 and Figures 6-32 through 6-40 for Unit 2. In each figure, the location of the upper extremity of the postulated through-wall crack is identified by the distance measured from the bottom of weld.

Head Vent

The only flaw tolerance chart that is necessary for the head vent region is for flaws at and above the weld, since there is no portion of the head vent which projects below the weld. Figure 6-8 (Unit 1) and Figure 6-28 (Unit 2) provide the projected growth of a part through flaw in the head vent at the attachment weld. The crack growth curves generated are based on the worst stress distribution at and above the attachment weld and therefore Figures 6-8 and Figure 6-28 are applicable for evaluating flaws at and above the attachment weld. The growth through the wall is relatively rapid, because the thickness of the head vent is small.

6.4 CIRCUMFERENTIAL FLAW PROPAGATION

Since circumferentially oriented flaws have been found at five plants (Bugey 3, Oconee 2, Crystal River 3, Davis Besse, and Oconee 3), it is important to consider the possibility of crack extension in the circumferential direction. The first case was discovered as part of the destructive examination of the tube with the most extensive circumferential cracking at Bugey 3. The crack was found to have extended to a depth of 2.25 mm in a wall thickness of 16 mm. The flaw was found at the outside surface of the penetration (number 54) at the downhill side location, just above the weld.

The circumferential flaws in Oconee Unit 3 were discovered during the process of repairing a number of axial flaws, whereas the circumferential flaw in Oconee Unit 2 and Crystal River Unit 3 were discovered by UT. Experience gained from these findings has enabled the development of UT procedures capable of detecting circumferential flaws reliably.

To investigate this issue completely, a series of crack growth calculations were carried out for a postulated surface circumferential flaw located just above the head penetration weld, in a plane parallel to the weld itself. This is the only flaw plane that could result in a complete separation of the penetration nozzle, since all others would result in propagation below the weld, and therefore there is no chance of complete separation because the remaining weld would hold the penetration nozzle in place.

[

]a,c,e

[

^{a,c,e} The results of this calculation are shown in Figure 6-21 for Unit 1 and Figure 6-41 for Unit 2. From these figures, it can be seen that the time required for propagation of a circumferential flaw to a point where the integrity of the CRDM penetration nozzle would be affected (330 degrees [10]) would be about 37 years and 21 years for Unit 1 and Unit 2 respectively. Due to the conservatism in the calculations (the time period for a surface flaw to become a through-wall flaw was conservatively ignored) the service life is likely to be even longer. In addition, due to uncertainties in the exact composition of the chemical environment in contact with the nozzle OD, a multiplicative factor of 2.0 is used in the Crack Growth Rate (CGR) for all circumferential surface flaws on the OD of the head penetration nozzles located above the elevation of the J-groove weld.

6.5 FLAW ACCEPTANCE CRITERIA

Now that the projected crack growth curves have been developed, the question remains as to what flaw size would be acceptable for further service.

Acceptance criteria have been developed for indications found during inspection of reactor vessel upper head penetration as part of an industry program coordinated by NEI (formerly NUMARC). Such criteria are normally found in Section XI of the ASME Code, but Section XI does not require in-service inspection of these regions and therefore acceptance criteria are not available. In developing the enclosed acceptance criteria, the approach used was very similar to that used by Section XI, in that an industry consensus was reached using input from both operating utility technical staff and each of the three PWR vendors. The criteria developed are applicable to all PWR plant designs.

Since the discovery of the leaks at Oconee and ANO-1, the acceptance criteria have been revised slightly to cover flaws on the outside diameter of the penetration below the attachment weld, and flaws in the attachment weld. These revised criteria are now formally endorsed by the NRC [13], and will be used in these evaluations. Portions of the acceptance criteria will be noted below.

The criteria presented herein are limits on flaw sizes, which are acceptable. The criteria are to be applied to inspection results. It should be noted that determination of the future service during which the criteria are satisfied is plant-specific and dependent on flaw geometry and loading conditions.

It has been previously demonstrated by each of the owners groups that the penetration nozzles are very tolerant of flaws and there is only a small likelihood of flaw extensions to larger sizes. Therefore, it was concluded that complete fracture of the penetration nozzle is highly unlikely. The approach used here is more conservative than that used in Section XI applications where the acceptable flaw size is calculated by placing a margin on the critical flaw size. For the current application, the critical flaw size would be far too large to allow a practical application of the approach used in Section XI applications, so protection against leakage is the priority.

The acceptance criteria presented herein apply to all the flaw types regardless of orientation and shape. Similar to the approach used in Section XI, flaws are first characterized according to established rules and then compared with acceptance criteria.

Flaw Characterization

Flaws detected must be characterized by the flaw length and preferably flaw depth. The proximity rules of Section XI for considering flaws as separate, may be used directly (Section XI, Figure IWA 3400-1). This figure is reproduced here as Figure 6-42.

When a flaw is detected, its projections in both the axial and circumferential directions must be determined. Note that the axial direction is always the same for each penetration, but the circumferential direction will be different depending on the angle of intersection of the penetration nozzle with the vessel head. The "circumferential" direction of interest here is along the top of the attachment weld, as illustrated in Figure 6-43. It is this angle which will change for each penetration nozzle and the top of the attachment weld is also the plane which could cause separation of the penetration nozzle from the vessel head. The location of the flaw relative to both the top and bottom of the partial penetration attachment weld must also be determined since a potential leak path exists when a flaw propagates through the penetration nozzle wall and up the penetration nozzle past the attachment weld. Schematic of a typical weld geometry is shown in Figure 6-44.

Flaw Acceptance Criteria

The maximum allowable depth (a_f) for axial flaws on the inside surface of the penetration nozzle, at or above the weld is 75 percent of the penetration wall thickness. The term a_f is defined as the maximum size to which the detected flaw is calculated to grow in a specified time period. This 75 percent limitation was selected to be consistent with the maximum acceptable flaw depth in Section XI and to provide an additional margin against through wall penetration. There is no concern about separation of the penetration nozzle from the vessel head, unless the flaw is above the attachment weld and oriented circumferentially. Calculations have been completed to show that the geometry of all penetrations can support a continuous circumferential flaw with a depth of 75 percent of the wall thickness.

Axial inside surface flaws found below the weld are acceptable regardless of depth as long as their upper extremity does not reach the bottom of the weld during the period of service until the next inspection. Axial flaws that extend above the weld are limited to 75 percent of the wall thickness.

Axial flaws on the outside surface of the penetration nozzle below the attachment weld are acceptable regardless of depth, as long as they do not extend into the attachment weld during the period of service until next inspection. Outside surface flaws above the attachment weld must be evaluated on a case by case basis, and must be discussed with the regulatory authority. These flaws must be repaired unless the regulatory authority is convinced otherwise.

Circumferential flaws located below the weld are acceptable regardless of their depth, provided the length is less than 75 percent of the penetration nozzle circumference for the period of service until the next inspection. Circumferential flaws detected in this area have no structural significance except that loose parts must be avoided. To this end, intersecting axial and circumferential flaws shall be removed or repaired since multiple intersecting axial and circumferential flaws can result in loose parts. Circumferential flaws at and above the weld must be discussed with the regulatory authority on a case by case basis. These flaws must be repaired unless the regulatory authority is convinced otherwise.

Surface flaws located in the attachment welds themselves are not acceptable regardless of their depth. This is because the crack growth rate is several times faster than that of the Alloy 600 material, and also because depth sizing capability does not yet exist for indications in the attachment weld.

The flaw acceptance criteria are summarized in Table 6-1. Flaws that exceed these criteria must be repaired unless analytically justified for further service. These criteria have been reviewed and endorsed by the NRC, as documented in references [7, 8, 13].

It is expected that the use of these criteria and crack growth curves will provide conservative predictions of the allowable service time.

6.6 EXAMPLE CALCULATIONS

The crack growth prediction curves in Figures 6-2 through 6-41 (Figures 6-2 through 6-21 for Unit 1 and Figures 6-22 through 6-41 for Unit 2) can be used with the acceptance criteria of Section 6.5 to determine the available service time for D. C. Cook Units 1 & 2. In this section, a few examples are presented to illustrate the use of some of these figures for Unit 2. The results for Unit 1 can be obtained using similar calculation process.

Example 1 – Determine the service life of an axially oriented inside surface flaw whose upper extremity is located 1.25" below the weld on the uphill side of penetration no. 75. First, the penetration locality angle is obtained from Table 1-2 and, in this case, the locality angle is 50.5 degrees. The initial flaw depth is 0.078" (a_{initial}) and the initial flaw length is 0.195" ($2c_{\text{initial}}$). Assuming that the initial aspect ratio of 2.5:1 is maintained throughout the time that the inside surface flaw becomes a through-wall flaw, the final length of the flaw ($2c_{\text{final}}$) will be 1.563". The upper extremity of the flaw is now located 0.566" below the weld and validates the use of a single

crack growth curve. The crack growth curve for the 50.5 degrees nozzle angle of Figure 6-22, which was developed for flaws located at 0.5" or more below the weld, is applicable and has been reproduced as Figure 6-45. The flaw is initially 12.5 percent of the wall thickness, and a straight line is drawn horizontally at $a/t = 0.125$ that intersects the crack growth curve. Using the acceptance criteria in Table 6-1, the service life can then be determined as the remaining time for this flaw to grow to the limit of 100 percent of the wall thickness or approximately 2.5- years (labeled as Service Life in Figure 6-45).

Example 2 – In this case, the flaw is identical in size to that used in Example 1, but located on the outside surface and on the downhill side of penetration no. 75. This flaw, just as the flaw in Example 1, will not cross into the weld region. The applicable curve to use is Figure 6-30. The ratio a/t and initial reference time are likewise found using the same approach as used in Example 1. Using the acceptance criteria in Table 6-1, the determination of service life is illustrated in Figure 6-46, where we can see that the result is approximately 1.3 years.

Example 3 – An axial inside surface flaw is located at the weld and on the downhill side of penetration no. 1. The initial length of the flaw is 0.250" and the initial depth is 0.05". From Table 1-2, the angle of this penetration nozzle is 0.0 degrees. The applicable curve is Figure 6-25 and is reproduced here as Figure 6-47. In this case, the initial flaw depth is 8.0 percent of the wall thickness. The initial reference time can be found by drawing a horizontal line at $a/t = 0.08$. Using the acceptance criteria in Table 6-1, the allowable service life can then be determined as the time for the flaw to reach a depth of 75 percent of the wall thickness. The final reference time is found through a horizontal line drawn at $a/t = 0.75$. The service life can be determined through the intersection points of these lines and the crack growth curve. The resulting service life is approximately 3.4 years, as shown in Figure 6-47.

Example 4 – In this case, we have postulated an axial inside surface flaw with an upper extremity located 1.0 inch below the attachment weld on the downhill side of penetration no. 23 (27.0 degrees). The flaw has an initial depth of 0.079" and an initial length of 0.395". Assuming that the initial aspect ratio of 5:1 ($0.395" / 0.079"$) is maintained as the flaw propagates into the nozzle wall, the final length of a through-wall flaw would be 3.125" long ($0.625" \times 5$). The location of the upper extremity of this flaw would have reached within 0.5 inch below the weld as it propagates into the nozzle wall ($1.0 - ((3.125" / 2) - (0.395" / 2))$). Therefore the evaluation will require the use of two flaw charts. The first step is to estimate the time required for the initial flaw to grow to within 0.5 inch of the weld. This can be accomplished with the use of Figure 6-23, which was developed for flaws located at 0.5" or more below the weld, and is reproduced here as Figure 6-48a. The upper extremity is 1 inch below the weld and is assumed to grow until the extremity is 0.5 inches below the weld. The final half-length of the flaw when it reaches 0.5 inches below the weld will be the sum of the initial half-length and the 0.5 inches it has grown or 0.6975" ($((0.395" / 2) + 0.5)$). Multiplying this by two and then dividing by the aspect ratio ($(2 \times 0.6975") / 5.0$) gives the flaw depth (0.279") when the upper extremity is 0.5 inches below the weld. Figure 6-48a can be used to find the time it takes to grow from 12.6% through-wall ($a/t = 0.079" / 0.625" = 0.126$) to 44.6% through-wall ($a/t = 0.279" / 0.625" = 0.446$). The time is estimated as 2.6 years. Using the flaw depth calculated previously ($a/t = 0.446$) as the initial flaw depth, the curves in Figure 6-25 reproduced here as Figure 6-48b, for inside surface flaws near the weld can be used to determine the remaining service time before the flaw depth reaches the

allowable flaw size ($a/t = 0.75$). Using the acceptance criteria in Table 6-1, Figure 6-48b shows an additional 0.6-years of service life for a total of 3.2years.

Example 5 – This case is an axial through-wall flaw with its upper extremity located 0.40 inches below the weld region on the uphill side of penetration no. 78. The angle of the penetration nozzle is 50.5 degrees as shown in Table 1-2. The crack growth curves of Figure 6-39 are applicable and has been reproduced as Figure 6-49. The initial reference time is found by drawing a horizontal line 0.40 inches below the line representing the bottom of the weld, then dropping a vertical line to the x axis. The final reference time is found by drawing a vertical line where the crack growth curve intersects the bottom of the weld horizontal line. The service life is estimated to be approximately 2.5 years for the postulated- flaw to grow to the bottom of the attachment weld.

The examples show that the most important figures used in evaluating the detected flaws in the head penetrations are the axial surface flaw figures (Figures 6-2 through 6-10 for Unit 1 and Figures 6-22 through 6-30 for Unit 2) and circumferential flaw figures (Figures 6-11 for Unit 1 and Figure 6-31 for Unit 2). The through-wall flaw figures (Figures 6-12 through 6-21 for Unit 1 and Figures 6-32 through 6-41 for Unit 2) provide valuable information on the projected growth of through-wall flaws, but may be of limited practical application with the current acceptance criteria.

Additional Guidelines

1. If a flaw is found in a penetration nozzle for which no specific analysis was performed and there is a uniform trend as a function of penetration nozzle angle, interpolation between penetration nozzles is the best approach.
2. If a flaw is found in a penetration nozzle for which no specific analysis was performed and there is no apparent trend as a function of penetration nozzle angle, the result for the penetration nozzle with the closest angle should be used.
3. If a flaw is found which has a depth smaller than any depth shown for the penetration nozzle angle of interest, the initial flaw depth should be assumed to be the same as the smallest depth analyzed for that particular penetration nozzle.
4. The flaw evaluation charts are applicable for aspect ratio of 6 or less. Consult with Westinghouse if the as-found flaw has an aspect ratio larger than 6.0.
5. For flaws whose upper extremities grow within 0.5" below the weld require the use of both the 0.5" below the weld and "at the weld" flaw tolerance charts. To avoid the use of these two charts, the "at the weld" charts may solely be used in determining the service life. This shall provide a conservative estimate of the crack growth due to a higher stress field.
6. All references to service life are in effective full power years.
7. Results are only provided for the uphill and downhill sides of the selected penetration nozzles. If flaws are found in locations between the uphill and downhill side, use the results for either the uphill or downhill location, whichever is closer.

| Table 6-1 Summary of R.V. Head Penetration Flaw Acceptance Criteria (Limits for Future Growth) | | | | |
|--|-------------------------|-----------------------|-------------------------|-----------------------|
| Location | Axial | | Circumferential | |
| | a_f | l | a_f | l |
| Below Weld (ID) | t | no limit | t | .75 circ. |
| At and Above Weld (ID) | 0.75 t | no limit | repair | repair |
| Below Weld (OD) | t | no limit | t | .75 circ. |
| Above Weld (OD) | repair | repair | repair | repair |
| <p>Note: PWSCC Surface flaws of any size in the attachment weld are not acceptable.</p> <p>a_f = Flaw Depth l = Flaw Length t = Wall Thickness</p> | | | | |

| Table 6-2 D. C. Cook Units 1 & 2 Penetration Geometries [11, 12] | | |
|---|-----------------------------|-----------------------------|
| Penetration Type | Wall Thickness (in.) | Penetration OD (in.) |
| CRDM (Units 1 & 2) | 0.625 | 4.000 |
| Head Vent (Unit 1) | 0.154 | 1.050 |
| Head Vent (Unit 2) | 0.218 | 1.050 |

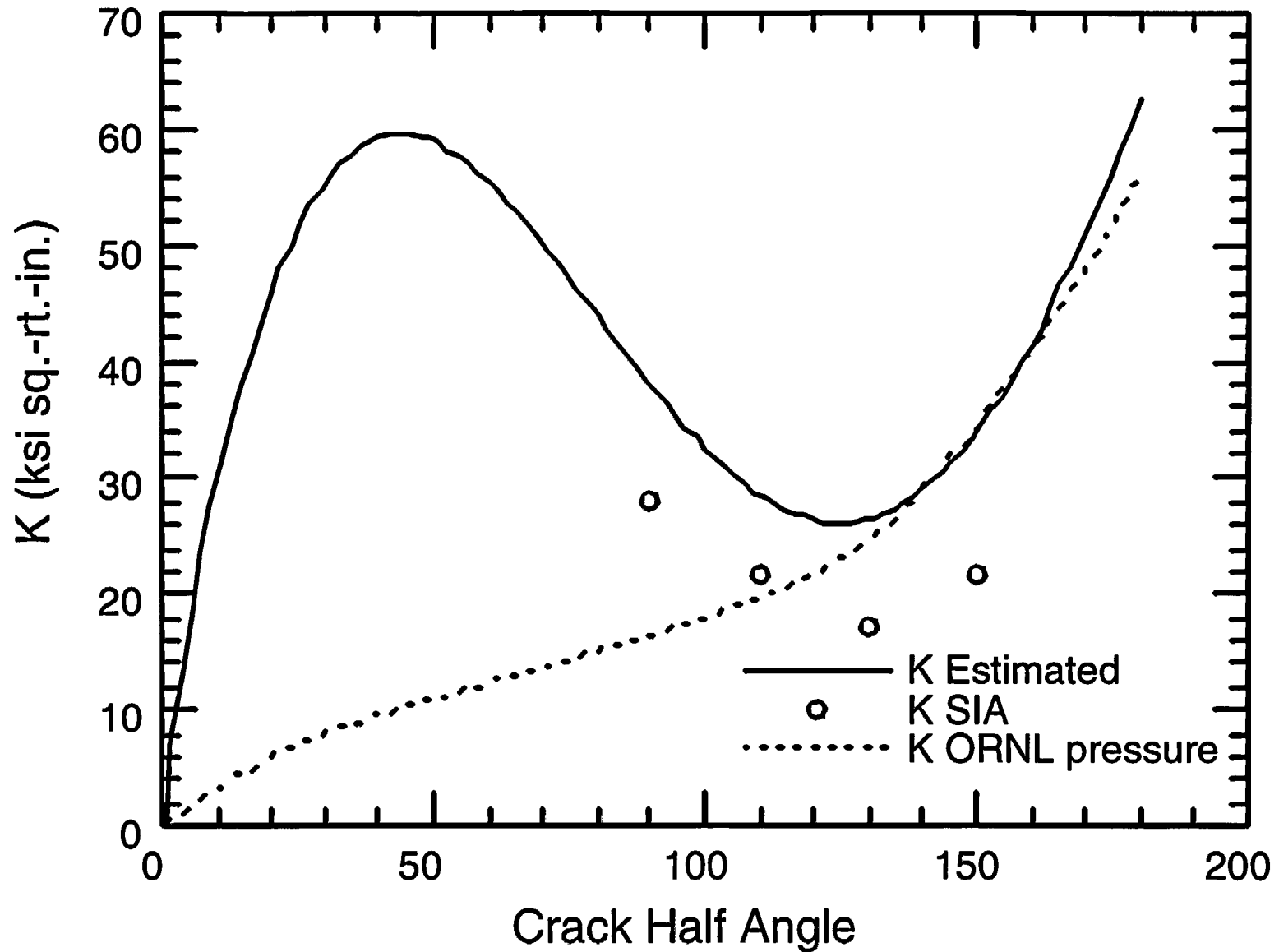


Figure 6-1 Stress Intensity Factor for a Through-Wall Circumferential Flaw in a Head Penetration

D. C. Cook Unit 1 Flaw Tolerance Charts

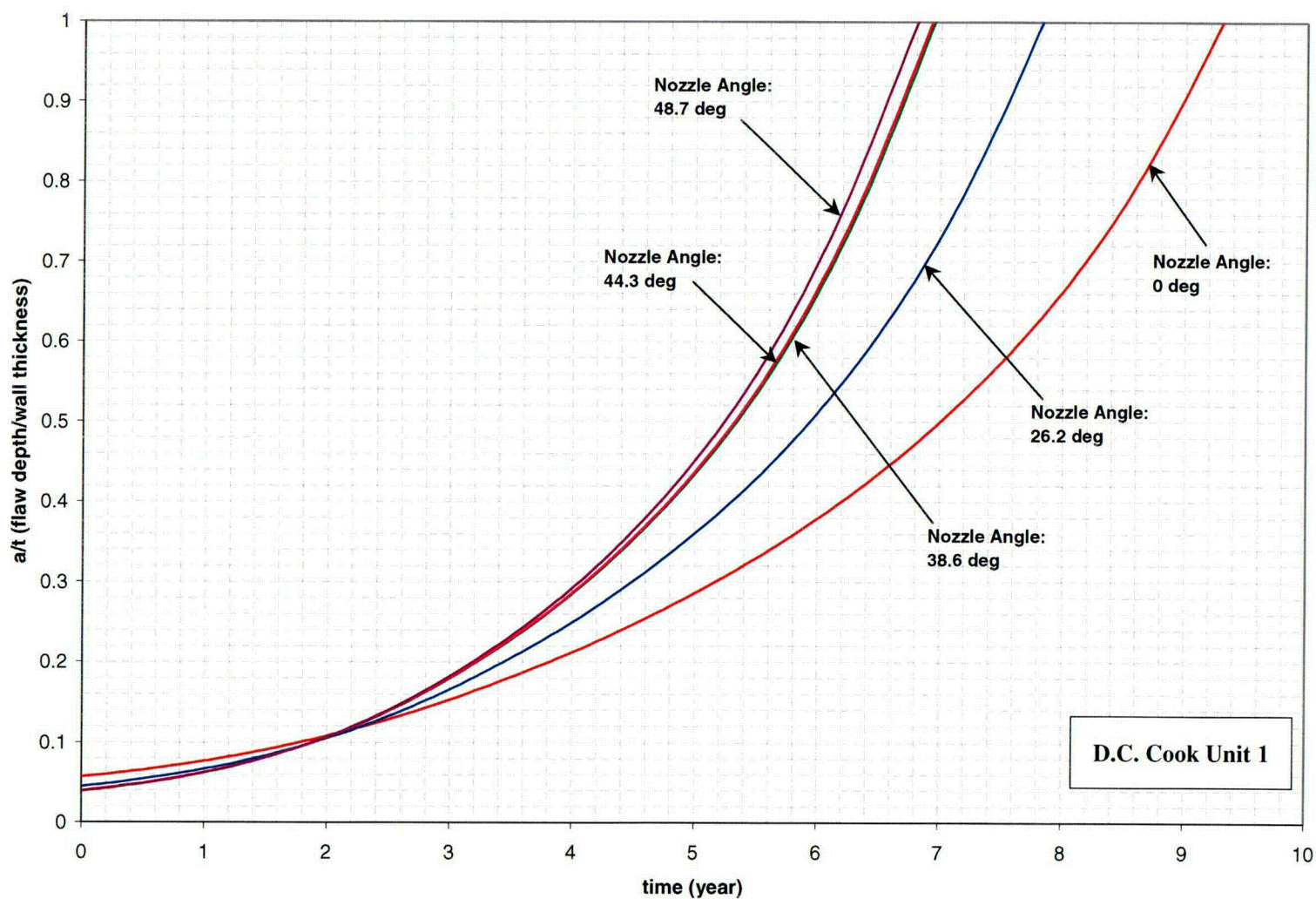


Figure 6-2 Inside, Axial Surface Flaws, .5" Below the Attachment Weld, Nozzle Uphill Side - Crack Growth Predictions for D. C. Cook Unit 1

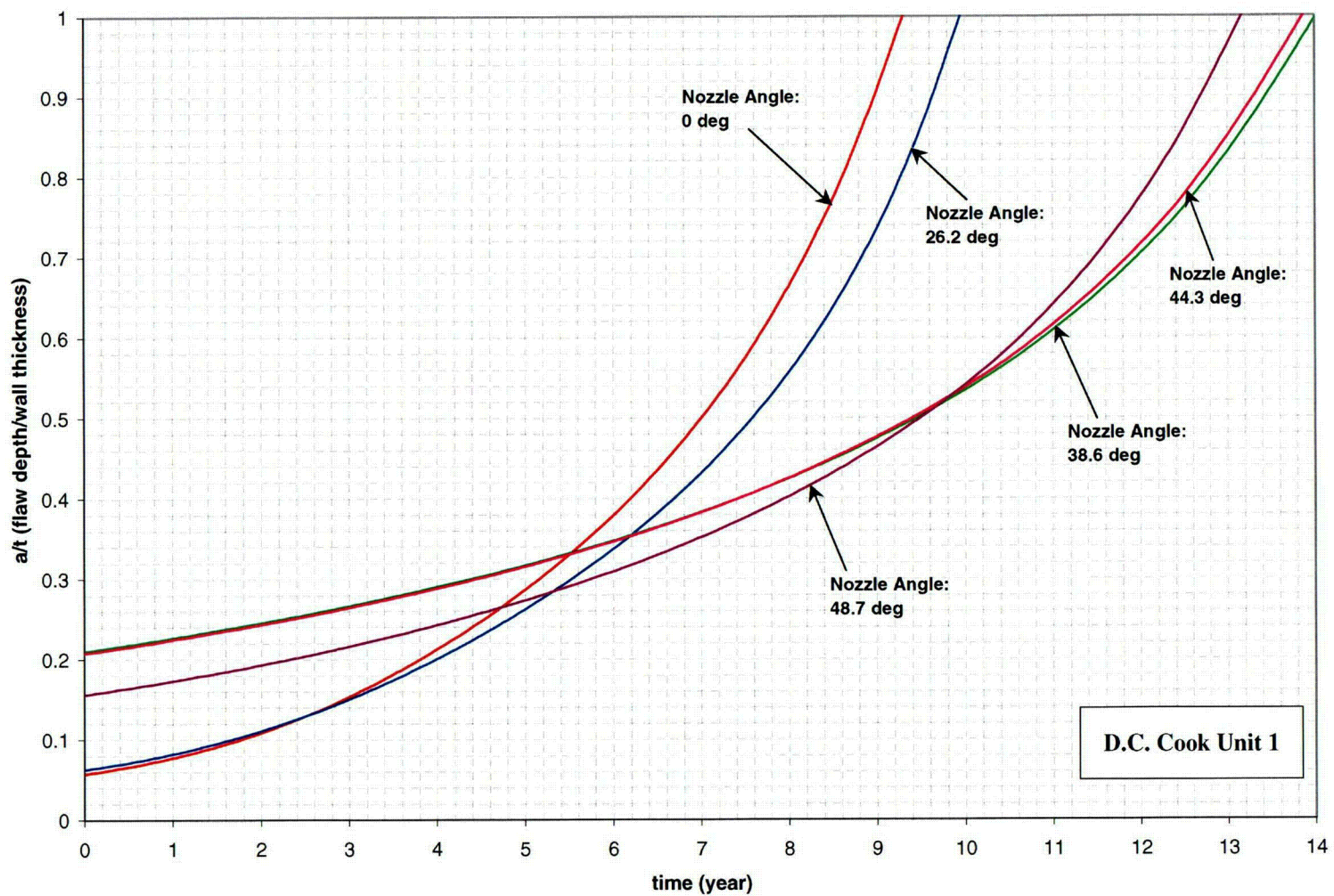


Figure 6-3 Inside, Axial Surface Flaws, .5" Below the Attachment Weld, Nozzle Downhill Side - Crack Growth Predictions for D. C. Cook Unit 1

C11

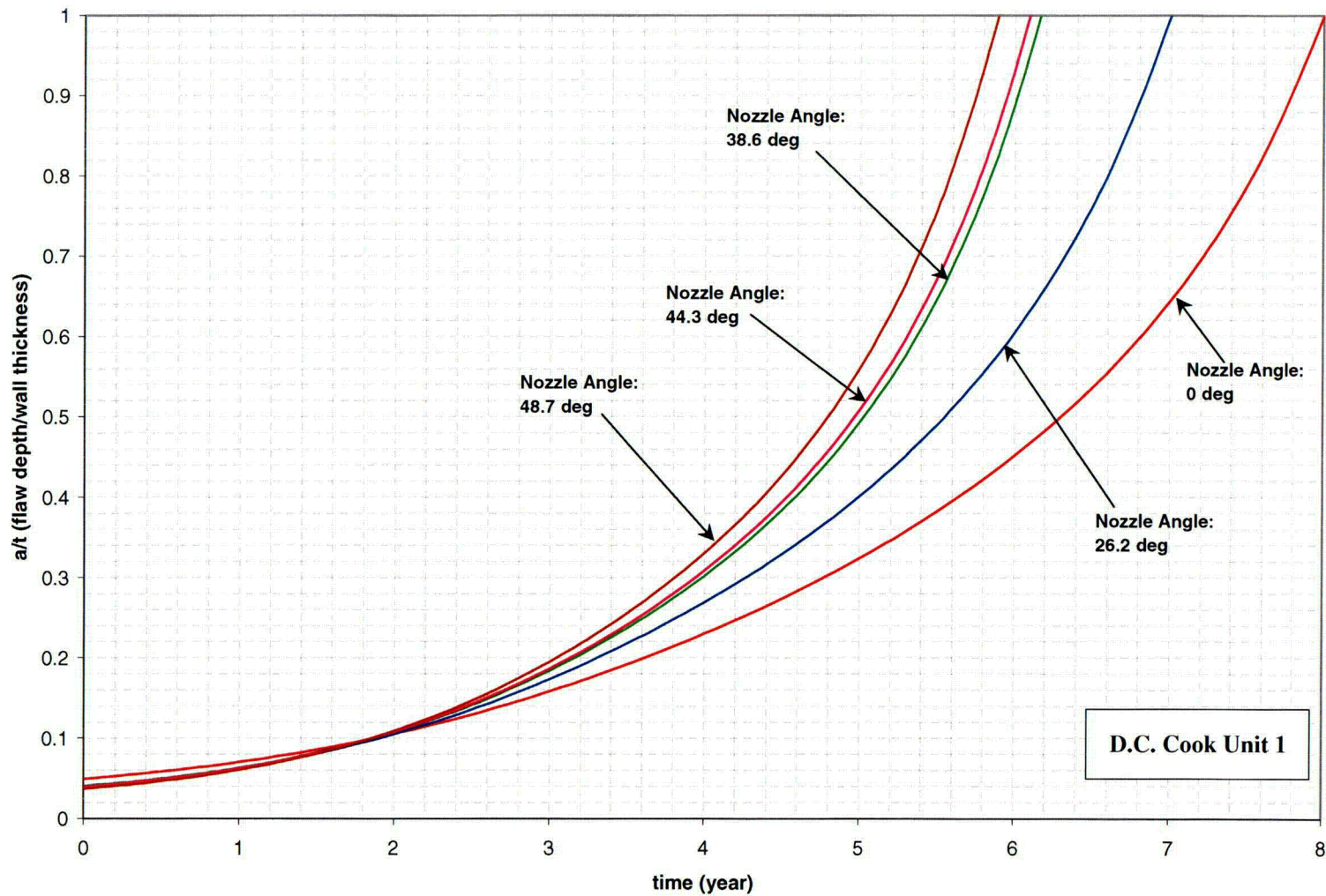


Figure 6-4 Inside, Axial Surface Flaws, At the Attachment Weld, Nozzle Uphill Side - Crack Growth Predictions for D. C. Cook Unit 1

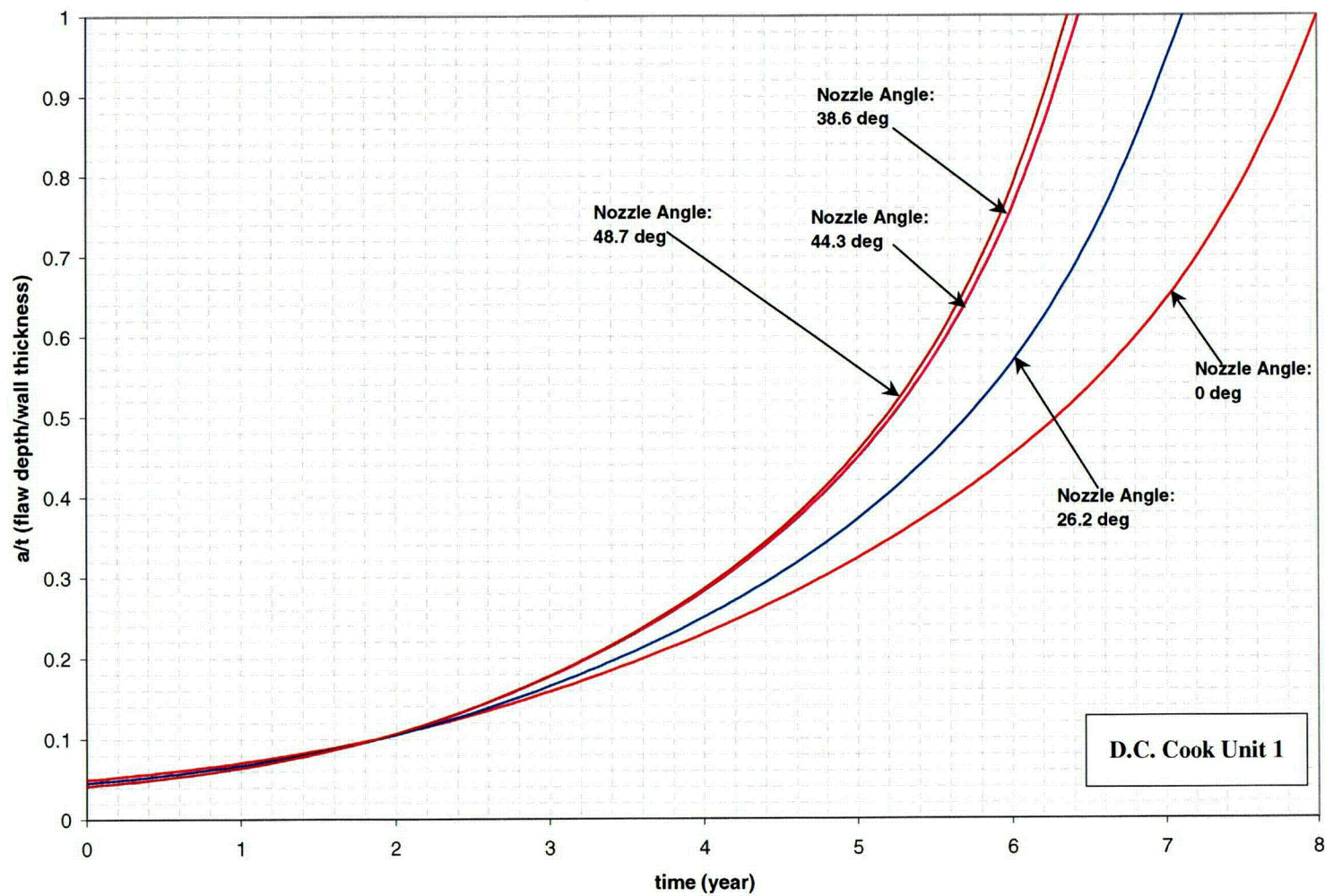


Figure 6-5 Inside, Axial Surface Flaws, At the Attachment Weld, Nozzle Downhill Side - Crack Growth Predictions for D. C. Cook Unit 1

C13

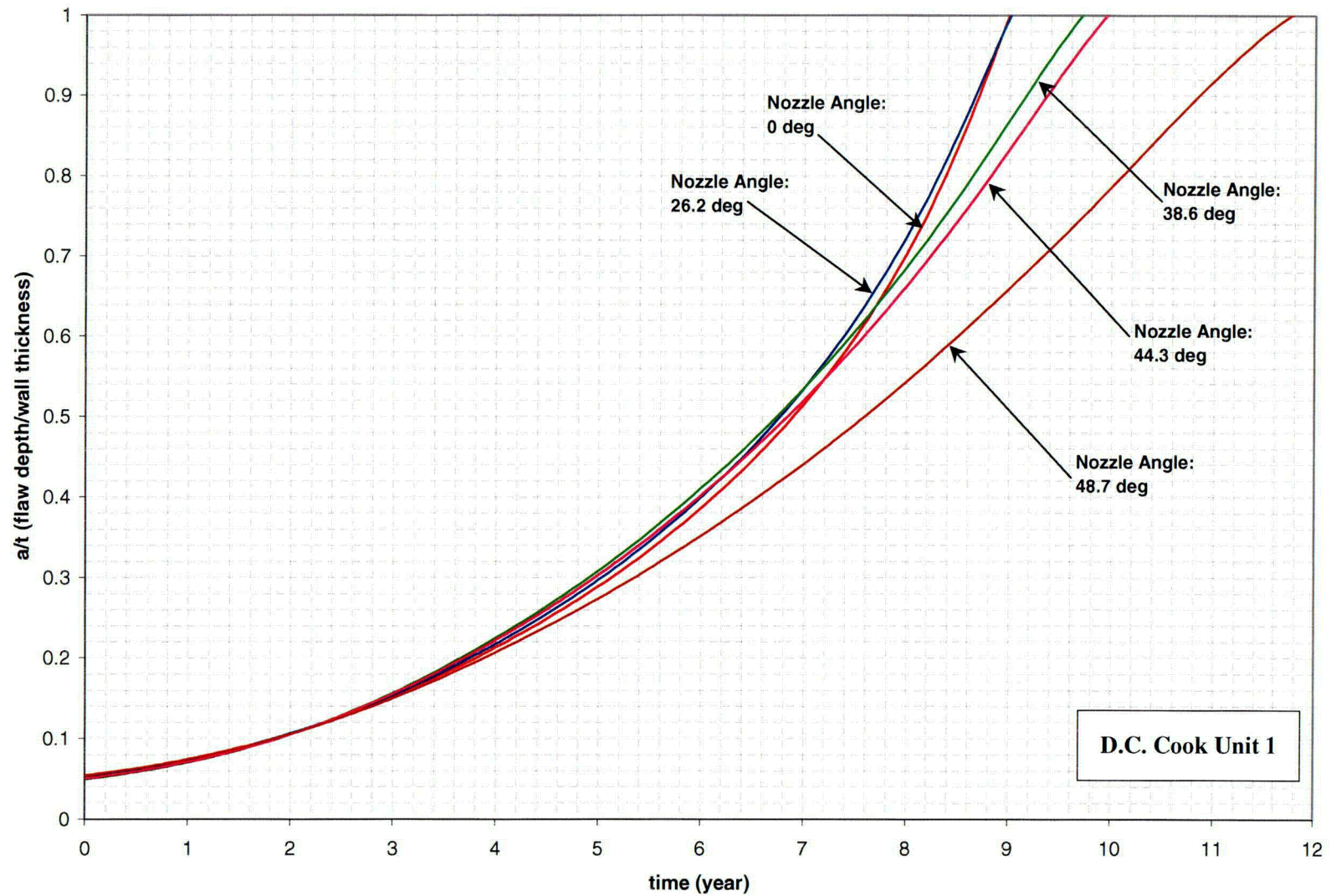


Figure 6-6 Inside, Axial Surface Flaws, .5" Above the Attachment Weld, Nozzle Uphill Side - Crack Growth Predictions for D. C. Cook Unit 1

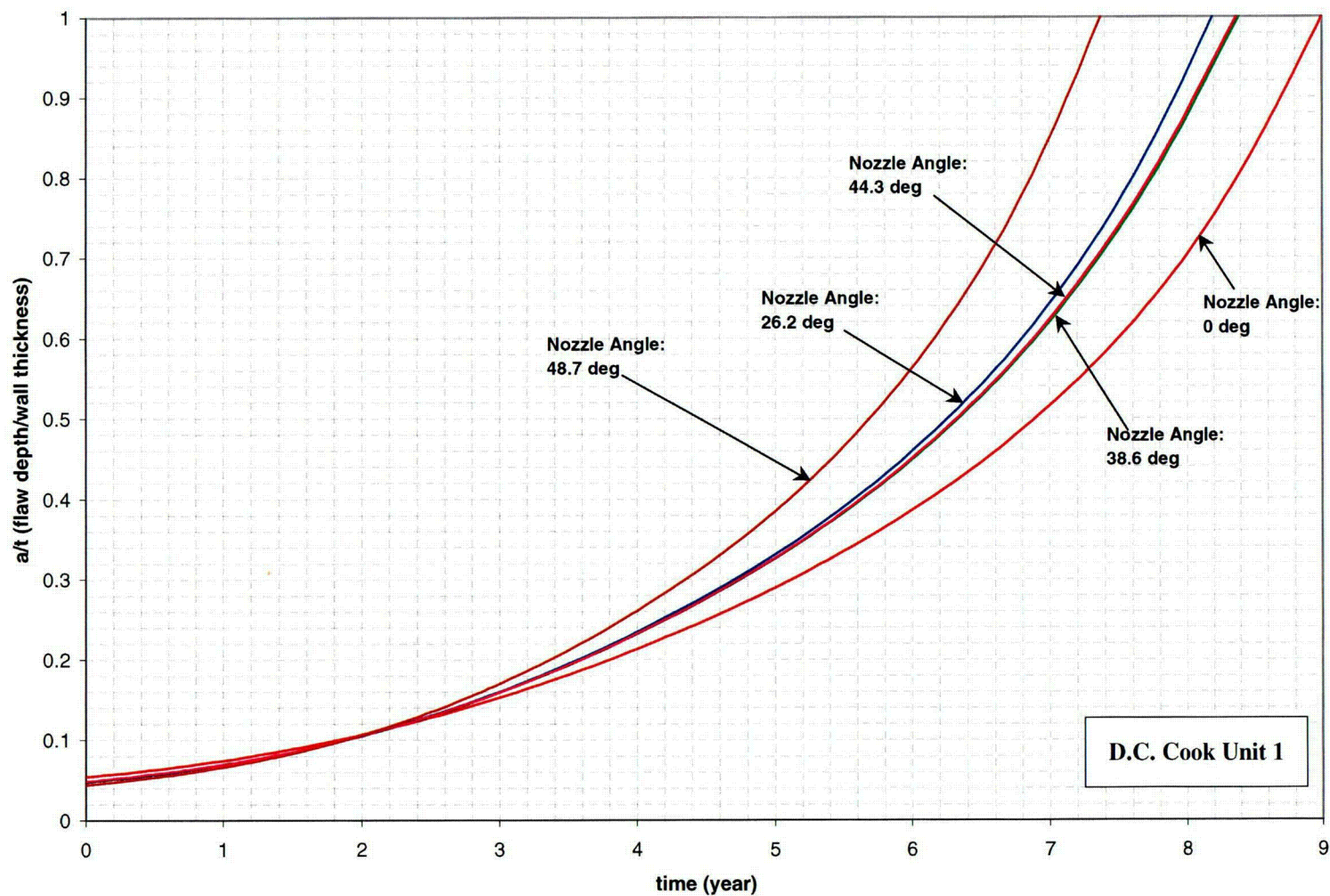


Figure 6-7 Inside, Axial Surface Flaws, .5" Above the Attachment Weld, Nozzle Downhill Side - Crack Growth Predictions for D. C. Cook Unit 1

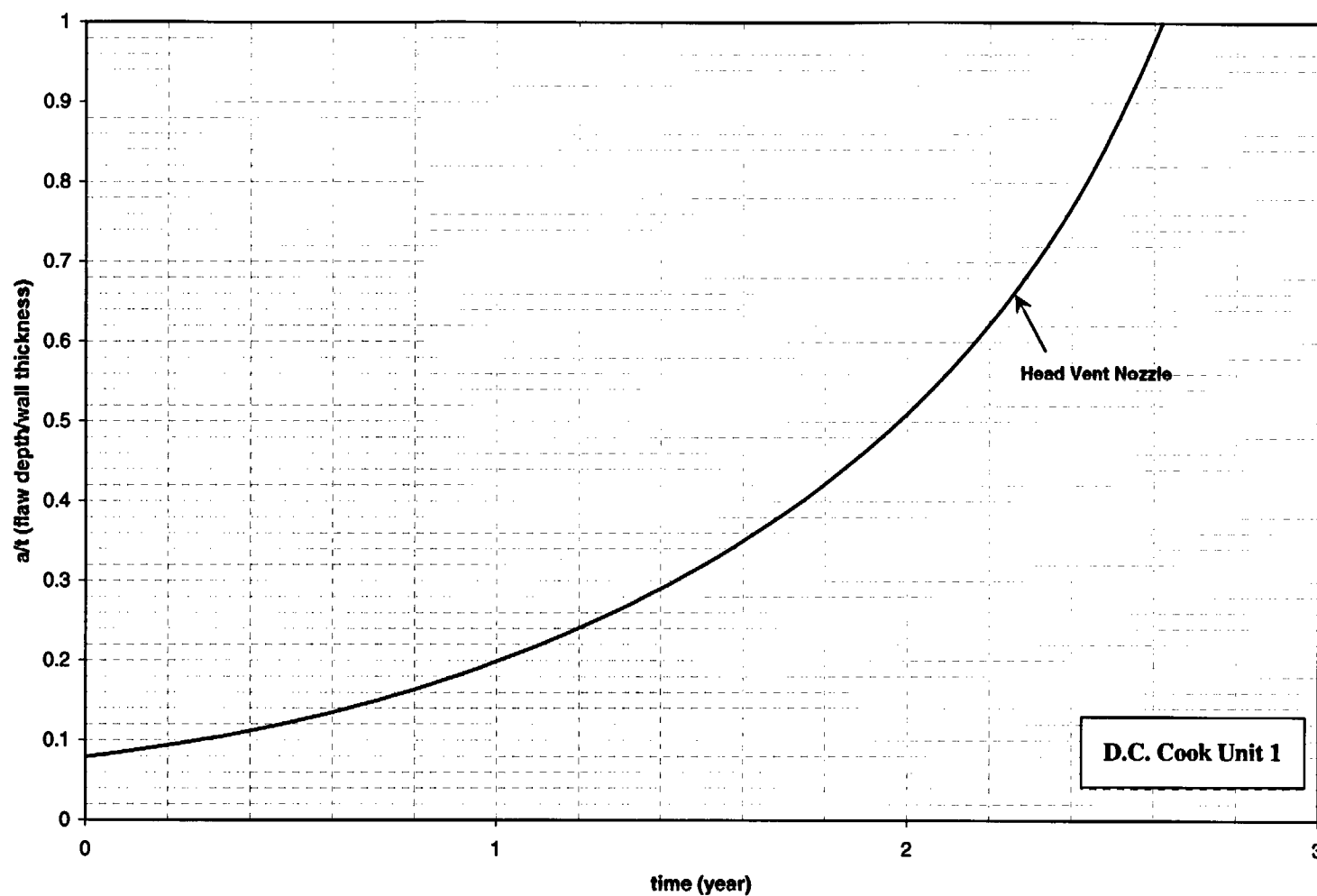


Figure 6-8 Inside, Axial Surface Flaws, At the Attachment Weld, Head Vent, Nozzle Downhill Side - Crack Growth Predictions for D.C. Cook Unit 1

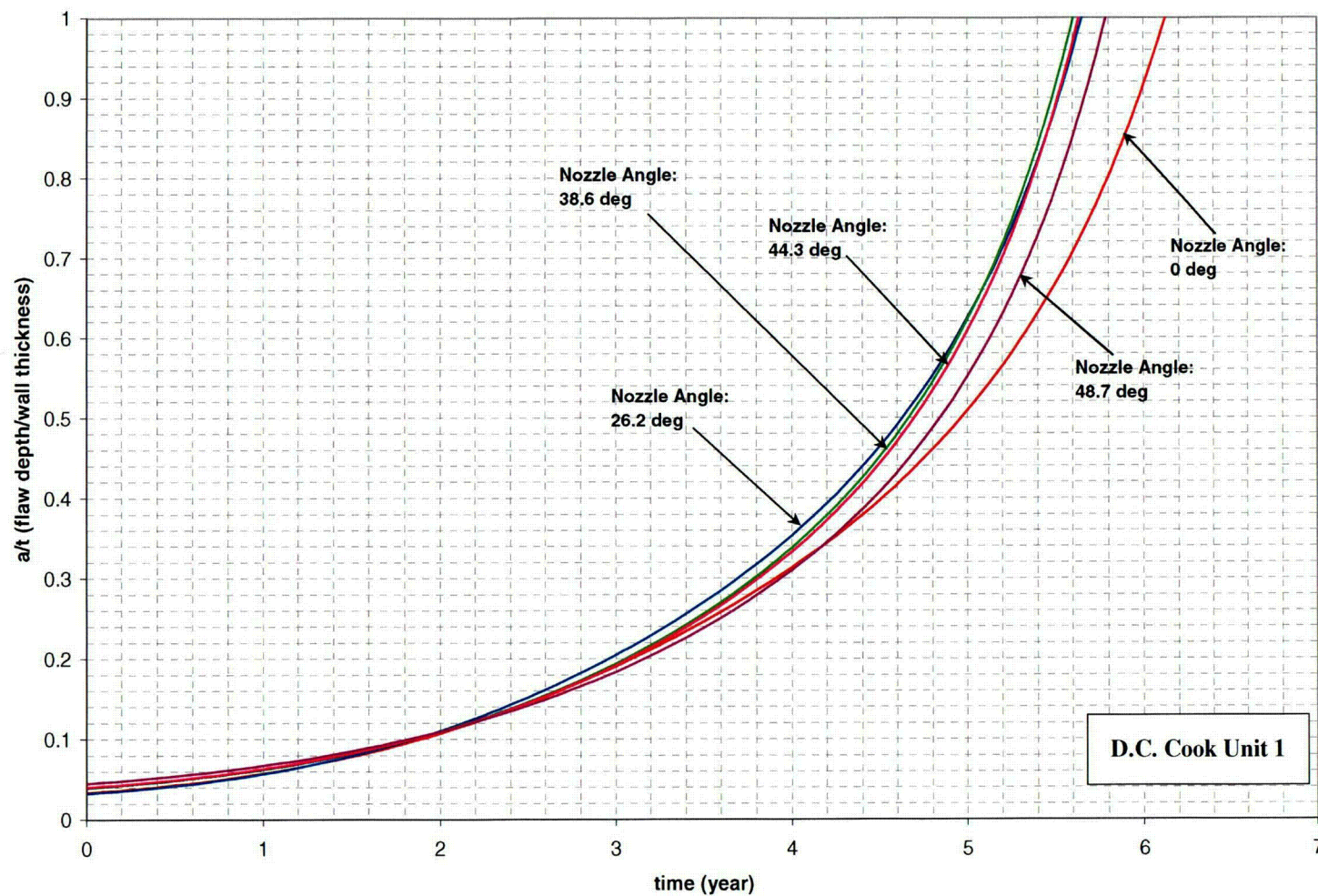


Figure 6-9 Outside, Axial Surface Flaws, Below the Attachment Weld, Nozzle Uphill Side - Crack Growth Predictions for D. C. Cook Unit 1

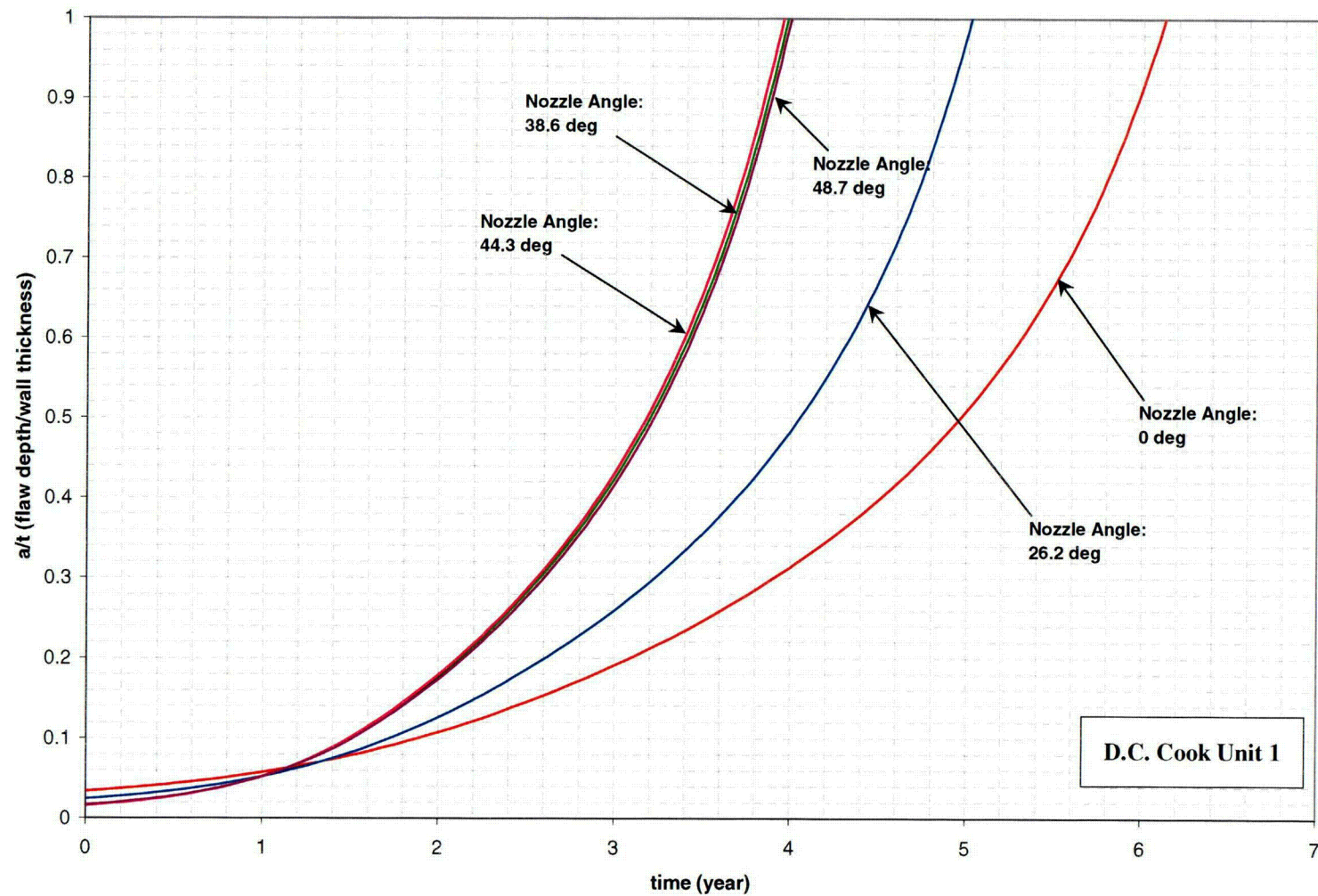


Figure 6-10 Outside, Axial Surface Flaws, Below the Attachment Weld, Nozzle Downhill Side - Crack Growth Predictions for D. C. Cook Unit 1

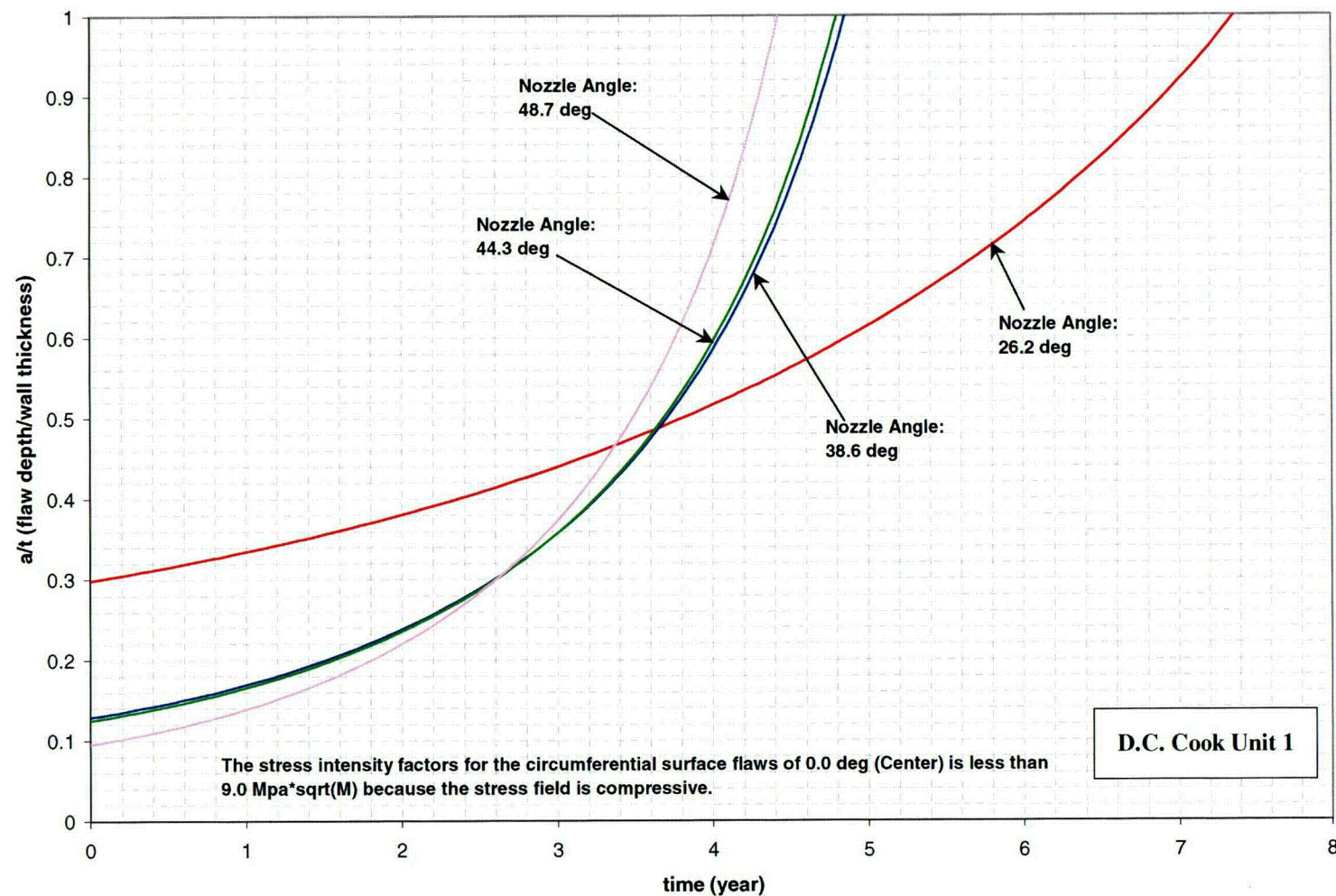


Figure 6-11 Outside, Circumferential Surface Flaws, Along the Top of the Attachment Weld - Crack Growth Predictions for D. C. Cook Unit 1 (MRP Factor of 2.0 Included)

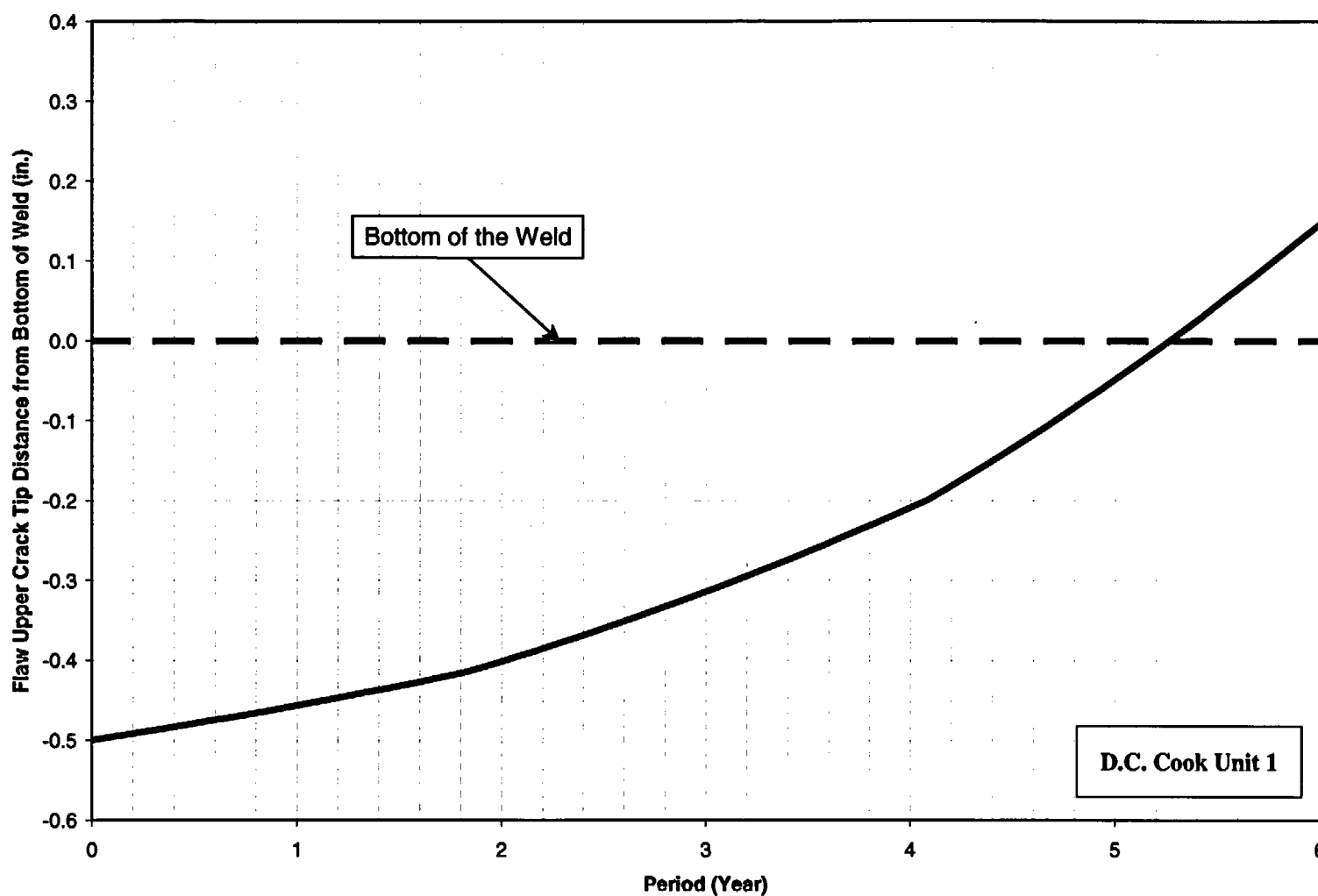


Figure 6-12 Through-Wall Axial Flaws Located in the Center CRDM (0.0 Degrees) Penetration, Uphill and Downhill Side - Crack Growth Predictions for D. C. Cook Unit 1

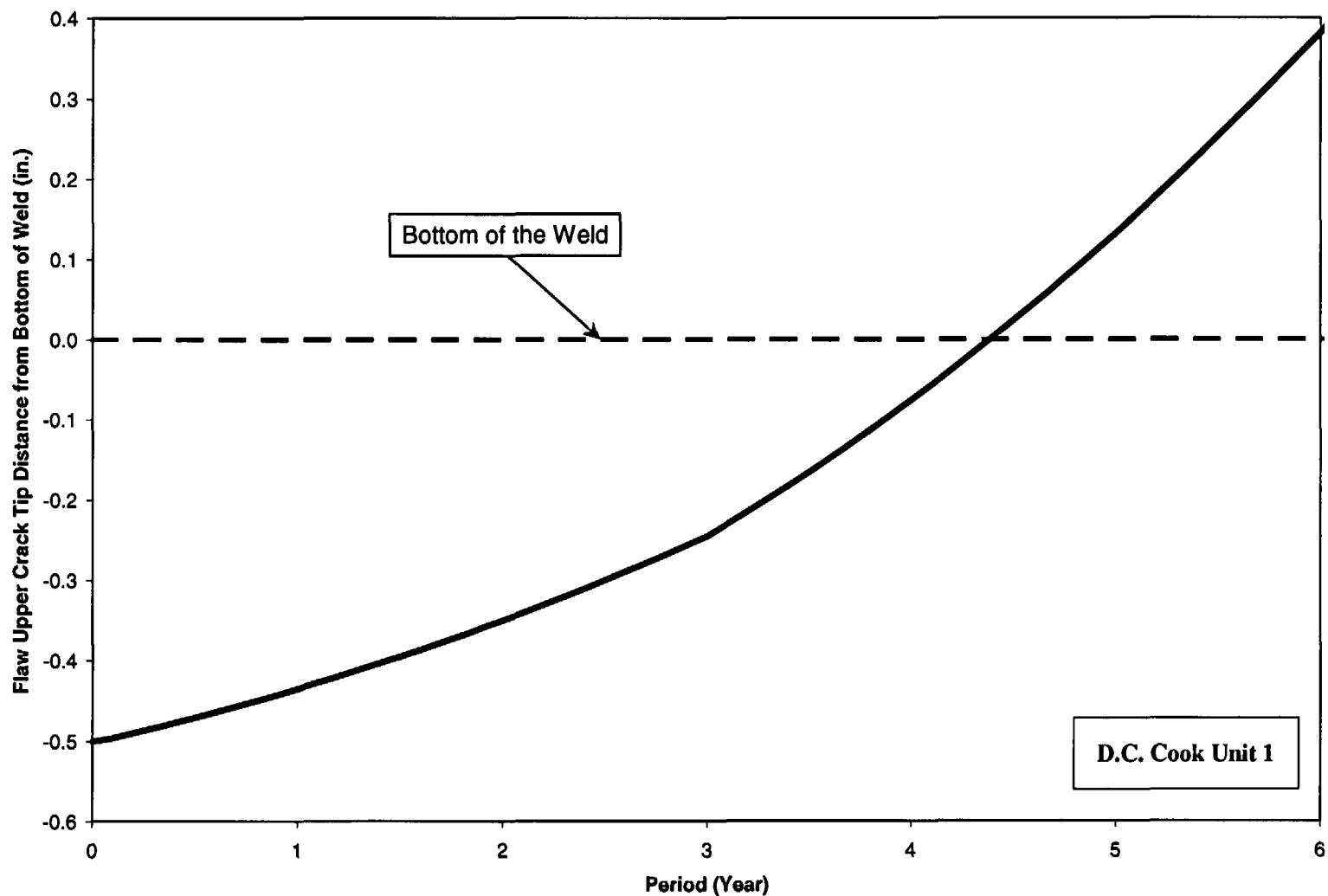


Figure 6-13 Through-Wall Axial Flaws Located in the 26.2 Degrees Row of Penetrations, Uphill Side - Crack Growth Predictions for D.C. Cook Unit 1

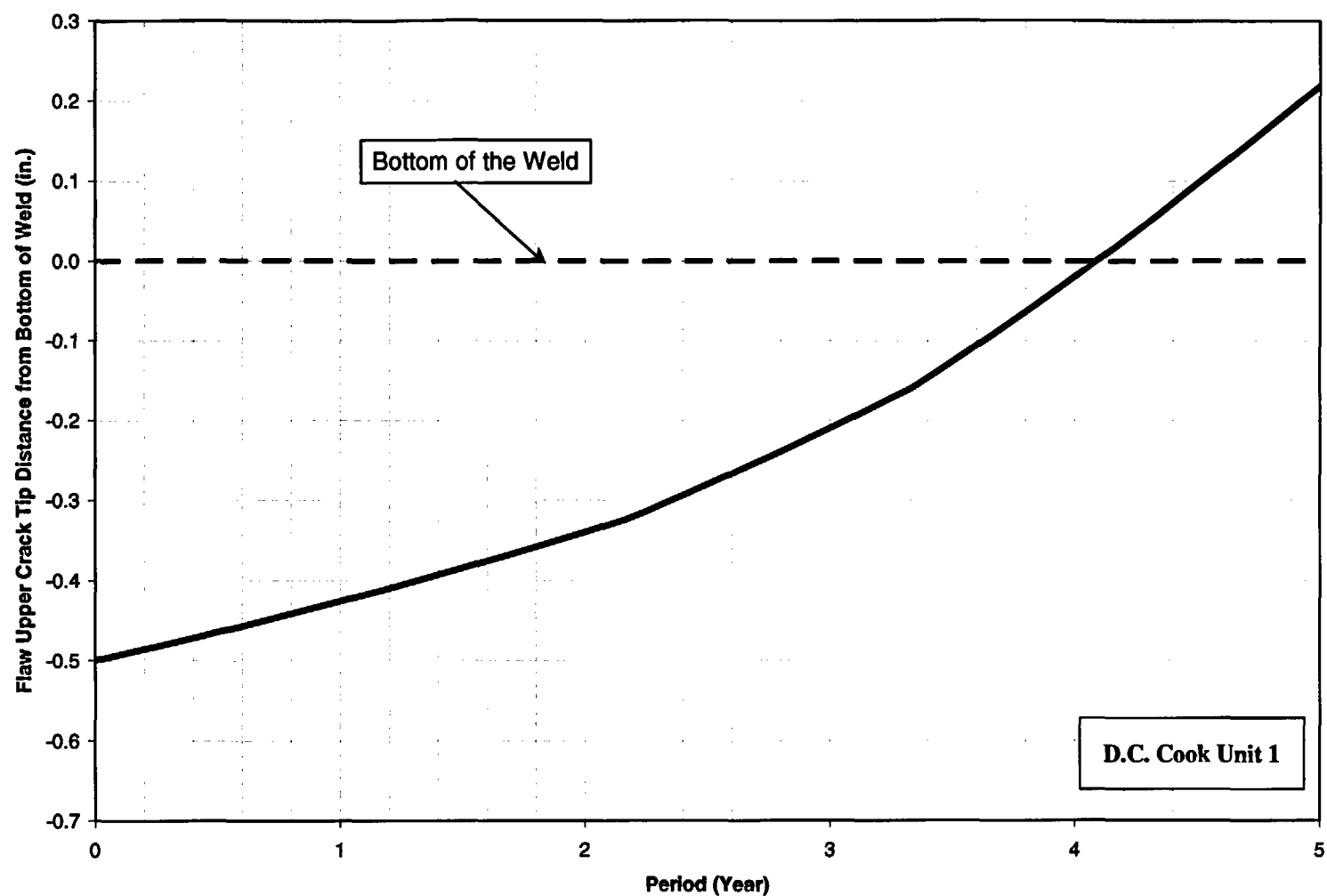


Figure 6-14 Through-Wall Axial Flaws Located in the 26.2 Degrees Row of Penetrations, Downhill Side - Crack Growth Predictions for D.C. Cook Unit 1

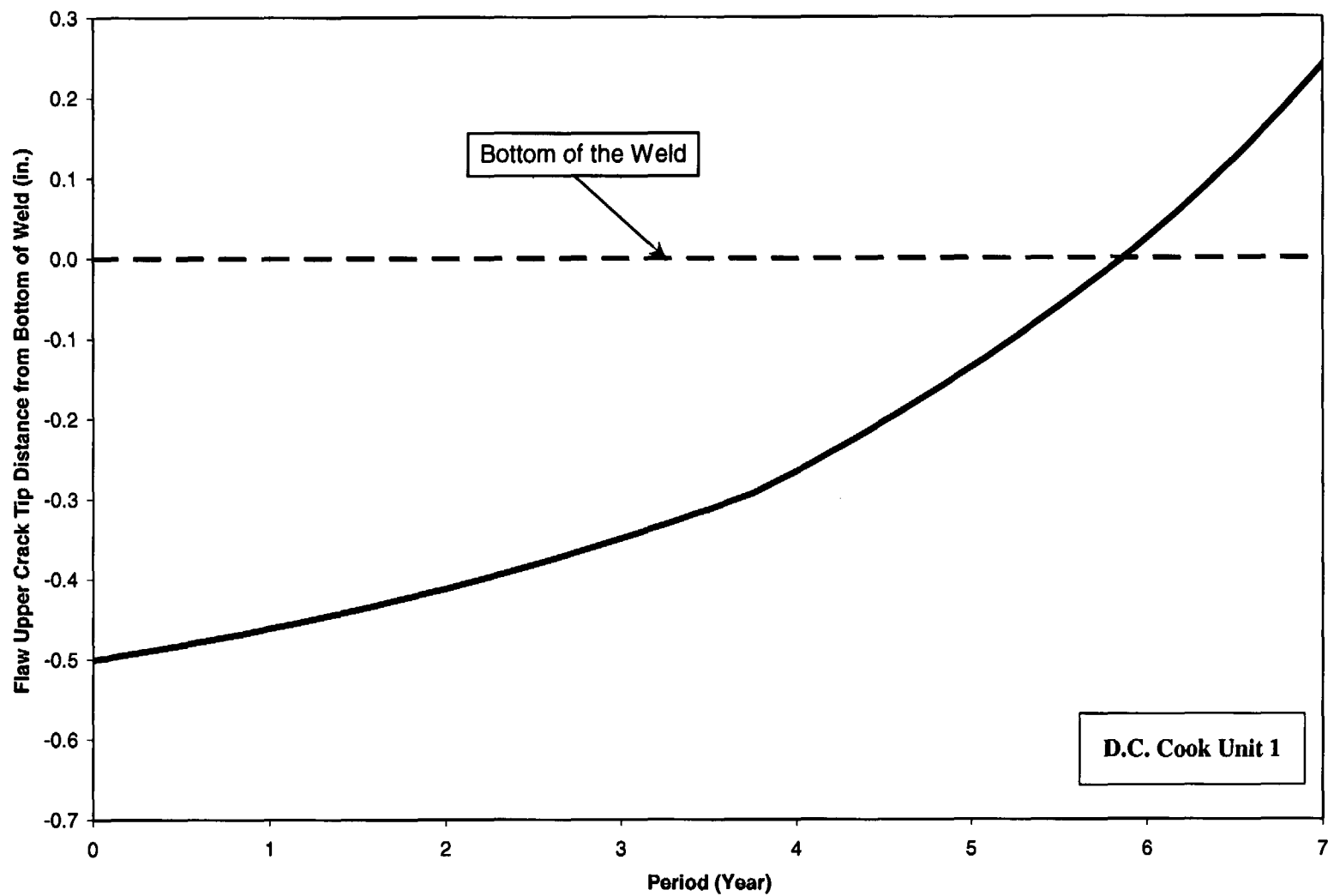


Figure 6-15 Through-Wall Axial Flaws Located in the 38.6 Degrees Row of Penetrations, Uphill Side - Crack Growth Predictions for D.C. Cook Unit 1

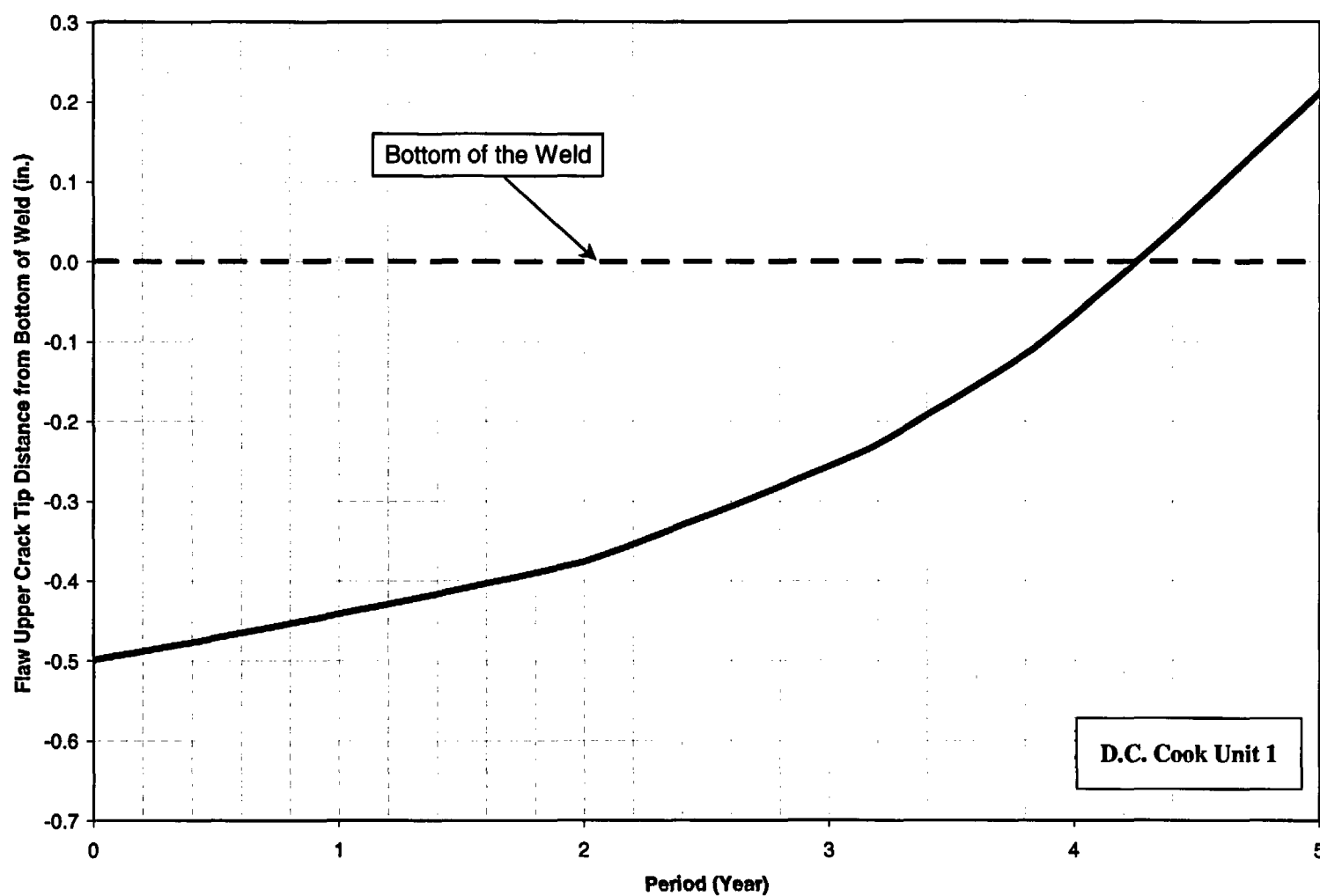


Figure 6-16 Through-Wall Axial Flaws Located in the 38.6 Degrees Row of Penetrations, Downhill Side - Crack Growth Predictions for D. C. Cook Unit 1

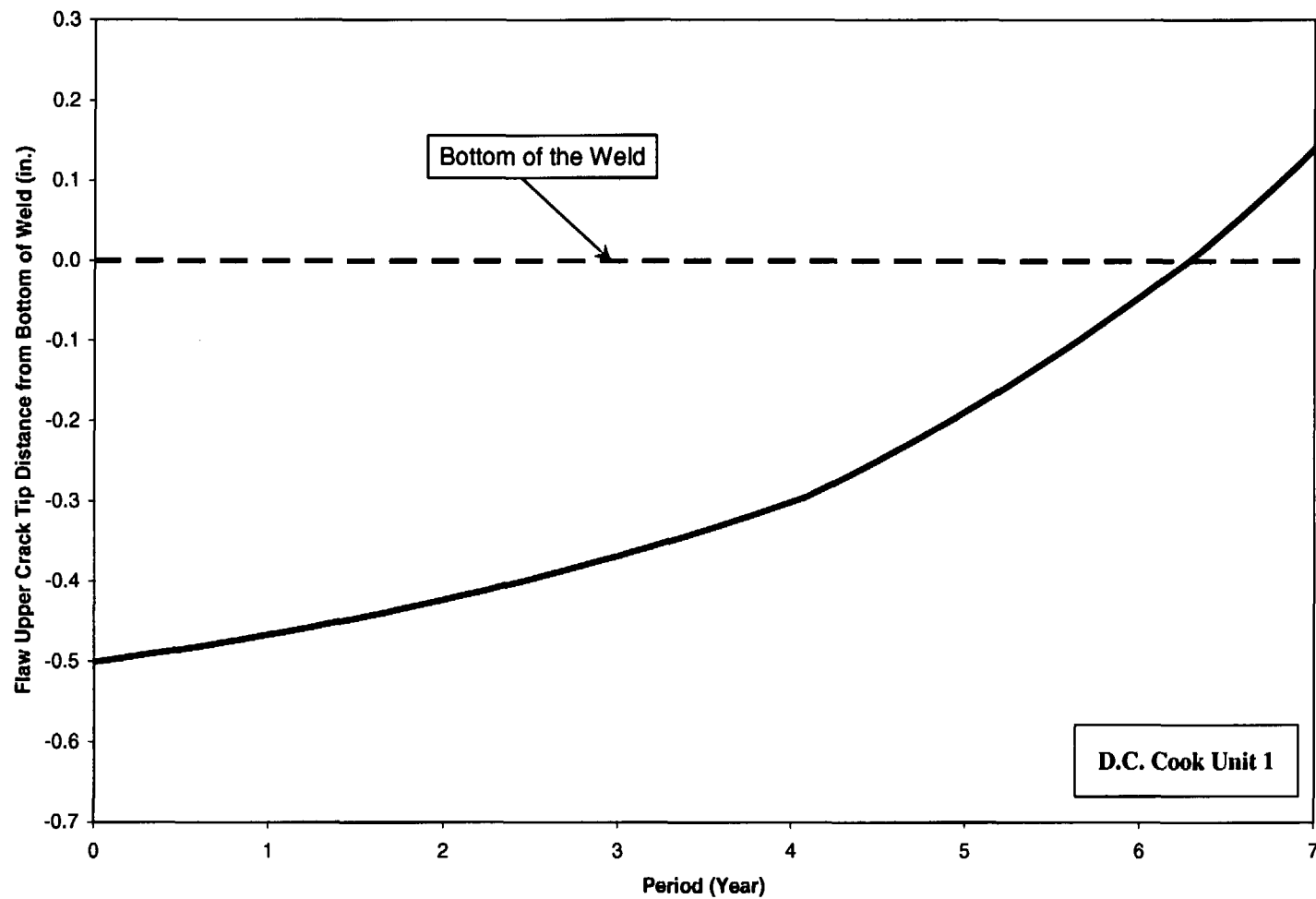


Figure 6-17 Through-Wall Axial Flaws Located in the 44.3 Degrees Row of Penetrations, Uphill Side - Crack Growth Predictions for D.C. Cook Unit 1

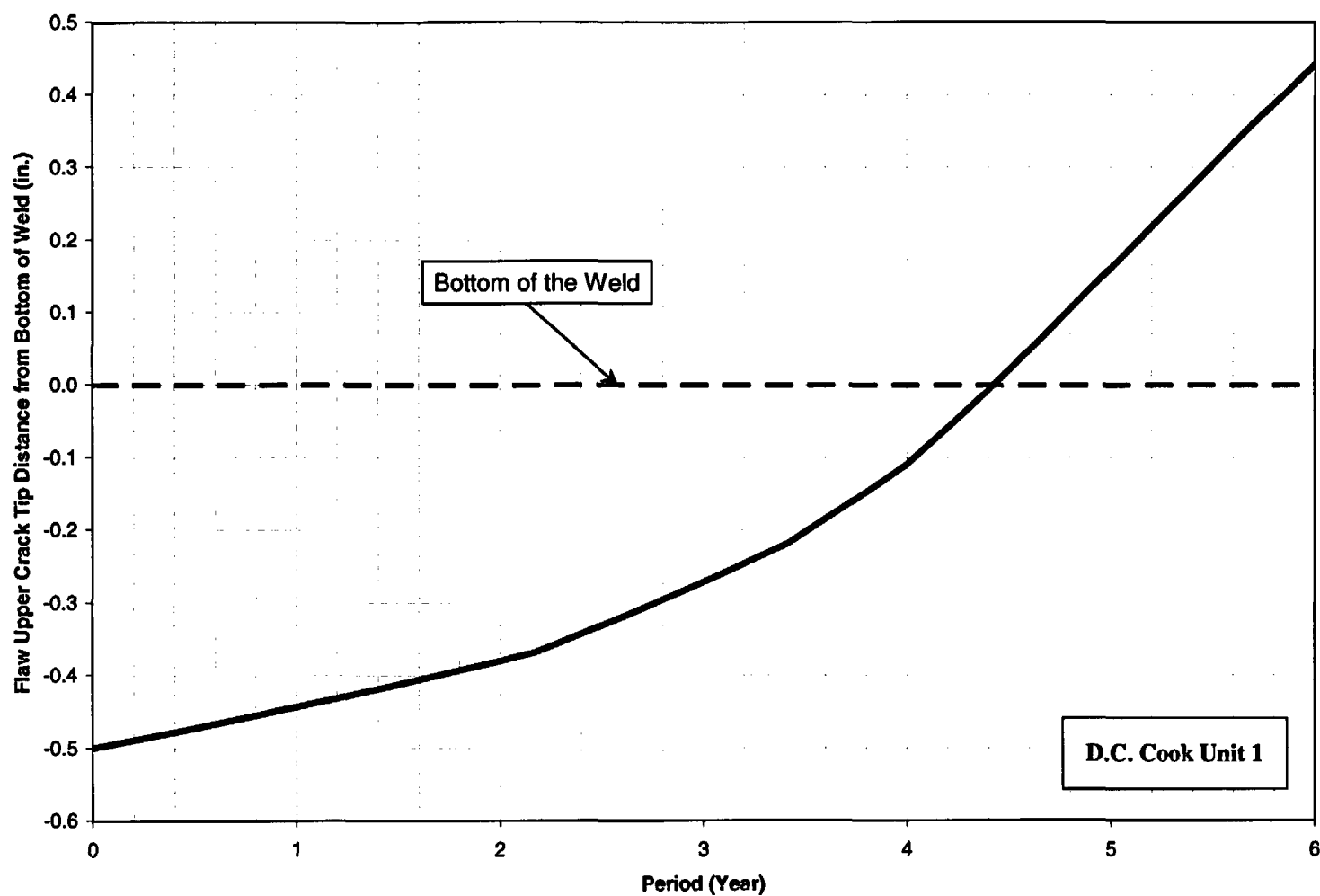


Figure 6-18 Through-Wall Axial Flaws Located in the 44.3 Degrees Row of Penetrations, Downhill Side - Crack Growth Predictions for D. C. Cook Unit 1

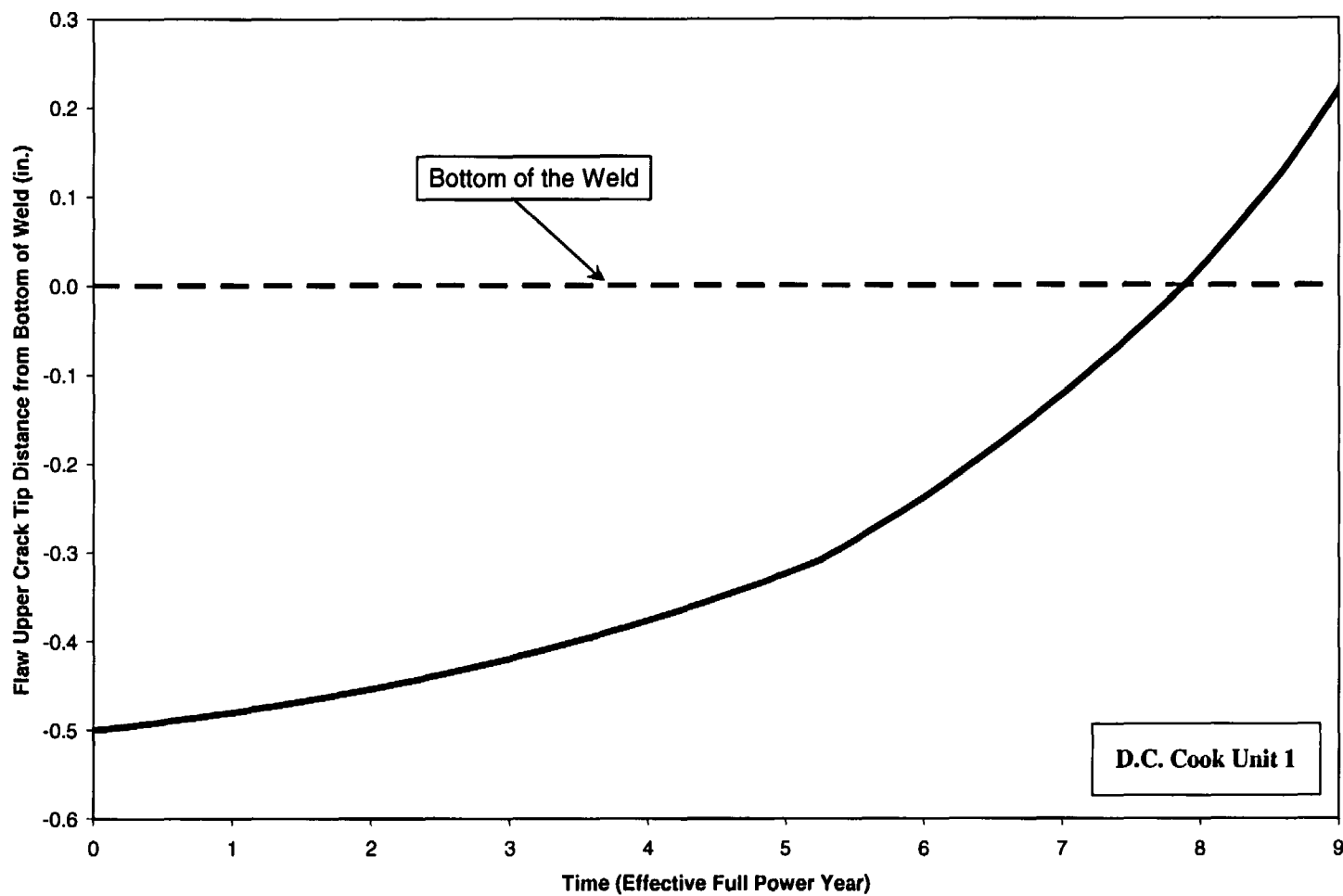


Figure 6-19 Through-Wall Axial Flaws Located in the 48.7 Degrees Row of Penetrations, Uphill Side - Crack Growth Predictions for D.C. Cook Unit 1

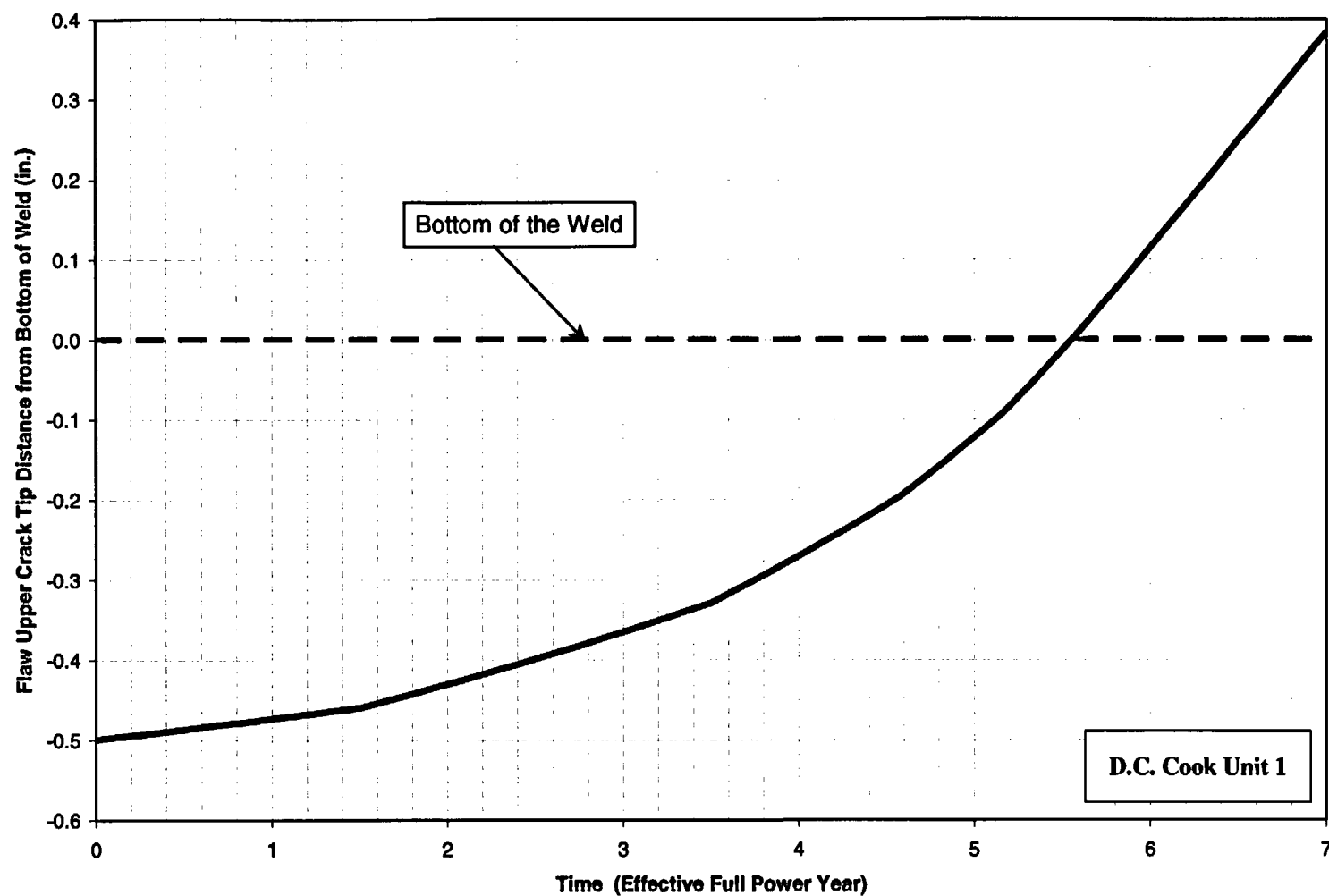


Figure 6-20 Through-Wall Axial Flaws Located in the 48.7 Degrees Row of Penetrations, Downhill Side - Crack Growth Predictions for D. C. Cook Unit 1

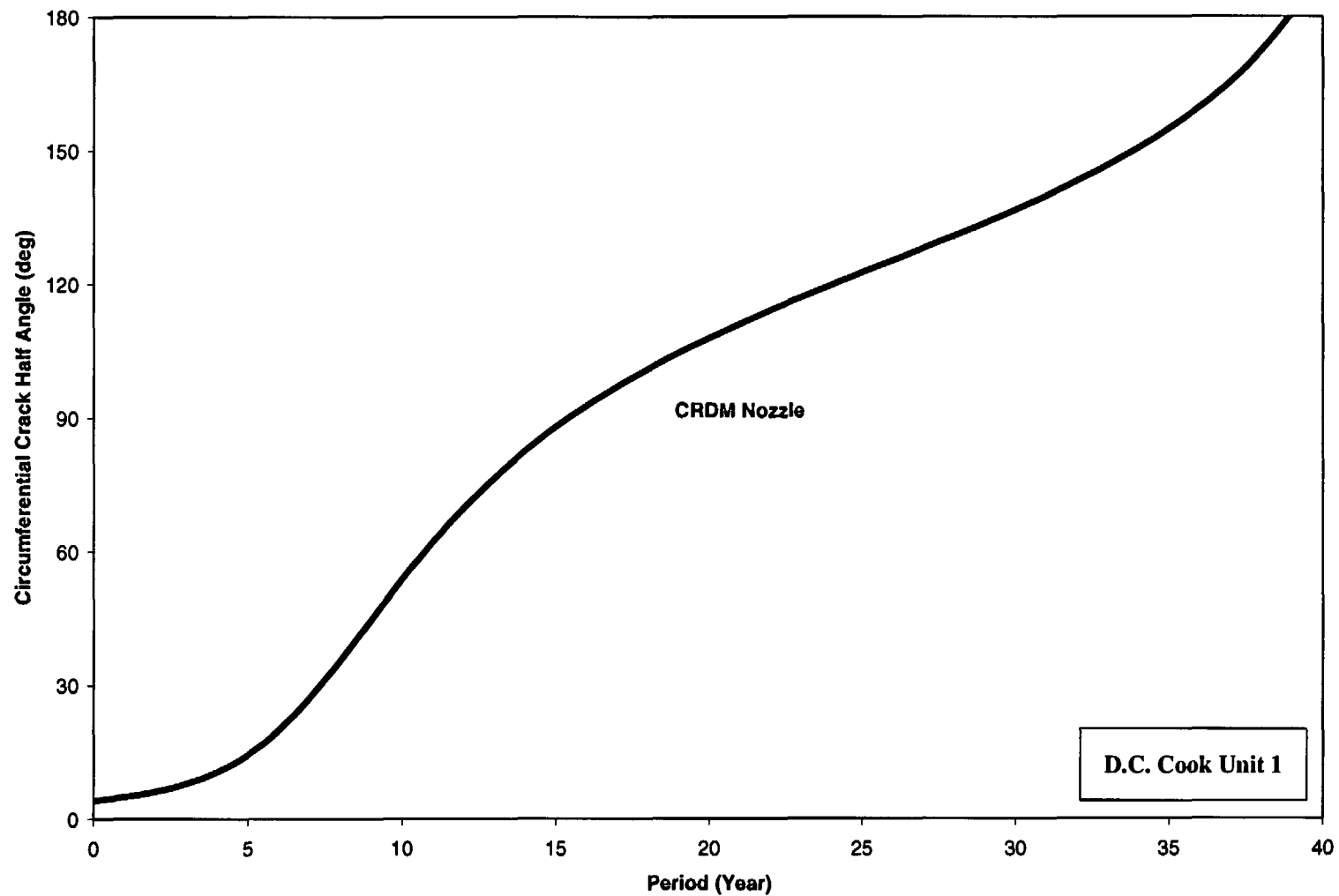


Figure 6-21 Through-Wall Circumferential Flaws Near the Top of the Attachment Weld for CRDM Nozzle - Crack Growth Predictions for D. C. Cook Unit 1 (MRP Factor of 2.0 Included)